About the influence of temperature and humidity level on pulse shape parameters of positive DC corona discharges in air

Ulrich Lühring, Daniel Wienold and Frank Jenau

***Abstract*—Partial discharges reduce the residual lifespan of operating equipment and can indicate serious deficiencies of electrical insulations at an early stage. Regarding AC voltage stress, the phase resolved pattern is an established diagnostic tool, which allows conclusions about the location and the type of fault. Despite the increasing importance of DC transmission systems, a comparable proceeding for DC voltage stress does not exist. This implies the development and evaluation of alternative and suitable basic approaches. Although diverse promising approaches are identified, recent research is focused on standard atmospheric conditions. Due to the fact that this is just partly consistent to real operating conditions, additional research is required. Focusing on the time domain analysis of corona discharges, occurring under positive DC voltage stress in air, a measurement method for investigating the influence of varying atmospheric quantities is presented. Measurements are carried out for five different relative humidity levels in the range of 20 % to 95 % and for four different temperature levels in the range of 20 °C to 65 °C. As characterizing pulse shape parameters, the rise time, the pulse width and the fall time are determined as well as the apparent charge. The gained values are compared to each other and reconciled with physical processes.**

***Index Terms*—corona discharge, DC voltage, humidity level, pulse shape parameter, temperature level**

I. Introduction

PARTIAL discharges are the result of a local electrical stress concentration and are defined as localized discharges, which partially bridge the electrical insulation between conductors [2]. Due to the damaging effect on the condition of isolation, the partial discharge (PD) diagnosis is a key component of electrical diagnostic procedures. In addition to a registration of local weak points, the focus of measurement and analysis techniques is in particular on the identification of the location and the type of fault. Regarding the latter, it is taken advantage of the fact that the appearance of PDs depends on various factors, which are influenced by the type of fault. Under AC voltage stress the phase resolved pattern is the best established and most commonly used diagnostic tool to distinguish between different types of fault [3]. This diagnostic procedure analyzes the link between discharge pulses and the phase angle of their occurrence with respect to the test voltage. The application is consequently restricted to AC voltage and not transferable to DC voltage. A similar recognized diagnostic tool for DC voltage stress does not exist.

The increasing importance of DC transmission systems requires the development and evaluation of alternative and suitable basic approaches. Therefore, the PD diagnosis at DC voltage stress is subject of current research, whereby diverse promising basic approaches could be identified. Regarding measurements based on the conventional PD measuring circuit, experimental tests indicate that an estimation of the magnitude of PDs [4], an analysis of the time lag between subsequent PD impulses [5] and the time domain analysis [6] are appropriated for a precise defect classification. In addition to that, unconventional measuring methods, such as the capturing of the electromagnetic spectrum by using a broadband antenna, are increasingly moving to the fore. With respect to DC applications it is e.g. shown in [7] and [8], that an evaluation of acquired data of the electromagnetic spectrum of PDs in the frequency domain respectively in the time domain is suited to distinguish between different types of fault.

An advantage of the time domain analysis is the direct relationship between the pulse shape of the PD impulse current and the causing processes. Furthermore, it is well known that the electromagnetic spectrum of PDs depends on the pulse shape of the discharge current [9]. The time domain analysis focusses on parameters, which are directly obtained from the pulse shape. The rise time, the pulse width and the fall time as primary parameters are considered as well as

This manuscript was submitted on June 8th, 2018 and revised on June 25th, 2018 as an extended version of the paper "*Influence of humidity on pulse shape parameters of positive corona discharges in air at DC voltage*" presented at the 17th International Conference on Environment and Electrical Engineering, Milan/Italy, June 2017 [1].

Ulrich Lühring, Daniel Wienold and Frank Jenau are with the Institute of High Voltage Engineering, TU Dortmund University, Dortmund, Germany (e-mail: ulrich.luehring@ tu-dortmund.de).

Supported by:

Federal Ministry for Economic Affairs and Energy

on the basis of a decision by the German Bundestag

This work has been funded by the German Federal Ministry for Economic Affairs and Energy (BMWi) as a part of the E²HGÜ project under grant number 03ET7514.

secondary parameters such as the coefficient of variation, the kurtosis or the skewness. A comparative analysis of these parameters, gained from PDs of idealized and artificial defects under DC voltage stress, outlines the possibility to differentiate between different types of fault [10] and defects in varying insulating media [11], [12]. Extensive experimental investigations and statistical evaluations, presented in [6], verify that the time domain analysis of PDs enables a precise defect classification. Comparative investigations of corona discharges occurring under AC and DC voltage stress point out, that the associated pulse shape parameters are not affected by the voltage waveform [13]. Based on these findings [14] demonstrates the general suitability of the time domain analysis to identify the type of fault at AC voltage as well.

The abovementioned investigations have in common that they are comprehensively realized under ambient atmosphere, which approximately corresponds to the reference atmosphere, and under a voltage stress which complies with the partial discharge inception voltage or a predefined voltage level above it. A variation of these parameters is not taken into consideration, which is just partly consistent with real operating conditions. Whereas detailed information regarding an influence of the test voltage level are outlined in [15], additional research concerning the influence of varying atmospheric parameters, such as the air pressure, the humidity level and the temperature level, on the appearance of PDs has to be carried out. Studies in relation to an influence of the gas pressure are outlined in [16] and [17]. Although detailed information from the presented measurement data are not derivable, these investigations indicate increasing discharge amplitudes and decreasing pulse widths as well as decreasing fall times if the gas pressure is raised. A consideration of a varying temperature and humidity level focuses on investigations regarding the PD intensity, the discharge inception voltage and the breakdown voltage. For example, [18] respectively [19] evince a slight decrease of the PD inception voltage and the breakdown voltage, if the temperature level is raised. Concerning a rising humidity level, a decreasing PD inception voltage and an increasing breakdown voltage is pointed out in [20] respectively [21]. This indicates a dependency between the partial discharge impulse current and the temperature level as well as the humidity level.

The purpose of this contribution is to investigate the influence of the temperature and the humidity level on the pulse shape by focusing on positive corona discharges in air. Therefore, corona discharges are generated by using a needle-to-plate set-up. The latter is part and parcel of an optimized measuring circuit. An appropriate measuring method is presented and applied to capture the pulse shape of corona discharges. To characterize the pulse shapes the rise time, the pulse width and the fall time are determined as well as the apparent charge for PDs occurring at temperature levels of 20 °C, 35 °C, 50 °C and 65 °C and for relative humidity levels of 20 %, 40 %, 60 %, 80 % and 95 %.

II. Experimental Set-Up

An accurate determination of pulse shape parameters presupposes a broadband measuring system, consisting of a measuring circuit and a measuring instrument. In [22] an overall bandwidth of at least 1 GHz is demanded to capture initial pulse shapes, which are not impaired by reflection and refraction processes. If this requirement is fulfilled, detailed information regarding the causing and influencing processes can be gained.

A. PD measuring circuit

The measurements are implemented by using a basic PD measuring circuit, which is in accordance to IEC 60270. As shown in Fig. 1, the PD measuring circuit consists of a coupling capacitor C_c, a measuring cell with a needle-to-plate set-up (DUT), a measuring impedances Z_{m1} respectively Z_{m2} and a decoupling impedance Z_d. The latter decouples the discharge current circuit from a high voltage power supply U_0, which provides a positive DC voltage with a low residual ripple. To determine the PD inception voltage an external quadripole of a PD measuring system is set as Z_{m1} in series to C_c. The pulse shapes are captured with a broadband oscilloscope, whose input resistor is set as Z_{m2} in series to the DUT.

B. Measuring Cell

A decoupling of the partial discharge impulse current from the weak point to the broadband oscilloscope devoid of distortions is enabled by using a measuring cell optimized from a high voltage and high frequency point of view. Core component of the measuring cell, whose sectional view is shown in Fig. 2, is a conical transmission line with a constant line impedance of approximately 50 Ω. The suitability of such a conical transmission line for an accurate measurement of the pulse shape is proven in [11] and [23]. In total four air inlets, which are arranged radially in the same height, ensure that the temperature and the humidity level within the measuring cell can comply with the external levels.

C. Test device

To generate corona discharges a sharp needle is attached to the cylindrical high voltage electrode. The air clearance between the ground electrode and the needle tip is set to 15 mm.

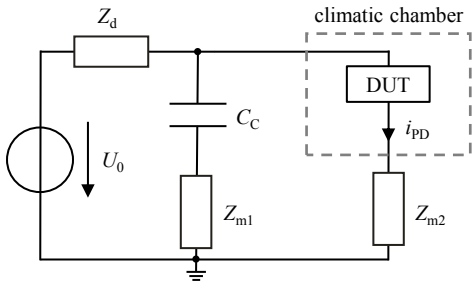

Fig. 1. PD measuring circuit according to IEC 60270 to determine the PD inception voltage and to capture the pulse shape.

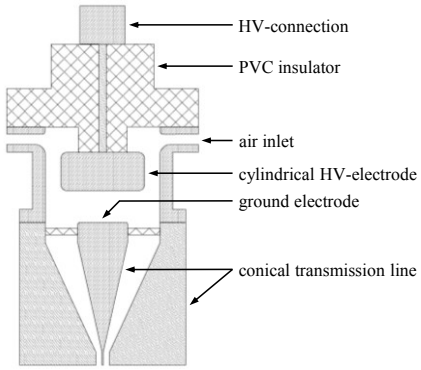

Fig. 2. Sectional view of the measuring cell optimized from a high voltage and high frequency point of view.

III. EXPERIMENTAL PROCEDURE

The influence of the temperature level and the humidity level on the pulse shape of positive corona discharges is investigated by considering different climatic conditions. As shown in in Fig. 3 13 different climatic conditions are considered, whereby the temperature level is varied in the range of 20 °C to 65 °C and the relative humidity level is varied in the range of 20 % to 95 %. A variation of these is made possible by placing the measuring cell in a climatic chamber, which is presented in [24]. The climatic chamber is characterized by a high long-term stability and an accurate regulation of the temperature and the relative humidity level.

To exclude an influence of the test voltage level, which occurs if the test voltage is raised above the inception voltage [15], all measurements are executed at the respective PD inception voltage. The latter is ascertained in advance for each climatic condition.

A. Determination of the inception voltage

Up to now, the term of the PD inception voltage under DC voltage stress is not clearly defined. In the framework of this investigation the PD inception voltage is determined by

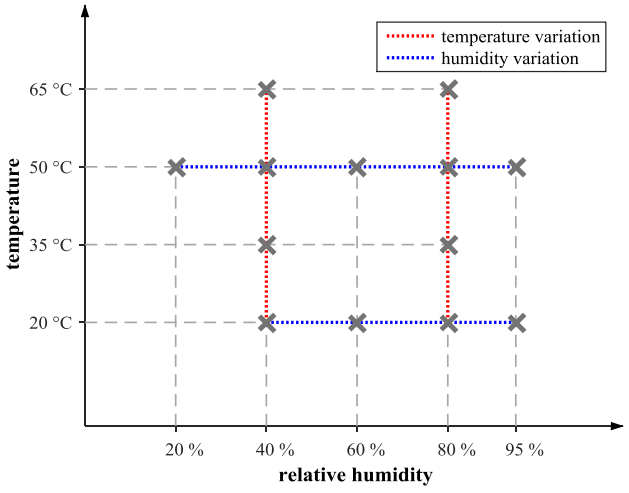

Fig. 3. Overview of the investigated climatic conditions.

increasing the test voltage in steps of 0.5 kV starting from zero. As shown in Fig. 4 the test voltage is enhanced by additional 0.5 kV, if PDs are not detected within one minute.

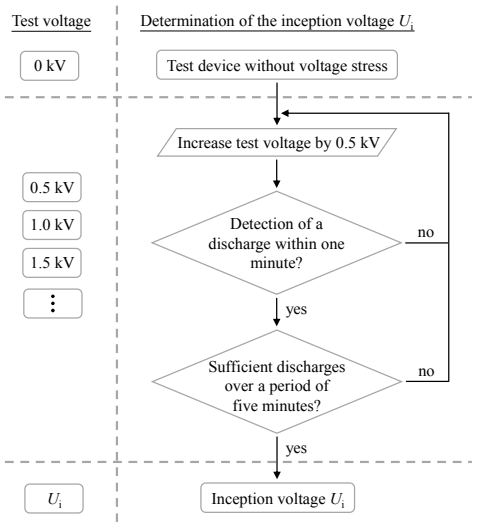

Fig. 4. Flow diagram for the determination of the PD inception voltage.

If sufficient PDs are measurable at a constant test voltage level over a period of five minutes, the PD inception voltage is assumed to be reached.

B. Capturing of the pulse shapes

The climatic conditions are successively provided by the climatic chamber, whereby special attention is paid in order to prevent the formation of condensate. In the case of a sole variation of the humidity level, an additional residence time of at least two hours is taken into consideration before performing a measurement after having reached a stationary state in the climatic chamber. If the temperature level is changed, the additional residence time is set to at least 12 hours. This ensures the desired climatic conditions within the measuring cell.

Previous investigations demonstrate that the first determinable pulse shapes reach larger amplitudes than the following [25], [26]. Due to these findings, the capturing of 100 sequent pulse shapes for each climatic condition is started after a stress duration of ten minutes. Furthermore, this ensures that the PDs are not mainly energized by the capacitive field [5].

IV. DATA ANALYSIS AND PRESENTATION

The captured pulse shapes are characterized by the determination of the rise time (20 % to 80 %), the pulse width (50 % to 50 %), the fall time (80 % to 20 %) and the apparent charge.

To present and compare the location and the distribution of the determined pulse shape parameters, box plots are used. This kind of graphic representation, which is among others shown in Fig. 5, divides the entire range of values into four subsets. The median is represented by the bar within the box, which itself contains the middle 50 % of all determined values. The boundaries of the box are the 25 % quartile and the 75 % quartile. Their distance delineates the interquartile range. Values, having a greater distance to the box than 1.5 times of the interquartile range, are designated as outliers and are characterized by a plus symbol.

V. RESULTS AND DISCUSSION

A. Appropriateness of the measurement method

The appropriateness of the experimental procedure presented in section III is evaluated by investigating selected climatic conditions more than once. To realize the different measurement series the climatic condition within the measuring cell is adjusted anew and the needle, which is attached to the high voltage electrode, is exchanged. In addition to that a long-term study is executed to examine the temporal development of the considered pulse shape parameters. In dependence on the reference atmosphere, these measurements are comprehensively carried out at a temperature level of 20 °C and an absolute humidity level of 11 g/m³.

In terms of two different measurement series, the box plots for 100 values of the determined pulse shape parameters are exemplarily shown in Fig. 5. Regarding the median the rise time evinces with approximately 10 % the largest deviation of all considered pulse shape parameters. In contrast, the deviation of the associated median values of the pulse width and the fall time are smaller than 5 % and therefore very low.

The temporal development of the pulse shape parameters, determined from the captured pulse shapes in a long-term study over a period of 360 minutes, is shown in Fig. 6. In the case of the rise time, the maximum deviation of all identified medians from that after a stress duration of ten minutes amounts to 5 %. For the pulse width and the fall time the maximum deviation is smaller than 1 %. A consideration of the illustrated temporal development clarifies that a significant decrease of the medians after a stress duration of 10 minutes is not ascertainable.

Accordingly, the presented measurement method is suited to investigate the influence of the temperature and the humidity level on pulse shape parameters with a high repeatability, if the defined stress duration is obeyed before starting the data acquisition.

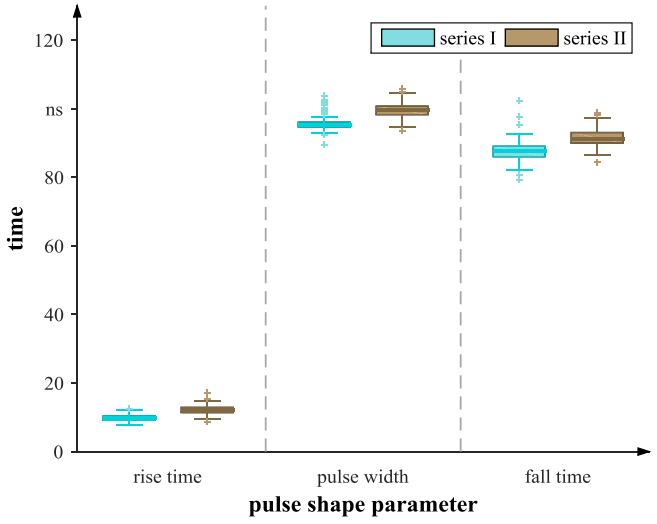

Fig. 5. Box plots for the pulse shape parameters rise time, pulse width and fall time of two different measurement series carried out at a temperature level of 20 °C and a absolute humidity level of 11 g/m³.

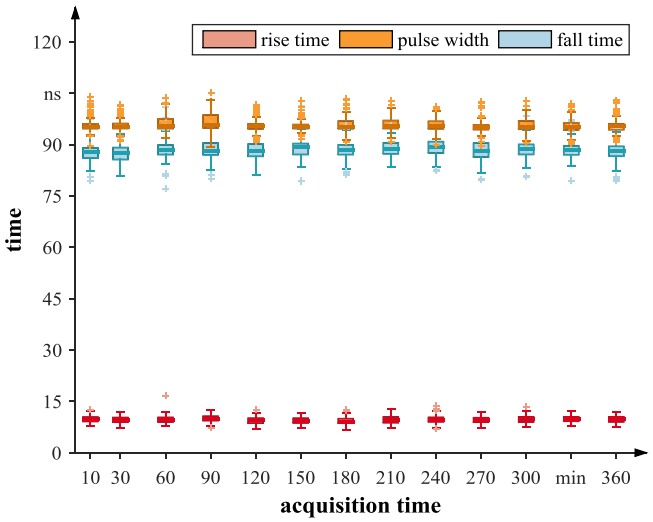

Fig. 6. Temporal development of the the pulse shape parameters rise time, pulse width and fall time as part of a long-term study carried out at a temperature level of 20 °C and an absolute humidity level of 11 g/m³.

B. Influence of the absolute humidity level

A consideration of the influence of a varying absolute humidity on the pulse shape parameters enables a simultaneous consideration of the temperature level and the relative humidity level. As stated in [27] a conversion is feasible according to equation (1).

$$AH = \frac{6.11 \cdot RH \cdot e^{\frac{17.6 \cdot T}{243+T}}}{0.4615 \cdot (273 + T)} \tag{1}$$

AH: absolute humidity level in g/m³
RH: relative humidity level in percent
T: temperature level of ambient air in °C

Fig. 7 exemplarily shows the medians for the pulse width and the fall time in dependence on the absolute humidity. It should be noted that the fundamental curve progression is identical for all considered temperature levels. This indicates that the absolute humidity level is the decisive influencing factor, whereby an additional influence of the temperature level on the pulse shape parameters cannot be excluded.

C. Influence of the temperature level

In Fig. 8 the box plots for 100 values of the determined pulse shape parameters rise time, pulse width and fall time are depicted as well as those for the apparent charge for positive corona discharges occurring at a varying temperature level. It is shown, that a variation of the temperature level affects the pulse shape for both considered relative humidity levels. All determined pulse shape parameters decrease with an increasing temperature level. This is particularly apparent in the case of the fall time and the pulse width. Focusing on the latter and on the measurements at a relative humidity level of 40 %, the median for a temperature level of 20 °C is in the range of 130 ns whereas the median for a temperature level of 65 °C is in the range of 22 ns. This corresponds to a reduction of almost one sixth.

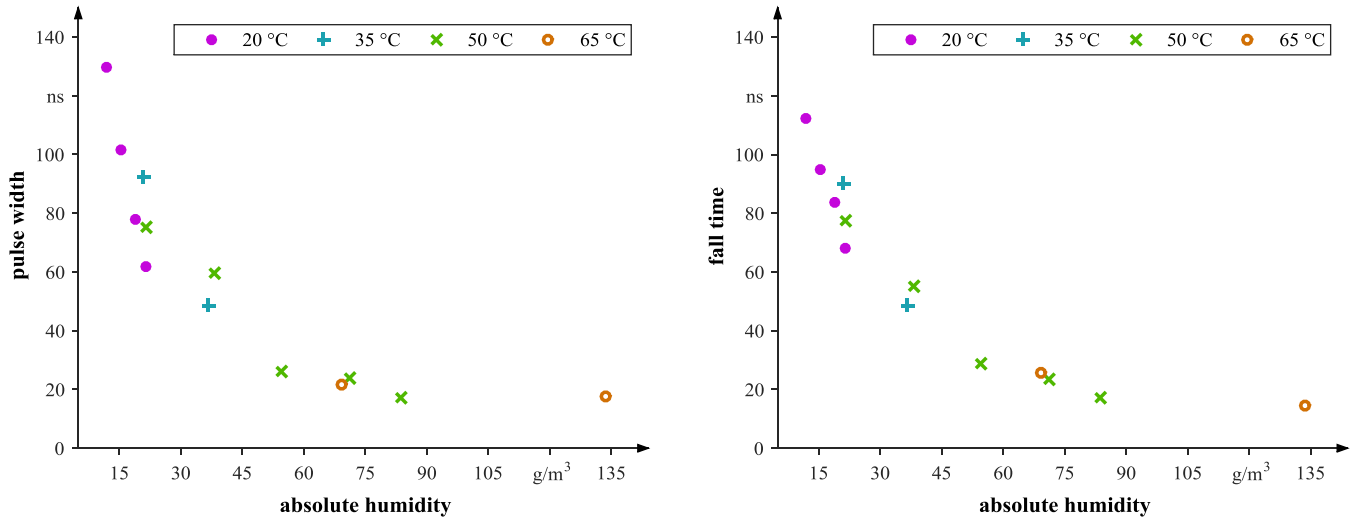

Fig. 7. Medians of the pulse width (left) and the fall time (right) for positive corona discharges in dependence of the absolute humdity.

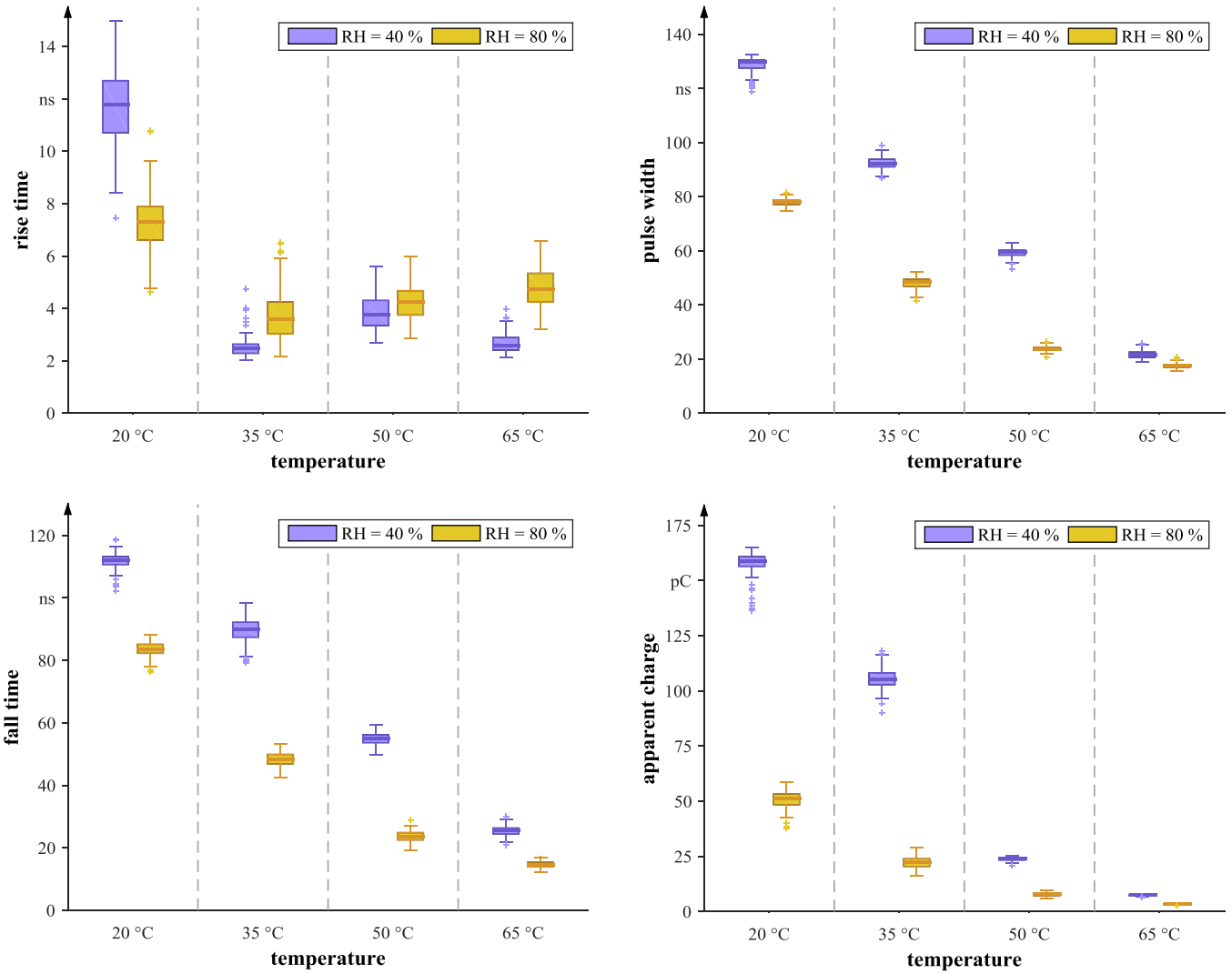

Fig. 8. Box plots for the pulse shape parameters rise time (top left), pulse width (top right), fall time (bottom left) and the apparent charge (bottom right) of positive corona discharges occuring under a varying temperature level for relative humidity levels of 40 % and 80 %.

D. Influence of the relative humidity level

The box plots for the determined values concerning an influence of the relative humidity level are illustrated in Fig. 9. The distribution and the location of the 100 gained values for the rise time, the pulse width, the fall time and the apparent charge clarifies that the pulse shape is affected by a varying relative humidity level. With the exception of the rise time, all considered parameters decrease with an increasing relative humidity level. In relation to the pulse shape parameters this is particularly apparent in the case of the pulse width and the fall time. Focusing on the fall time and on the measurements at 50 °C, the median for a relative humidity level of 20 % is in the range of 77 ns whereas the median for a relative humidity level of 95 % is in the range of 17 ns. This corresponds to a reduction of almost one fifth. Besides the fundamental influence of the relative humidity level on the pulse shape parameters, the box plots, illustrated in Fig. 9, suggest a linear dependency between the location of the pulse shape parameters and the relative humidity level for the measurements at 20 °C. For the measurements at 50 °C the change in value suspects a non-linear relationship. This indicates that the relative humidity level is not the decisive influencing factor.

E. Reconciliation with physical processes

Independent of the considered climatic condition, the captured pulse shapes are characterized by a steep ascent and a slower descent. Relating to [28] this fundamental curve progression is directly traceable to involved physical processes. The needle-to-plate setup generates a strongly inhomogeneous electric field. Prerequisite for the development of a partial discharge process is the availability of a free electron in the area of the highest electric field strength. In the current case of a needle, appearing as positive high voltage electrode, the free electron is accelerated into the area of increasing field strength. This is associated with an energy absorption. Collisions with gas molecules lead to the emergence of secondary electrons and positive ions if the ionization energy is reached. A continued existence of the necessary ionization condition results in an avalanche effect, which causes the steep ascent of the pulse shape. An increase

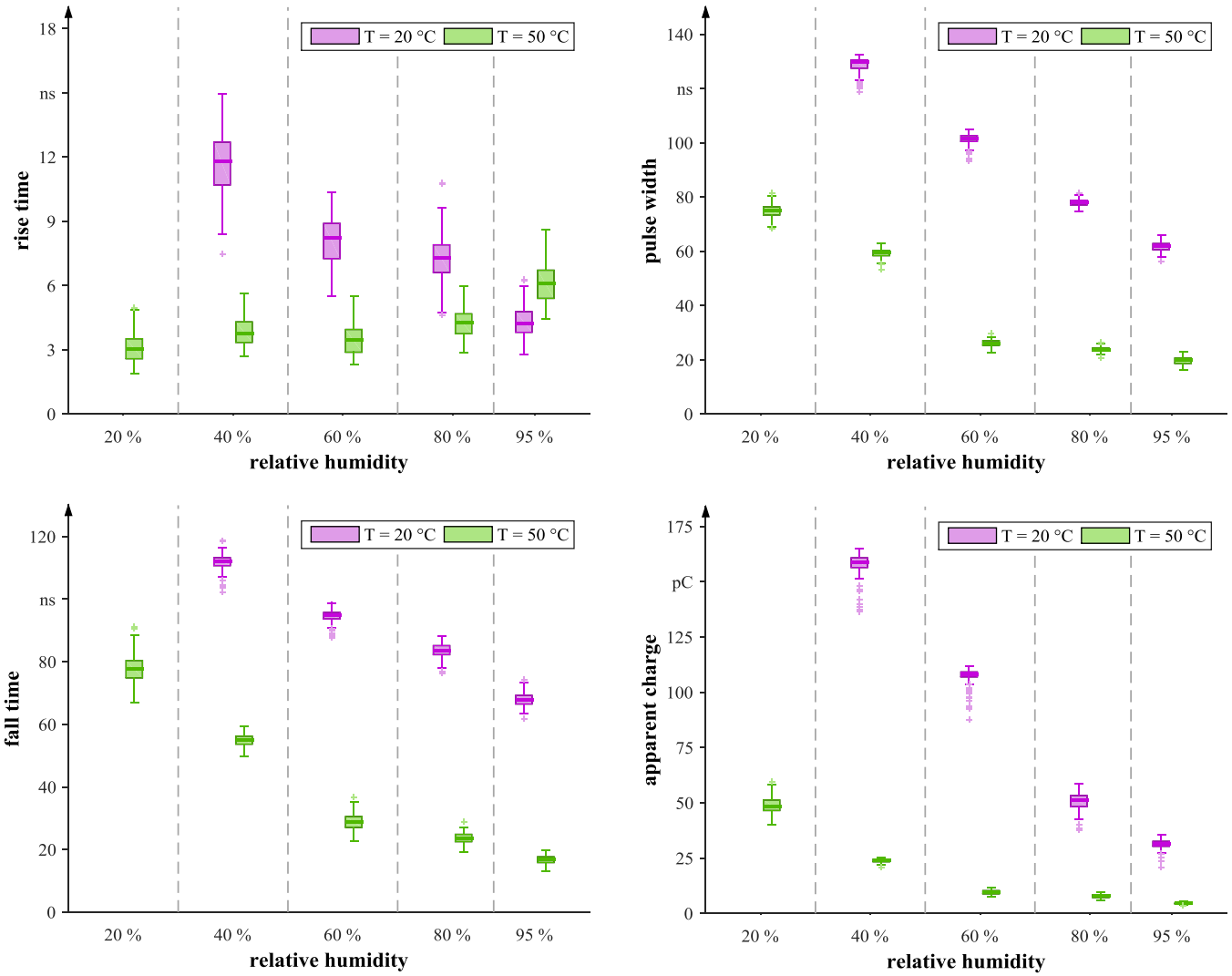

Fig. 9. Box plots for the pulse shape parameters rise time (top left), pulse width (top right), fall time (bottom left) and the apparent charge (bottom right) of positive corona discharges occuring under a varying relative humidity level for temperature levels of 20 °C and 50 °C.

of the mean free path, e.g. by reducing the air density as a result of a rising temperature level, favors this effect. Whereas the electrons move very rapidly towards the needle tip and are accepted by the anode or attached to molecules with a high electron affinity, the positive ions form a positive space charge. Because of the low mobility of the positive ions, the space charge drifts very slowly in the direction of the cathode. This entails a reduction of the effective field strength near the needle tip, which hampers the ionization process, favors the attachment process and leads to a decreasing discharge current. Therefore, the characteristic of the pulse shape is significantly dependent on the ionization and the attachment coefficient

Experimental tests prove that a surge of the humidity level goes along with an increasing attachment coefficient [29] and an increasing ionization coefficient [30]. The same applies to a rise of the temperature level [31]. This knowledge is already utilized to explain the impact of the temperature and the humidity level on the breakdown voltage and the PD inception voltage. Coupled with the fact that the mean free path is magnified, which favors relevant collision processes, a declaration of the ascertained influence of a varying temperature and humidity level on the pulse shape parameters is enabled.

Considering the temporal progression of the PD process described above, an increasing ionization coefficient results in a steeper ascent of the pulse shape and a decreasing rise time. Apart from a growing number of free electrons, the hampering positive space charge is build up in a shorter time span. This is accompanied by a reduction of the pulse width and the amplitude. The minimization of the effective field strength near the anode enhances the possibility of attachment processes. These are favored by an upward attachment coefficient, which results in a decreasing fall time. Consequently, the apparent charge decreases as well, if all abovementioned parameters decline.

VI. Conclusions

To obtain detailed information regarding the influence of the temperature and the humidity level, the pulse shapes of corona discharges are captured for 13 different climatic conditions. By performing a long-term study and carrying out investigations at one climatic condition more than once, it is proven that the proposed measuring method is suited to investigate the influence of the temperature and the humidity level. Regarding the latter, a determination of the pulse shape parameters results in comparable values, so that a high repeatability is achieved. This applies also if the needle, which emulates corona discharges, is substituted. A comparative analysis of pulse shape parameters, gained from measurements at different climatic conditions, illustrates that an increasing temperature level at a constant relative humidity level as well as an increasing humidity level results in decreasing pulse shape parameters. Therefore, the interpretation of PD impulses requires a consideration of the climatic condition. The dependency can be reconciled with the reliance of the ionization coefficient and the attachment coefficient on the varying atmospheric parameter. Regarding the influence of the humidity level it is assumed that the absolute humidity is the decisive influencing factor. To verify this assumption, it is recommended to carry out supplementary investigations. This should entail an investigation of a varying temperature level at a constant absolute humidity.

References

[1] U. Lühring, D. Wienold and F. Jenau, “Influence of humidity on pulse shape parameters of positive corona discharges in air at DC voltage”, 17th International Conference on Environment and Electrical Engineering, Milan/Italy, June 2017.

[2] IEC 60270:2000, “High-voltage test techniques – Partial discharge measurement (IEC 60270:2000); German version EN 60270:2001”, DIN Deutsches Institut für Normung e.V. und VDE Verband der Elektrotechnik Elektronik Informationstechnik e.V., Berlin, 2001.

[3] D. König and Y. N. Rao, “Partial discharges in electrical power apparatus”, Berlin: VDE-Verlag, 1993.

[4] R. S. Bever and J. L. Westrom, “Partial Discharge Testing Under Direct Voltage Conditions”, IEEE Transactions on Aerospace and Electronic Systems, Vol. AES-18, No. 1, January 1982.

[5] U. Fromm, “Interpretation of Partial Discharges at dc Voltages”, IEEE Transactions on Dielectrics and Electrical Insulation, Vol. 2, No. 5, October 1995.

[6] T. Vogt, “Teilentladungsdiagnose bei Gleichspannung”, Dissertation Technische Universität Dortmund, 2015.

[7] D. Wienold, U. Lühring and F. Jenau, “Detection and distinction of partial discharges in air at DC voltage by using a non-conventional approach in the high-frequency range“, 17th International Conference on Environment and Electrical Engineering, Milan/Italy, June 2017.

[8] D. Wienold, U. Lühring and F. Jenau, “Data analysis and verification for DC PD measurements in the high frequency range”, 2nd IEEE International Conference on Dielectrics, Budapest/Hungary, 2018, in press.

[9] T. Mutakamihigashi, R. Sakurai, S. Okada and H. Ueno, “Relationship between electric field strength and characteristic frequency in partial discharge”, 18th International Symposium on High Voltage Engineering, Seoul/Korea, August 2013.

[10] T. Klueter, J. Wulff, F. Jenau and D. Wienold, “Evaluation of Surface- and Corona Discharges at DC Voltage”, 13th International Conference on Environment and Electrical Engineering, Wroclaw/Poland, November 2013.

[11] T. Klueter, J. Wulff and F. Jenau, “Time Domain Analysis of Partial Discharges at DC Voltage in Air and Insulation Oil”, 12th International Conference on Environment and Electrical Engineering, Wroclaw/Poland, May 2013.

[12] T. Klueter, J. Wulff and F. Jenau, “Measurement and Statistical Analysis of Partial Discharges at DC Voltage”, 48th International Universities´ Power Engineering Conference UPEC 2013, Dublin/Ireland, September 2013.

[13] U. Lühring, D. Wienold and F. Jenau, “Comparative investigation on pule shape parameters of partial discharges in air under AC and DC voltage stress”, 51st International Universities´ Power Engineering Conference UPEC 2016, Coimbra/Portugal, September 2016.

[14] U. Lühring, D. Wienold and F. Jenau, “Investigation on the Applicability of the Time Domain Analysis of Discharges in Gases for the Defect Identification at AC Voltage”, Transactions on Environment and Electrical Engineering, Vol. 2, No. 1, January 2017.

[15] U. Lühring, D. Wienold and F. Jenau, “Investigation on the pulse shape of DC corona discharges in air under varying test voltage level”, 2nd IEEE International Conference on Dielectrics, Budapest/Hungary, July 2018, in press.

[16] D. A. Scott and G. N. Haddad, “Negative point-to-plane corona pulses in oxygen”, Journal of Physics D: Applied Physics 19, January 1986.

[17] X. Liu, D. G. Kasten and S. A. Sebo, “Partial Discharge Measurements for a Twisted Pair of Insulated Conductors at Low Pressures in Air, Argon and Helium“, IEEE International Symposium on Electrical Insulation, June 2006.

[18] M. Abdel-Salam and N. L. Allen, “Current-voltage characteristics of corona in rod-plane gaps as influenced by temperature”, IEE Proceedings – Science, Measurement and Technology, Vol. 150, No 3, May 2003.

[19] N. L. Allen, M. Abdel-Salam and I. Cotton, “Effects of temperature and pressure change on positive corona and sparkover under direct voltage in short airgaps”, IET Science, Measurement & Technology, Vol. 1, No. 4, July 2007.
[20] X. Bian, L. Wang, J. M. K. MacAlpine and Z. Guan, “Positive Corona Inception Voltages and Corona Currents for Air at Various Pressures and Humidities”, IEEE Transaction on Dielectrics and Electrical Insulation, Vol. 17, No. 1, February 2010.
[21] E. Kuffel, “Influence of humidity on the breakdown voltage of sphere-gaps and uniform-field gaps”, Proceedings of the IEE, Paper 3322M, February 1961.
[22] P. Morshuis, “Assessment of dielectric degradation by ultrawide-band PD detection”, IEEE Transactions on Dielectrics and Electrical Insulation, Vol. 2, No. 5, October 1995.
[23] M. Kurrat and D. Peier, “Wideband measurement of partial discharges for fundamental diagnostics”, 7th International Symposium on High Voltage Engineering, Dresden/Germany, August 1991.
[24] R. Schmerling, M. Freiburg, F. Jenau, T. Weissgerber and F. Pohlmann, „Development and application of a climate chamber for testing large dimensioned high voltage components up to 100 kV”, 18th International Symposium on High Voltage Engineering, Seoul/Korea, August 2013.
[25] H. Okubo and N. Hayakawa, “A novel technique for partial discharge and breakdown investigation based on current pulse waveform analysis”, IEEE Transactions on Dielectrics and Electrical Insulation, Vol. 12, No. 4, August 2005.
[26] K. Nanao, Y. Murakami and M. Nagao, “Analysis of Internal Partial Discharge Based on PD Current Waveform”, Annual Report: Conference on Electrical Insulation and Dielectric Phenomena, October 2008.
[27] IEC 60060-1:2010, “High-voltage test techniques – Part 1: General definitions and test requirements (IEC 60060-1:2010); German version EN 60060-1:2010”, DIN Deutsches Institut für Normung e.V. und VDE Verband der Elektrotechnik Elektronik Informationstechnik e.V., Berlin, 2011.
[28] L. B. Loeb, “Electrical coronas – Their basic physical mechanism”, Berkeley and Los Angeles: University of California Press, 1965.
[29] E. Kuffel, “Electron Attachment Coefficients in Oxygen, Dry Air, Humid Air and Water Vapour”, Proceedings of the Physical Society, Vol. 74, No. 3, April 1959.
[30] W. Bauke, “Über den Einfluß des Wasserdampfgehaltes der Luft auf den elektrischen Durchschlag im inhomogenen Feld bei Wechselspannung”, Dissertation Technische Universität Berlin, 1968.
[31] W. S. Zaengl, S. Yimvuthikul and G. Friedrich, “The Temperature Dependence of Homogeneous Field Breakdown in Synthetic Air”, IEEE Transactions on Electrical Insulation, Vol. 26, No. 3, June 1991.

Theoretical analysis of the efficiency of a V2G wireless charger for Electric Vehicles

Alicia Triviño, Jose M. Gonzalez-Gonzalez, and Jose A. Aguado

***Abstract*—V2G (Vehicle-to-grid) technology will report important benefits for the operation and safety of the grid. In order to facilitate the expansion of the V2G technology in a future, it is recommended to offer the drivers with easy to use methods to charge and discharge their EV batteries. In this sense, wireless chargers are expected to play a relevant role in the future electrical networks as it reduces the users' intervention. The development of this kind of system is still open to improve them in terms of their operation, their compliance and their control. An important issue for the evaluation of these systems is the efficiency, which measures the power losses occurring in the system. This paper addresses a deep study about the losses in a bidirectional wireless charger. Then, it provides with a mathematical model to characterize them. This model is validated by means of experimental results conducted in a 3.7-kW prototype.**

***Index Terms*—V2G, wireless charge, wireless discharge, losses, efficiency, electric vehicle, inductively-coupled power system, ICPT, bidirectional.**

I. Introduction

ELECTRIC vehicles (EV) represent a clear eco-friendly mobility solution. Firstly, it is able reduce CO2 emissions [1–3]. On the other hand, it also helps for the integration of renewable energy sources [3, 4]. Despite these potential benefits, the proliferation of electric vehicles must be carefully controlled as a big number of them stands out for a considerable aggregated load to the grid. Market-driven solutions [5] aims at prompting the charge of the vehicles in those times when it is more convenient for the grid, avoiding the periods with a high demand too [6].

In a V2G context, the vehicles operate in an active discharge mode that needs to be also controlled [6]. Specifically, when recommended, the vehicles could decide to deliver energy to the grid from their batteries. If correctly coordinated, this operation leads to important advantages for the grid.

In order to promote the controlled charge and discharge modes and to obtain important advantages, it is highly recommended to reduce the user's intervention. This can be achieved with wireless chargers for Electric Vehicles (EV) [7].

Wireless power transfer technology can be realized by different techniques. By now, the most popular one is the one based on a pair of loosely coupled coils operating under resonant conditions. This is known as Inductively Coupled Power Transfer or ICPT [7]. In this technique, one coil is placed in the pavement (named the primary side) and the other in the chassis (known as the pickup or secondary side). The current through the primary coil induces a voltage in the secondary coil, which is used to charge the battery. The magnetic field involved in this charger is ranged in the 20 kHz - 100 kHz interval [8]. To generate this high-frequency sinusoidal current, power converters need to be included in the charger.

The non-idealities of the switches of the power converters and the parasitic resistances of the reactive components are responsible for the losses in the whole system, which degrades the charger efficiency. This paper addresses the proposal and verification of a model to characterize the efficiency of a bidirectional wireless charger. The main contribution of our work are the following ones:

- In contrast to [9, 10], our work is focused on a bidirectional wireless charger operating at 85 kHz and 3.7 kW. The change in the frequency and on the power requires the use of specific semiconductors. In particular, SiC MOSFETs are used [11, 12]. The particularities of these devices need to be considered for the model as they clearly affect in the losses of the system and in the efficiency.
- It extends the work in [13] by focusing on the efficiency and adding a comprehensive analysis of the experimental results, which is the basis for the computation of this parameter in a prototype.

The rest of the paper is structured as follows. Section II reviews some related works about the study of losses in wireless chargers basing on ICPT technology. Section III presents the ICPT wireless charger topology used in this work. The theoretical model to compute the efficiency and the losses is presented in Section IV. Section V evaluates the methods basing on the real measurements performed in a 3.7-kW prototype. Finally, Section VI describes the main conclusions of this work.

II. Related work

The losses of an EV wireless charger are mainly due to the semiconductors employed in the power converters and the parasitic resistance of the real reactive elements.

Ideal semiconductors in the power converters are operated in such a way that no losses result. However, the real behavior leads to conductive and switching losses for these elements. Conductive losses are produced because of the difference of the element from an ideal switch. To understand the losses by this event, we can rely on semiconductors models, which represent the device as an equivalent circuit with parasitic components such as resistances or capacitors. Conductive

A. Triviño, J. M. Gonzalez-Gonzalez and J. A. Aguado are with the Electrical Engineering Department, Universidad de Málaga, Málaga, Spain (e-mail: atc@uma.es).

losses occur because of the resistances. When the current flows through the resistances, losses occur. On the other hand, the capacitors prevents the semiconductors from having instantaneous commutations, which implies switching losses.

As for the reactive components, the conductive losses are due to the resistance offered by the cables on which they are built. An equivalent model for these elements adds a series resistance to the reactive component. It is known as the ESR (Equivalent Series Resistance) and its value greatly depends on the material of the reactive components. For instance, Litz wire minimizes the skin effect and, in turn, the ESR [14].

The work in [9] makes a deep theoretical study about the switching losses of a wireless charger. The impact of them depends on the fact whether they are hard or soft. A similar study but in a low-power application is proposed in [10]. The prototype under evaluation uses a different power transfer technique working at 6.78 MHz and transferring 2 W.

The work in [15] presents the model for the computation of the switching losses for MOSFET in a unidirectional wireless charger. However, they do not rely on the equivalent model and they employ the parameters observed in the experimental results to derive this type of loss. The use of the parasitic capacitors, as we do in the present work, eases the estimation of the losses before the prototype is built.

Our present work uses the model presented in [9] to derive the efficiency of an EV bidirectional wireless charger. It represents an extension to the study presented in [13] as it makes a deep analysis of the experimental results.

III. ICPT WIRELESS CHARGER FOR EV

In this work, we will focus on ICPT technology for charging and discharging the battery of an EV. The generic scheme of a unidirectional wireless charger is represented in Figure 1.

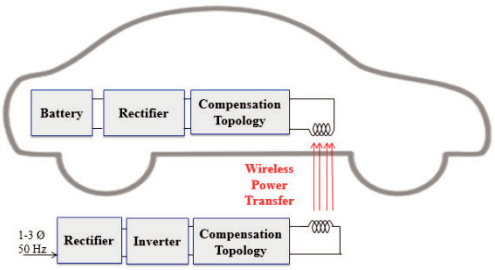

Fig. 1. Structure of a unidirectional wireless charger.

The charger is connected to the grid, whose alternating current has a frequency of 50 Hz or 60 Hz depending on the region. Nevertheless, these frequency values are not enough to transfer power inductively. Consequently, it is necessary to convert this current to high frequency current, using power electronics for that. Firstly, the alternating current is converted to direct current using a rectifier. Both single-phase and three-phase rectifiers can be used. Despite its higher cost, the three phase rectifier has some advantages as for example lower losses, lower ripple factor and higher transformer utilization factor. The direct current is necessary to obtain high frequency current using an inverter. The generated high frequency current flows through the primary coil, creating a magnetic field which mainly depends on the coil structures. The magnetic field created by the primary coil induces an alternating voltage in the secondary coil, which is rectified again to provide Direct Current, which is appropriate for the battery. Additionally, a compensation system composed of capacitors is introduced on both sides to enable the operation under resonant conditions.

When implementing a bidirectional wireless charger, the power flow must be also allowed from the battery to the grid. As a consequence, the power converters should have a dual behavior to cope with the two senses of the power flows. This modification can be observed in Figure 2.

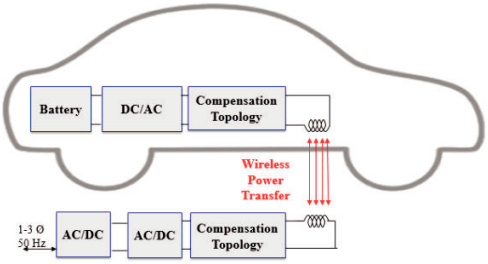

Fig. 2. Structure of a bidirectional wireless charger.

In order to allow the power flow in both senses, the primary inverter has to be capable to work also as a rectifier, while the rectifiers have to perform the functions of an inverter. This issue is solved using bidirectional AC/DC converters. As in the unidirectional wireless charger, the connection to the grid can be done through both a single-phase and three-phase converter. The three-phase converter has benefits to the single-phase converter because using three phases allows to convert the same power with less current per phase, thereby reducing the losses on the components of the converter.

IV. THEORETICAL MODEL FOR THE EFFICIENCY

The efficiency (η) of a wireless charger measures the relationship between the real power delivered to the load (P_{load}) and the real power generated by the source (P_{source}). So that:

$$\eta = \frac{P_{load}}{P_{source}} \tag{1}$$

At resonant operation and with ideal components, all the power generated by the source is delivered to the battery, that is η equals 1. However, due to conduction and switching losses (L_{cond} and L_{sw} respectively), this parameter decreases as follows:

$$\eta = \frac{P_{source} - L_{cond} - L_{sw}}{P_{source}} \tag{2}$$

where the calculation of L_{cond} and L_{sw} is presented in the following subsection.

Despite having similar structures in both sides, wireless chargers can use different components in the primary and the secondary sides. One important component of the charger

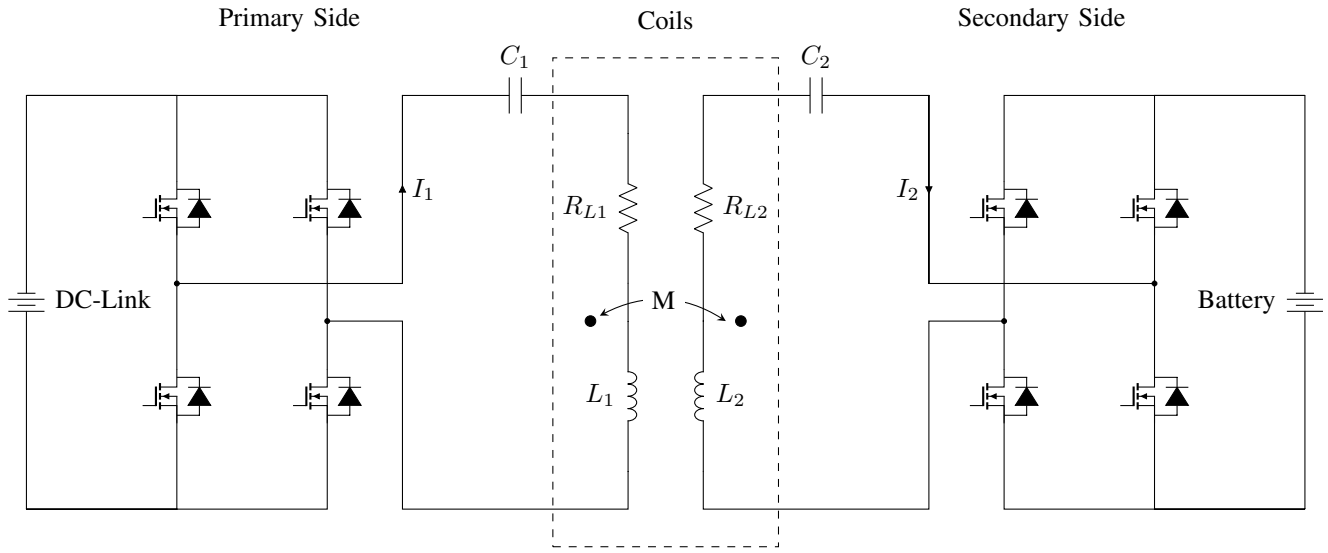

Fig. 3. Topology of the analyzed bidirectional wireless charger.

which can differ are the coils because having a bigger coil on the primary side can help with misalignments. Different coils also require different compensation systems. Due to this asymmetrical structure of the bidirectional wireless charger, it is necessary to define two efficiencies, one for each sense of the power flow. Thus, we have η^{ch} to characterize the power flow from the grid to the battery and η^{dis} to define the charger performance in the opposite sense. We can reformulate Eq. 2 as:

$$\eta^{ch} = \frac{P_{grid} - L^{ch}_{cond} - L^{ch}_{sw}}{P_{grid}} \tag{3}$$

and

$$\eta^{dis} = \frac{P_{grid} - L^{dis}_{cond} - L^{dis}_{switch}}{P_{grid}} \tag{4}$$

where P_{grid} represents the real power generated by the grid and P_{bat} is the real power delivered by the EV battery.

In the next subsections, we formulate the equations to estimate both efficiencies for the bidirectional wireless charger topology presented in Fig. 3.

A. Charge mode

In this operation mode, the DC/AC power converter in the primary side acts an inverter whereas the AC/DC power converter in the pickup is a rectifier. The conduction losses are:

$$L^{ch}_{cond} = L^{ch}_{con,inv} + L^{ch}_{con,rec} + L^{ch}_{coils} + L^{ch}_{match} \tag{5}$$

where $L^{ch}_{con,inv}$ are the conductions losses of the inverter, $L^{ch}_{con,rec}$ are the conductions losses of the rectifier, L^{ch}_{coils} are the losses in the coils and L^{ch}_{match} are the losses in the compensation system. The superscript ch indicates that these values correspond to the charging mode.

In order to simplify the control, a full-bridge topology with a phase-shift control of a duty cycle equal to 50% is employed. In this scheme, there is only one transistor in each leg in conduction. Thus, the conduction losses of the inverter are:

$$L^{ch}_{con,inv} = 2 \cdot R_{ds} \cdot \widehat{I}_1^2 \tag{6}$$

being $\widehat{I}_1$ the rms (root-mean squared) current in the primary side and R_ds the internal resistance drain-source of the MOSFET in the inverter.

For the conduction losses of the rectifier, we also rely on the equivalent model of the diodes. In a full-bridge rectifier, two diodes are simultaneously conducting, both of them provoking some losses as:

$$L^{ch}_{con,rec} = 2 \cdot R_d \cdot \widehat{I}_{rec}^2 + 2 \cdot V_{th} \cdot \widehat{I}_{rec} \tag{7}$$

where R_d represents the internal resistance of the diodes, V_th their forward voltage and $\widehat{I}_{rec}$ the rms value of the current traversing these elements. In a series-series compensation topology as we are using in this work, I_rec equals I_2, that is, the secondary current.

The coils and the matching networks also incur in conduction losses to the system due to their parasitic resistances. Specifically, the losses of the coils are estimated as:

$$L_{coils} = R_{L1} \cdot \widehat{I}_1^2 + R_{L2} \cdot \widehat{I}_2^2 \tag{8}$$

where R_{L1} and R_{L2} are the resistances associated to the primary and secondary coil respectively.

The currents injected to the coils are the same as those in the capacitors as a series-series compensation network is used. Thus, the conduction losses in the matching networks are:

$$L_{match} = R_{C1} \cdot \widehat{I}_1^2 + R_{C2} \cdot \widehat{I}_2^2 \tag{9}$$

where R_{C1} and R_{C2} are the resistances associated to the primary and secondary capacitors respectively

Concerning the switching losses, they are due to the inverter. Theoretically, these losses can be estimated by the addition of multiple terms, being the one due to the output capacitance (C_{oss}) the most relevant (L_{Coss}). Thus, we simplify as:

$$L_{sw}^{ch} \cong L_{Coss} = \frac{1}{2} f_s C_{oss} V_{ds}^2 \tag{10}$$

being f_s the switching frequency and V_{ds} the voltage between the drain and the source.

B. Discharge mode

In the discharge mode, the power flow from the battery to the grid. Making use of the dual behavior of the power converters, in this operation mode, the power converter attached to the battery acts as an inverter while the power converter in the primary side works as a rectifier.

In this way, the conduction losses can be expressed as:

$$L_{cond}^{dis} = L_{con,inv}^{dis} + L_{con,rec}^{dis} + L_{coils}^{dis} + L_{match}^{dis} \tag{11}$$

where the superscript ch indicates these values correspond to the discharging mode.

Although the conduction losses of the coils (L_{coils}) and the compensation system (L_{match}) can be calculated following the same equations of the charging mode (Eq. 8 and 9), the conduction losses of the inverter and the rectifier differ in the current values because in this mode they are working on the secondary and the primary side respectively. Theses losses can be computed as:

$$L_{con,inv}^{dis} = 2 \cdot R_{ds} \cdot \widehat{I_2^2} \tag{12}$$

$$L_{con,rec}^{dis} = 2 \cdot R_d \cdot \widehat{I_1^2} + 2 \cdot V_{th} \cdot \widehat{I_1} \tag{13}$$

Finally, the switching losses are estimated following the same equation of the charging mode (Eq. 10).

V. Validation of the model: experimental results

The developed theoretical model is verified with a 3.7-kW bidirectional prototype based on ICPT technology. The coils are both square but with different sizes. The compensation networks are uniresonant and in series with the coils. As for the magnetic field, it is generated at 85 kHz as recommended by SAE TIR J2954 [16]. CREE C2M0080120D SiC MOSFETs are the components of the power converters as they support the power demanded and the switching frequency. The main properties of the charger, including the values related to the non-idealities of the components, are summarized in Table I.

Firstly, we derive the theoretical results for the losses and the efficiencies considering the model presented in the previous Section. These results are exposed in Table II.

The resistance of the coils has the highest impact in the efficiency of the system. The rest of the components of the system have similar losses with the exception of the switching losses of the inverter which, thanks to the use of SiC MOSFETs, are negligible. Due to security reasons with the operation of the battery, the power transferred in the discharge mode has been reduced.

TABLE I
Parameters of the ICPT system.

Charger specifications		**TX-RX parameters (prototype values)**	
Output	3.7 kW 300V	$L_1[mH]$	240.5
fs $[kHz]$	85	$L_2[mH]$	230.6
Coils geometry		$C_1[nF]$	14.3
Primary coil $[m^2]$	0.75 x 0.75	$C_2[nF]$	15.6
Secondary coil $[m^2]$	0.5 x 0.5	$R_{L_1}[m\Omega]$	196
C2M0080120D MOSFET		$R_{L_2}[m\Omega]$	143
$R_d[m\Omega]$	40	$R_{C_1}[m\Omega]$	67
$V_{th}[V]$	0.98	$R_{C_2}[m\Omega]$	52
$C_{oss}[pF]$	80	$M[mH]$	54.5
$R_{ds}[m\Omega]$	80	$k = M(L_1L_2)^{1/2}$	0.231

TABLE II
Computed losses.

Charge mode		**Discharge mode**	
$L_{con,inv}[W]$	25	$L_{con,inv}[W]$	3.3
$L_{sw,inv}[W]$	1	$L_{sw,inv}[W]$	1
$L_{con,rec}[W]$	34	$L_{con,rec}[W]$	15
$L_{coils}[W]$	64	$L_{coils}[W]$	11
$L_{match}[W]$	23	$L_{match}[W]$	4

To validate the computed results, the losses are also carried out by obtaining the real power which flows for each component of the system. To get these values is necessary to analyze the oscilloscope captures both at the input and at the output of the components, with which the current and voltage are taken into account. Figure 4 shows an oscilloscope capture of the current and the voltage measure at the output of the primary DC/AC converter in charge mode. As can be observed, voltage measurement consists on a square signal which can be used to computed the real power assuming a fundamental harmonic approximation. The difference between input and output real power of each component corresponds to the losses.

The measurements of the electrical signals in the prototype leads to the values exposed in Table III.

The following subsections presents the calculation methods to obtain the results from the experimental measurements. Using these equations and the measures of Table III, the prototype losses has been computed to validate the model. These losses are shown in Table IV.

As can be observed, the use of the model based on the nonidealities leads to higher losses estimation in comparison with those derived from the analysis of the waveforms. In particular, for the charge mode, the inverter is assumed to loss 26 W whereas the waveform analysis states that these losses

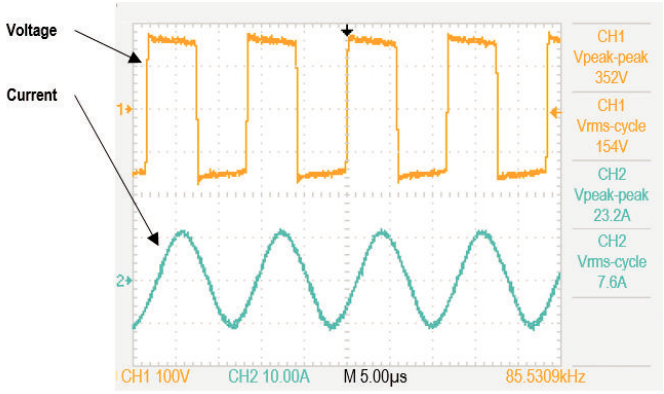

Fig. 4. Voltage (channel 1) and current (channel 2) measurements at the output of the primary DC/AC converter.

TABLE III
ELECTRICAL SIGNALS MEASURED IN THE PROTOTYPE.

Electrical signals	Charge mode	Discharge mode
$V_{inv_{input}}[V]$	288	298
$V_{inv_{output}}[V]$	290	293
$I_{inv_{input}}[A]$	12.56	4.56
$V_{inv_{input}}[A]$	13.78	5.14
$V_{rec_{input}}[V]$	285	247
$V_{rec_{output}}[V]$	288	250
$I_{rec_{input}}[A]$	13.74	6.02
$I_{rec_{output}}[A]$	12.16	5.30

are 20 W. Concerning the rectifier operation, this difference is 11 W. For the discharge mode, there are also some deviations. Specifically, the difference in the inverter is 1.3 W whereas the rectifier is associated to a deviation equals to 1 W. Taking into account the total values, the differences are significant. This is due to the errors in the measurements, which impact on both the waveform analysis and on the model based on the nonidealities.

A. Charge mode

Concerning the output of the primary inverter, the voltage is a square-wave of $V_{inv_{output}}$ amplitude while the current is in-phase and sinusoidal (with a peak value equals to $I_{inv_{output}}$). The shape and phase of the output current is the consequence of forcing the system to operate under resonant conditions. For the active power, we must extract the peak value of the fundamental harmonic of the voltage signal ($V^1_{inv_{output}}$) and operate as follows:

$$P^{ch}_{inv_{output}} = \frac{V^1_{inv_{output}} \cdot I_{inv_{output}}}{2} = \frac{4 \cdot V_{inv_{output}} \cdot I_{inv_{output}}}{\pi \cdot \sqrt{2}} \tag{14}$$

Thus, the losses in the primary inverter (L^{ch}_{inv}) are:

$$L^{ch}_{inv} = P^{ch}_{inv_{input}} - P^{ch}_{inv_{output}} \tag{15}$$

TABLE IV
LOSSES COMPUTED FROM THE ELECTRICAL SIGNALS MEASURED IN THE PROTOTYPE.

Charge mode		Discharge mode	
$L^{ch}_{inv}[W]$	20	$L^{dis}_{inv}[W]$	3
$L_{coils} + L_{match}[W]$	73	$L_{coils} + L_{match}[W]$	17
$L^{ch}_{rec}[W]$	23	$L^{dis}_{rec}[W]$	14

The rectifier input consists of a square-wave voltage (with a peak value of $V_{rec_{input}}$) and a sinusoidal current wave with a peak value equal to $I_{rec_{input}}$. Applying the decomposition of harmonics, we can state that:

$$P^{ch}_{rec_{input}} = \frac{4 \cdot V_{rec_{input}} \cdot I_{rec_{input}}}{\pi \cdot \sqrt{2}} \tag{16}$$

The output of the rectifier in conjunction of the low-pass filter results in two constant signals for voltage and current. The voltage equals to $V_{rec_{output}}$ while the current is $I_{rec_{output}}$. This lead to an output power computed as follows:

$$P^{ch}_{rec_{output}} = V_{rec_{output}} \cdot I_{rec_{output}} \tag{17}$$

Consequently, the losses in the controlled rectifier (L^{ch}_{rec}) are:

$$L^{ch}_{rec} = P^{ch}_{rec_{input}} - P^{ch}_{rec_{output}} \tag{18}$$

B. Discharge mode

In the discharge mode, the battery of the EV provides energy to the grid so that the power flow is reverse to the previous mode. This means that the power converter attached to the battery acts as an inverter while the power converter in the primary side works as a rectifier. The waveforms of the converters change according to their new functionality but it follows a form equivalent to the previous case. Thus, these are the losses that are defined in a different way in comparison with the afore mentioned definitions. Alternatively, $L_{con,inv}$, $L_{sw,inv}$, $L_{con,rec}$, L_{coils} and L_{match} can be computed as previously. In the discharge mode, for the inverter attached to the battery:

$$P^{dis}_{inv_{output}} = \frac{V^1_{inv_{output}} \cdot I_{inv_{output}}}{2} = \frac{4 \cdot V_{inv_{output}} \cdot I_{inv_{output}}}{\pi \cdot \sqrt{2}} \tag{19}$$

$$P^{dis}_{inv_{input}} = V_{inv_{input}} \cdot I_{inv_{input}} \tag{20}$$

On the other hand, the losses in the primary inverter (L^{dis}_{inv}) are:

$$L^{dis}_{inv} = P^{dis}_{inv_{input}} - P^{dis}_{inv_{output}} \tag{21}$$

The rectifier input, which is now in the primary side, corresponds with a square-wave voltage (with a peak value of $V_{rec_{input}}$) and a sinusoidal current wave with a peak value equal to $I_{rec_{input}}$. Applying the decomposition of harmonics, we can assure that:

$$P_{rec_{input}}^{dis} = \frac{4 \cdot V_{rec_{input}} \cdot I_{rec_{input}}}{\pi \cdot \sqrt{2}} \quad (22)$$

The output of the rectifier is now connected to the grid. The voltage equals to $V_{rec_{output}}$ while the current is $I_{rec_{output}}$. Both signals are constant as a low-pass filter is used. This implies that the output power is computed as follows:

$$P_{rec_{output}}^{dis} = V_{rec_{output}} \cdot I_{rec_{output}} \quad (23)$$

As a consequence, the losses in the controlled rectifier for the discharge mode (L_{rec}^{dis}) are:

$$L_{rec}^{dis} = P_{rec_{input}}^{dis} - P_{rec_{output}}^{dis} \quad (24)$$

VI. Conclusion

This paper presents a model for the estimation of the charge and discharge efficiency in a bidirectional ICPT wireless charger for EV. Specifically, the model relies on the equivalent circuit of the semiconductors and of the reactive components to derive the conduction and the switching losses of the system. The model is contrasted with the experimental results obtained in a 3.7 kW wireless charger at 85 kHz. There exist some differences among them, which are assumed to be due to measurement errors.

As future work, we intend to model the switching losses when the resonant conditions do not hold because of misalignments between the two coils.

References

[1] L. Canals Casals, E. Martinez-Laserna, B. Amante García, and N. Nieto, "Sustainability analysis of the electric vehicle use in Europe for CO2 emissions reduction," *Journal of Cleaner Production*, vol. 127, pp. 425–437, 2016.

[2] E. A. Moreira Falcão, A. C. Rodrigues Teixeira, and J. R. Sodré, "Analysis of CO2emissions and techno-economic feasibility of an electric commercial vehicle," *Applied Energy*, vol. 193, pp. 297–307, 2017.

[3] A. Triviño, M. Longo, and F. Foiadelli, "Reduction of CO2 emissions using RES to recharge EVs : the Spanish case," *International Conference on Renewable Energies and Power Quality (ICREPQ'17)*, vol. 1, no. 15, 2017.

[4] K. E. Forrest, B. Tarroja, L. Zhang, B. Shaffer, and S. Samuelsen, "Charging a renewable future: The impact of electric vehicle charging intelligence on energy storage requirements to meet renewable portfolio standards," *Journal of Power Sources*, vol. 336, pp. 63–74, 2016.

[5] M. A. Lopez, S. De La Torre, S. Martin, and J. A. Aguado, "Demand-side management in smart grid operation considering electric vehicles load shifting and vehicle-to-grid support," *International Journal of Electrical Power and Energy Systems*, vol. 64, pp. 689–698, 2015.

[6] K. M. Tan, V. K. Ramachandaramurthy, and J. Y. Yong, "Integration of electric vehicles in smart grid: A review on vehicle to grid technologies and optimization techniques," *Renewable and Sustainable Energy Reviews*, vol. 53, pp. 720–732, 2016.

[7] K. A. Kalwar, M. Aamir, and S. Mekhilef, "Inductively coupled power transfer (ICPT) for electric vehicle charging - A review," *Renewable and Sustainable Energy Reviews*, vol. 47, pp. 462–475, 2015.

[8] A. Triviño-Cabrera, J. Aguado, and J. González, "Analytical characterisation of magnetic field generated by ICPT wireless charger," *Electronics Letters*, vol. 53, no. 13, pp. 871–873, jun 2017.

[9] G. Di Capua, J. A. A. Sanchez, A. T. Cabrera, D. F. Cabrera, N. Femia, G. Petrone, and G. Spagnuolo, "A losses-based analysis for electric vehicle wireless chargers," in *2015 International Conference on Synthesis, Modeling, Analysis and Simulation Methods and Applications to Circuit Design (SMACD)*. IEEE, sep 2015, pp. 1–4.

[10] G. Di Capua, N. Femia, G. Petrone, G. Lisi, D. Du, and R. Subramonian, "Power and efficiency analysis of high-frequency Wireless Power Transfer Systems," *International Journal of Electrical Power & Energy Systems*, vol. 84, pp. 124–134, jan 2017.

[11] N. Oswald, P. Anthony, N. McNeill, and B. H. Stark, "An Experimental Investigation of the Tradeoff between Switching Losses and EMI Generation With Hard-Switched All-Si, Si-SiC, and All-SiC Device Combinations," *IEEE Transactions on Power Electronics*, vol. 29, no. 5, pp. 2393–2407, may 2014.

[12] R. A. Wood and T. E. Salem, "Evaluation of a 1200-V, 800-A All-SiC Dual Module," *IEEE Transactions on Power Electronics*, vol. 26, no. 9, pp. 2504–2511, sep 2011.

[13] A. Trivino, J. M. Gonzalez-Gonzalez, and J. A. Aguado, "Evaluation of losses in a bidirectional wireless power transfer system for electric vehicles," in *2017 IEEE International Conference on Environment and Electrical Engineering and 2017 IEEE Industrial and Commercial Power Systems Europe (EEEIC / I&CPS Europe)*. IEEE, jun 2017, pp. 1–5.

[14] Q. Deng, J. Liu, D. Czarkowski, M. K. Kazimierczuk, M. Bojarski, H. Zhou, and W. Hu, "Frequency-Dependent Resistance of Litz-Wire Square Solenoid Coils and Quality Factor Optimization for Wireless Power Transfer," *IEEE Transactions on Industrial Electronics*, vol. 63, no. 5, pp. 2825–2837, may 2016. [Online]. Available: http://ieeexplore.ieee.org/document/7383291/

[15] A. Moradi, F. Tahami, and M. A. GhaziMoghadam, "Wireless Power Transfer Using Selected Harmonic Resonance Mode," *IEEE Transactions on Transportation Electrification*, vol. 3, no. 2, pp. 508–519, 2017. [Online]. Available: http://ieeexplore.ieee.org/document/7903716/

[16] SAE International, "Wireless Power Transfer for Light-Duty Plug-In/Electric Vehicles and Alignment Methodology (SAE TIR J2954)." [Online]. Available: http://standards.sae.org/wip/j2954/

Control Strategy of Thyristors Switched SVCs with High Power Quality

D. I. Panfilov
Department of industrial electronics
Moscow power engineering institute
Moscow, Russia
Dmitry.panfilov@inbox.ru

Ahmed E. ElGebaly
Electrical power and machines department
Faculty of engineering- Tanta university
Tanta, Egypt
Ahmed.elgebaly@f-eng.tanta.edu.eg

M. G. Astashev
G. M. Krzhizhanovsky power engineering institute
(JSC ENIN)
Moscow, Russia
astashev@eninnet.ru

Alexander N. Rozhkov
Department of industrial electronics
Moscow power engineering institute
Moscow, Russia
rozhkovan@eninnet.ru

***Abstract*—In this paper, new static VAR compensators SVCs schemes for inductive and capacitive reactive power are developed. The provided schemes improve the flexibility and power system quality of SVCs by developing new circuit topologies with new control strategy of the reactive power. New circuit schemes are introduced for thyristors switched reactors TSR and thyristors switched capacitors TSC to design harmonic-free SVC with higher discrete number of reactive power levels. This paper provides the control algorithm and block diagram of the new SVCs schemes. The switching strategies of TSR and TSC are described and implemented. The new scheme of TSC requires special modifications to decrease transient effects and implementation of specific switching strategies to acquire SVC with high power quality indexes.**

Keywords—static VAR compensators, thyristor switched reactors, thyristor switched capacitors

I. Introduction

Static VAR compensators SVC play an important role in electrical power systems because of their capability to dynamically compensate the reactive power. The SVC fundamentally is made up of inductive reactive power source, such as thyristor-controlled reactor TCR or thyristors switched reactors TSR, and capacitive reactive power source, for instance fixed capacitor FC and thyristors switched capacitors TSC [1]. The advance of SVC has various research trends such as optimization of the device rating and the place of installation in the power network [2], improvement of power electronics structure in the schemes [3,4,5] and development of SVC control system structure and operation [6]. TSR is considered as a solution to eliminate high order harmonics which are commonly produced in SVC based on TCR scheme. The new TSR topologies have flexible performance than the simple equal parallel branches or binary TSR schemes [7]. The existed TSC has one of the following topologies: equal rating parallel TSC branches and binary TSC [8].

The study was performed at Stock Company G. M. Krzhizhanovsky Power Engineering Institute within the framework of the project "Development of a controlled source of reactive power with the absence of the higher-order harmonics currents during the regulation of the electrical energy and with the improved technical and economicl indicators on the basis of the domestic component base of power electronics for automatic control of the voltage and the power flows in the electric power distribution networks of 6-110 kV (RFMEFI57917X0140)" with the financial support of the Ministry of Education and Science of the Russian Federation

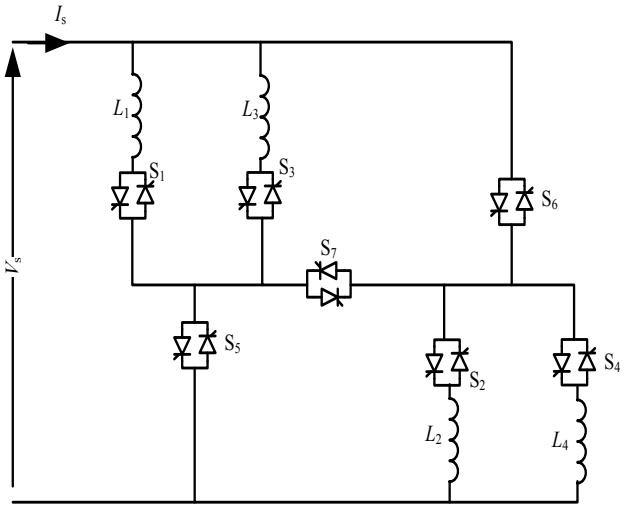

Fig. 1. TSR with 25 power steps

In the paper, new developed circuit topologies for both of TSR and TSC are developed with essential idea of increasing the number of steps of reactive power compensation with the same number of passive elements (reactors and capacitors). This paper demonstrates the principle of the new schemes operation. The characteristics of the new schemes that relates between the required and developed reactive power is provided in this paper. Furthermore, the control strategy and construction of the new developed schemes are clarified. The modification of TSC operation during transients is implemented with special algorithm and circuitry.

II. Circuits Topologies of Improved TSC and TSR

TSR and TSC new schemes are developed to control the reactive power with zero harmonic content but with discrete manner. The earlier schemes of TSR control the developed reactive power by varying the equivalent inductance of the parallel connected reactors. The developed schemes control the reactive power not only by changing the parallel connected branches but also by series connection of passive elements [9]. Fig. 1 illustrates a new circuit scheme for TSR which consists

four reactors and seven back-to-back thyristor switches. This scheme allows to obtain 25 different equivalent inductances; thus, it produces 25 reactive power steps. It can become evident that with additional three switches, the number of steps are increased from 16 steps in binary TSR to 25 steps in the new scheme [10]. TABLE I shows the different equivalent inductances and the states of operation of the switches where + means series connection and // means parallel connection of reactors. The total apparent power of reactors in the new scheme equals the total apparent power of the reactor used in conventional TCR and binary TSR [10]. With the same manner, the number of reactors may be more than four, but the number of switches will be more than the number of reactor by 3. These three switches are S_5, S_6 and S_7 in Fig. 1.

TABLE I. THE EQUIVALENT INDUCTANCE OBTAINED BY NEW TSR WITH FOUR REACTORS AND SEVEN SWITCHES

No.	Equivalent inductance	Switches state						
		S_1	S_2	S_3	S_4	S_5	S_6	S_7
1	0	OFF	OFF	OFF	OFF	OFF	OFF	OFF
2	L_1+L_2	ON	ON	OFF	OFF	OFF	OFF	ON
3	L_2+L_3	OFF	ON	ON	OFF	OFF	OFF	ON
4	$(L_1//L_3) + L_2$	ON	ON	ON	OFF	OFF	OFF	ON
5	L_2	OFF	ON	OFF	OFF	OFF	ON	OFF
6	L_1+L_4	ON	OFF	OFF	ON	OFF	OFF	ON
7	$(L_2//L_4) + L_1$	ON	ON	OFF	ON	OFF	OFF	ON
8	L_3+L_4	OFF	OFF	ON	ON	OFF	OFF	ON
9	$(L_2//L_4) + L_3$	OFF	ON	ON	ON	OFF	OFF	ON
10	L_1	ON	OFF	OFF	OFF	ON	OFF	OFF
11	$(L_1//L_3) + L_4$	ON	OFF	ON	ON	OFF	OFF	ON
12	$(L_1//L_3)+ (L_2//L_4)$	ON	ON	ON	ON	OFF	OFF	ON
13	$L_1//L_2$	ON	ON	OFF	OFF	ON	ON	OFF
14	L_3	OFF	OFF	ON	OFF	ON	OFF	OFF
15	L_4	OFF	OFF	OFF	ON	OFF	ON	OFF
16	$L_2//L_3$	OFF	ON	ON	OFF	ON	ON	OFF
17	$L_2//L_4$	OFF	ON	OFF	ON	OFF	ON	OFF
18	$L_1//L_3$	ON	OFF	ON	OFF	ON	OFF	OFF
19	$L_1//L_4$	ON	OFF	OFF	ON	ON	ON	OFF
20	$L_1//L_2//L_3$	ON	ON	ON	OFF	ON	ON	OFF
21	$L_1//L_4//L_2$	ON	ON	OFF	ON	ON	ON	OFF
22	$L_3//L_4$	OFF	OFF	ON	ON	ON	ON	OFF
23	$L_3//L_4//L_2$	OFF	ON	ON	ON	ON	ON	OFF
24	$L_1//L_4//L_3$	ON	OFF	ON	ON	ON	OFF	OFF
25	$L_1//L_2//L_3//L_4$	ON	ON	ON	ON	ON	ON	OFF

Fig. 2 demonstrates the new scheme of TSC which contains four capacitors and seven switches. This topology can produce 25 steps of operation such as that of the new TSR in Fig. 1. This scheme is better than binary TSC that contains four branches because the new topology provides 25 steps instead of 16 steps which can produced by binary TSC. Although the topologies of TSR and TSC have the same principle of operation by varying the developed reactive power by changing the equivalent reactance, the method of control of each scheme is different [11,12] as will explained in section IV.

III. CHARACTERISTICS OPTIMIZATION OF THE DEVELOPED TSC AND TSR TOPOLOGIES

The characteristic of the SVC system is the relation between the required reactive power as a reference from the control system and the actual produced reactive power from SVC. The characteristics of the new TSR or TSC schemes have discrete form. Consequently, it is very vital to adjust the SVC characteristics to be most near to the continuous characteristic

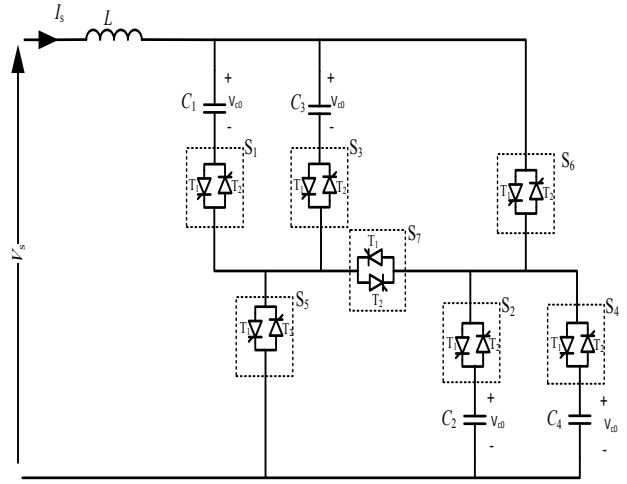

Fig. 2. TSC with 25 power steps

of SVC with TCR. Optimization technique can determine the parameters of each of the new developed schemes to obtain the smoothest variation in the produced reactive power [3]. In this section, the optimization technique is applied for TSR and with the same way it can be applied for TSC [3]. By assuming that, each equivalent inductance $L_x(n)$ produces the inductive reactive power Q_d:

$$Q_d(n) = \frac{V^2}{\omega L_x(n)} \tag{1}$$

In the case of the capacitive reactive power, each equivalent capacitance $C_x(n)$ produces capacitive reactive power according the following equation $Q_d(n) = V^2 \omega C_x(n)$, where n is the number of the equivalent circuits which depend on the switches states in Fig. 2. An objective function should be applied to optimize the distribution of the produced reactive power. This objective function *O.F.D* designates the difference between two consecutive developed reactive power ($Q_d(n)$, $Q_d(n+1)$), while this difference shouldn't exceed certain determined value ΔQ.

$$O.F.D = \sum_{n=1}^{m-1} \left(Q_d(n+1) - Q_d(n) \right) - \Delta Q \tag{2}$$

where m is the total number of steps obtained by the developed scheme.

This objective function is used for both of new TSR and TSC schemes. Optimization technique that depends on genetic algorithm GA is used to solve this objective function. The constraint for the variables is the ratio between the maximum and the minimum variables (maximum and minimum inductance or capacitance of passive elements) doesn't exceed 8. So, the parameters of TSR and TSC can be determined as a function of rated inductance L_{eq} and rated capacitance C_{eq} correspondingly. The values of inductances to obtain the finest solution are as the following: $L_1 = 5.1\ L_{eq}$, $L_2 = 10.8\ L_{eq}$, $L_3 = 3\ L_{eq}$, $L_4 = 2.6\ L_{eq}$. While the value of capacitance for TSC optimal design $C_1 = 0.2\ C_{eq}$, $C_2 = 0.0998\ C_{eq}$, $C_3 = 0.3248\ C_{eq}$,

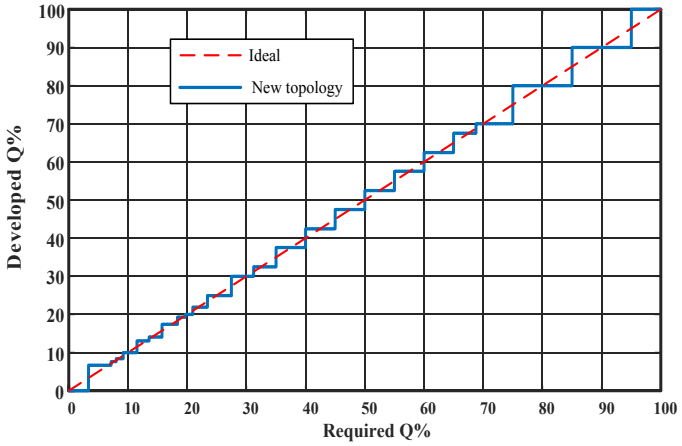

Fig. 3. The optimal characteristics of the new TSR and TSC characteristics

C_4 = 0.3754 C_{eq}. The predetermined parameters offer the characteristic for each of TSR or TSC as demonstrated in Fig. 3. This characteristic links between the required reactive power from the scheme and the discrete produced reactive power. It can be noted that this characteristic may be inductive or capacitive according to the type of the scheme. To get certain required reactive power, certain step of 25 steps should be realized consistent with its percentage. The grouping between the two new TSC and TSR schemes provides more smooth variation in the group characteristic.

IV. Algorithms of Thyristors Controlling in New SVC Schemes

Fig. 4 demonstrates the general block diagram of SVC with discrete TSR and TSC. The required susceptance B (the required reactive power) is converted to required inductive susceptance and required capacitive susceptance [4]. The required susceptance B is converted by the control system to specified step according to the characteristics of TSR or TSC. This control system is essential for the discrete control SVC schemes and has the required blocks to diminish the effect of the discrete characteristics [4].

The inductive reactive power control is occurred because of the changing of the inductance value consistent with the certain step as in Fig. 5. The varying of inductance value is simple because it should be occurred at zero crossing of current. For inductive current, the current zero crossing occurs at voltage phase angles of 90° and 270° i.e. at the moment of maximum instantaneous voltage. Therefore, the maximum time delay in this case equals half cycle of the fundamental frequency. Fig. 6 illustrates the block diagram of the TSR control system which contains three main components; the first is the block responsible for the synchronization between the TSR and the power grid; the second is the block responsible for the determination of the required susceptance and therefore the required operated switches; the third block is the firing circuit of thyristors. Fig. 7 shows the waveforms of TSR current and voltage throughout the changing from one step to another. If new step is required by the control system, the implementation of the new step happens only at the zero-crossing of the current or the maximum amplitude of instantaneous voltage.

Conversely, the capacitive reactive power control of TSR is more complicated. There is no opportunity to switch on a switch in series with sinusoidal power supply and capacitor because there is a need to avoid the sudden change of voltage on the capacitor which leads to excessive level of current which may lead to the damage of the switch and the capacitor. In some cases, when the firing angle of the switch occurs at zero crossing of voltage, the high value of current change *di/dt* is very hazard for the switch. Consequently, connection of small damping inductors in series with capacitor will reduce the high values of current or its rate of change [11].

For the new scheme of TSC, it is preferred to install a reactor L in series with power supply as in Fig. 2. This reactor plays vital role not only for switching on the capacitors with lower transients but also for preparing the capacitors for the next step. The developed topology depends on the series connection and parallel connection. Nonetheless, the connection of capacitors in series needs the discharging of all capacitors to prevent residual DC charge on capacitors during producing of capacitive current. Consequently, the control

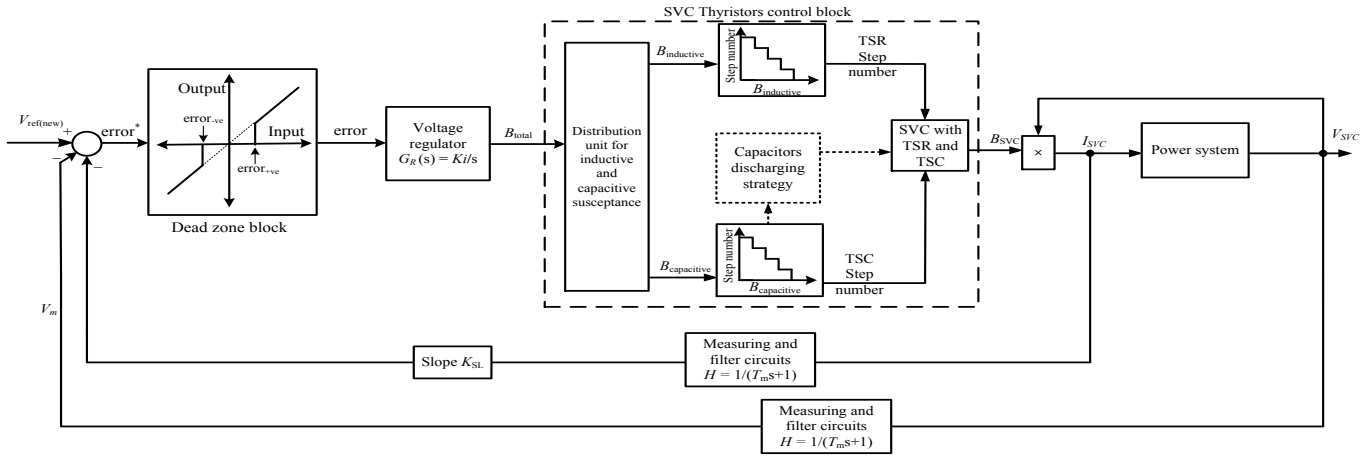

Fig. 4. The block diagram of control system for thyristors switched SVC

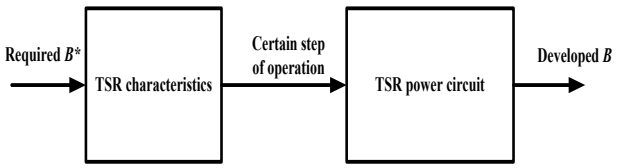

Fig. 5. Flow chart for controlling thyristors switched reactors

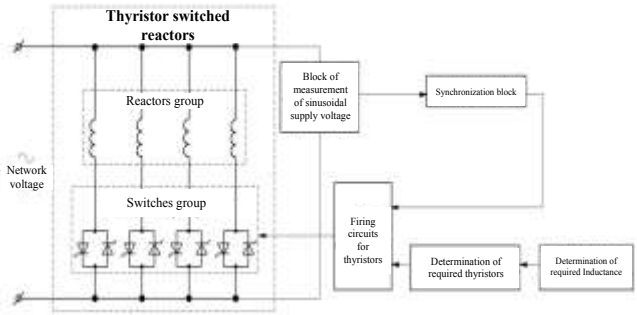

Fig. 6. Block diagram of TSR control system

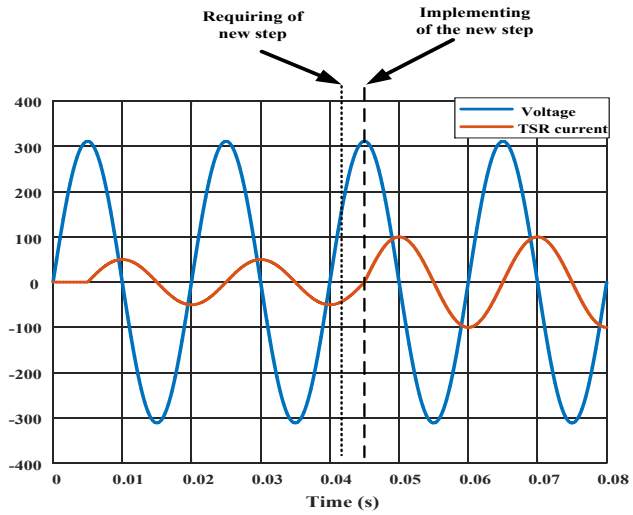

Fig. 7. TSR voltage and current waveforms during transition from one step to another

algorithm of TSC should contain the discharging process earlier than the starting of the new step of operation. After the capacitors discharging, the new connection of the capacitors starts at the next voltage zero crossing. Fig. 8 illustrates the flow chart of the control algorithm of TSC to start new step of operation. Consistent with this algorithm, if there is requirement of new value of susceptance B, the discharging process should be activated before the implementation of new value of B. Fig. 9 demonstrates the detailed block diagram of the TSC control system which contains the blocks required for the changing of the required susceptance and the discharging of the capacitors. Fig. 10 (a) demonstrates the waveforms of the supply voltage and the current of the TSC in the transition between two steps where the TSC current equals zero during the discharging period except the impulse current due to capacitor discharge. Fig. 10 (b) shows the voltage of certain

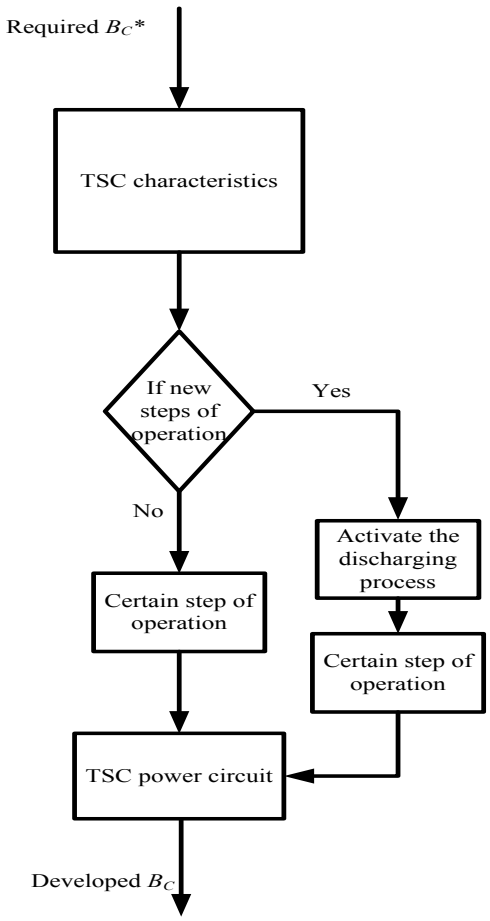

Fig. 8. Flow chart of algorithms for controlling thyristors switched

capacitor in the transition process the voltage is kept constant till the moment to discharge it to zero voltage.

The special discharging process for capacitors is applied within only one quarter of the fundamental period to keep the fast response of the overall system. If the capacitors are charged with positive or negative charge from the previous state of operation, this energy could be regenerated to the power supply depending on the reactor L. Therefore, the inductance L of installed reactor and the equivalent capacitance C_{eq} should provide resonance frequency higher than the fundamental frequency ω_0 to end the discharging process in very short time. The resonance frequency recommended in this paper equals 24 times the fundamental frequency. So, the value inductance L can be determined with maximum capacitance C_{eq} and resonance frequency of 24 ω_0.

$$L = \frac{1}{(24\omega_0)^2 C_{eq}} \tag{3}$$

For delta connected TSC 200 kVAR, 400 V-line voltage, the value of C_{eq} equals 1315 μF and the value of inductance equals 13.2 μH. The control algorithm for the discharging can be explained according to the following example: assume all capacitors have remaining voltages V_{c0} illustrated in Fig. 2 which equals $220\sqrt{2}$ V. The goal is the regeneration of this

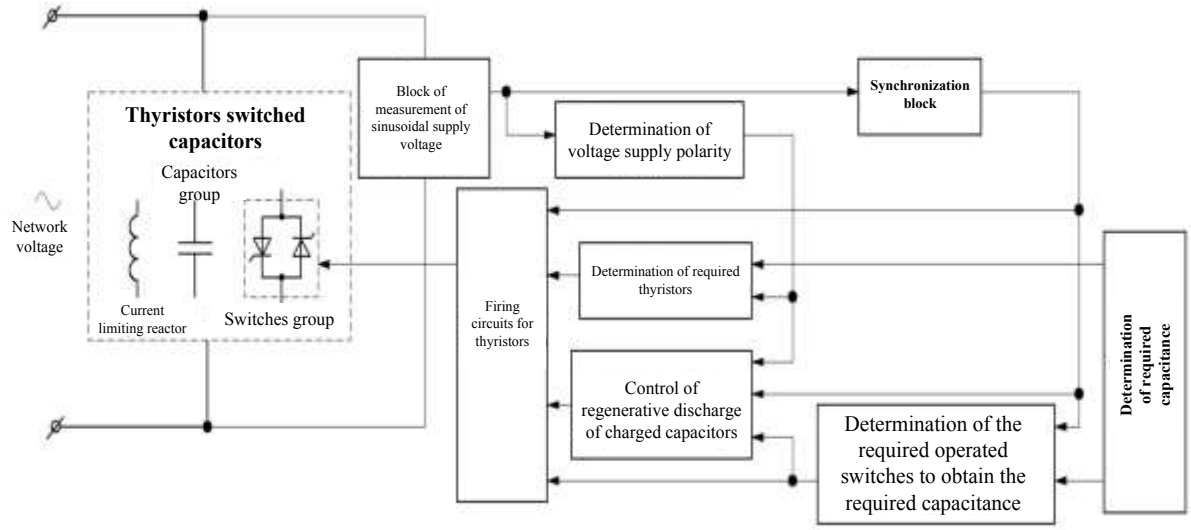

Fig. 9. Block diagram of new topology of TSC control system

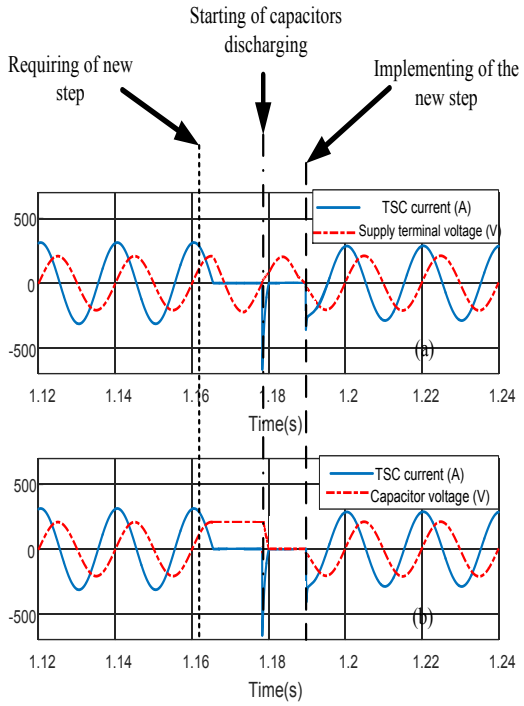

Fig. 10. The waveform of the applied voltage on TSC and its current and a voltage on one capacitor

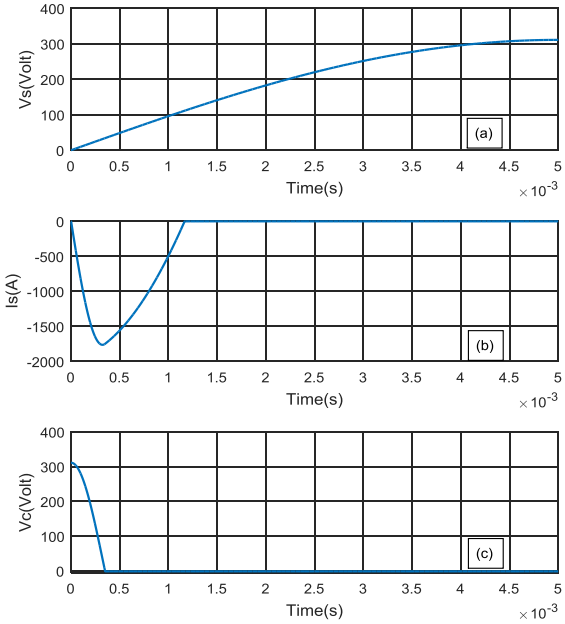

Fig. 11. Discharging process for capacitor of TSC with regeneration of energy (a) the supply voltage, (b) the supply current and (c) the capacitors voltage

stored energy to the supply to reduce the capacitor voltage to zero level. The starting of discharging happens when the waveform of voltage passes through zero to the positive values as in Fig. 11 (a) and the thyristors T_2 for all switches are fired in this moment. Fig. 12 illustrates the flow of current during discharging of capacitors where all switches except S_7 operate in the direction enables to discharge the capacitors. In this moment, the voltage of capacitors is more than the instant value of supply voltage; so, all capacitors produce currents passes through reactor *L* and thyristors T_2 in all switches except S_7. This current has negative sign with respect to the power supply as in Fig. 11 (b). At the moment when the capacitors voltage reaches zero Fig. 11 (c) (0.35 µs) the thyristors T_2 in the switches S_1, S_2, S_3 and S_4 are changed to off state (open circuit). But, the inductor current continuous passing in the same direction through thyristors T_2 in switches S_5, S_6 and S_7. The positive voltage of the supply forces the current to decay to zero as in Fig. 11 (b) in the period 0.35 to 1.1 µs. Then the capacitors are ready to the next connection through the power supply at the next voltage zero crossing. With the same strategy the discharging of capacitors can be applied if the capacitors are charged with negative sign.

V. CONCLUSION

This paper has provided new topologies of thyristors switched SVC which control the reactive power with zero

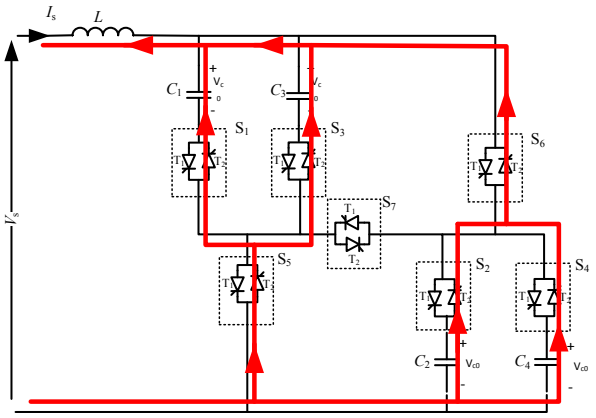

Fig. 12. Discharging path for positively charged capacitors of TSC

harmonic content. The power circuitries for inductive and capacitive schemes of the new SVC are introduced. The principle of operation of new SVC has been explained to illustrate the basics of the control system algorithm. The block diagram of the control system of the new SVC system has been introduced with some modifications than the conventional SVC. The control algorithm for TSR of the new SVC schemes has been explained. The control algorithm for TSC is developed including the switching strategy required for the discharging of capacitors.

ACKNOWLEDGMENT

The study was performed at Stock Company G. M. Krzhizhanovsky Power Engineering Institute within the framework of the project " Development of a controlled source of reactive power with the absence of the higher-order harmonics currents during the regulation of the electrical energy and with the improved technical and economical indicators on the basis of the domestic component base of power electronics for automatic control of the voltage and the power flows in the electric power distribution networks of 6-110 kV (RFMEFI57917X0140)" with the financial support of the Ministry of Education and Science of the Russian Federation.

REFERENCES

[1] L. Gyugyi, “Power electronics in electric utilities: static VAR compensators”, Proceedings of the IEEE, Vol: 76, Issue: 4, April 1988

[2] Sharma, P. R. Kumar, A. Kumar, N. Optimal Location for Shunt Connected FACTS Devices in a Series Compensated Long Transmission Line. // Turk J Elec Engin. 15, 3(2007), pp. 321-328.

[3] D. I. Panfilov, A. E. ElGebaly, M. G. Astashev and Alexander N. Rozhkov, “New Approach for Thyristors Switched Capacitors Design for Static VAR Compensator Systems” 19th International Conference of Young Specialists on Micro/Nanotechnologies and Electron Devices June 29 - July 3, 2018

[4] D. I. Panfilov, A. E. ElGebaly and M. G. Astashev, “Design and Optimization of New Thyristors Controlled Reactors with Zero Harmonic Content”, 18th International Conference of Young Specialists on Micro/Nanotechnologies and Electron Devices June 29 - July 3, 2017

[5] D. I. Panfilov, A. E. ElGebaly and M. G. Astashev, “Design and evaluation of control system for static VAR compensators with thyristors switched reactors” IEEE 58th International Scientific Conference on Power and Electrical Engineering of Riga Technical University (RTUCON), Riga, Latvia, 12-13 October 2017

[6] D.I. Panfilov, A. E. ElGebaly, “Modified Thyristor Controlled Reactors for Static VAR Compensators” 2016 IEEE 6th International Conference on Power and Energy (PECON 2016) , Melaka, Malaysia, November 2016

[7] D. I. Panfilov, A. E. ElGebaly and M. G. Astashev, “Topologies of thyristor controlled reactor with reduced current harmonic content for static var compensators” 17th EEEIC concerence, Milan, Italy, 6-9 June 2017

[8] A. E. Elgebaly, D. I. Panfilov and M. G. Astashev “Comparative Evaluation of Binary and Conventional Static VAR Compensators” Mechanics, Materials Science & Engineering journal (mmse), vol. 17, 2018

[9] D. I. Panfilov, A. E. Elgebaly and M. G. Astashev, “Design and Assessment of Static VAR Compensator on Railways Power Grid Operation under Normal and Contingencies Conditions”, 16th EEEIC conference, Florence, Italy, 7-10 June 2016

[10] D. I. Panfilov, A. E. ElGebaly and M. G. Astashev, “Thyristors Controlled Reactors for Reactive Power Control with Zero Harmonics Content”, 17th IEEE International Conference on Smart Technologies IEEE EUROCON 2017, Ohrid, Macedonia, 6 - 8 July 2017

[11] N. Garcia , A. Medina “Fast periodic steady state solution of systems containing thyristor switched capacitors”, 2000 power engineering society summer meeting Seattle, Washington USA, 16 - 20 July 2000

[12] A.N. Vasconcelos, et.al, “Detailed Modeling of An Actual Static Var Compensator for Electromagnetic Transient Studies”, IEEE Transactions on Power Systems, Vol. 7, No. 1, February 1992.

Stair-like Multivariable Generalized Predictive Control of Pulverizing System in Thermal Power Plants

ZHANG Jiansheng[1]
Electricity Production Department
Shenhua Guoneng Energy Group Corporation, Limited
Beijing, China
zjs3241@163.com

Gao Yaokui[3]
School of Control and Computer Engineering
North China Electric Power University
Beijing, China
Gaoyaokui05@126.com

ZHANG Gang[2]
School of Control and Computer Engineering
North China Electric Power University
Beijing, China
1562820108@qq.com

Hu Yong[4]
School of Control and Computer Engineering
North China Electric Power University
Beijing, China
ncepu_hu@yahoo.com

***Abstract*—Pulverizing system is an important part in the clean and efficient utilization of coal in thermal power plant, the optimal control of the system is an important way to achieve this goal. This paper presents a stair-like multivariable generalized predictive control scheme for a pulverizing system. This scheme focuses on the problem of predictive control algorithm in practical application, especially when it incorporates feedforward control ideas. Simulation results showed that the scheme are able to realize the decoupling control of the pulverizing system, avoid the problem of matrix inversion, reduce the amount of calculation, and has certain engineering application value.**

Keywords—Power Plants; Pulverizing System; Predictive Control;

I. INTRODUCTION

"Rich in coal but poor in oil and gas" is a distinctive feature of China's present energy structure. The National Potential Assessment of Coal Resources shows that China's total coal resources are 5.9 trillion tons, which accounts for 94% of the total primary energy resources; however, the oil and natural gas resources account for only 6%. The total energy consumption in 2016 is about 4.36 billion tons of standard coal, of which, 2.7 billion tons of coal were consumed, which accounts for 62% of the total energy consumption; in which, the coal consumed for power generation accounts for 53% [1,2]. Further, Coal-fired power generation capacity accounted for more than 60% of the total installed power generation capacity in China (about 14 billion kilowatts). Therefore, the clean and efficient use of coal in China is crucial, especially in coal-fired power plants, which will be of great significance in alleviating the pressure on China's resources and the environment, and will ensure the sustainable development of the China's energy system.

In coal-fired power plants, the clean and efficient use of coal is affected by many factors, such as coal quality, type and dryness, distribution of primary and secondary air, burner structure, operating conditions of units, etc. These factors involve the pulverizing, air distribution, desulfurization, denitration, dust removal, and coordination system, which make it difficult to analyze them integrally. In this paper, we mainly study the optimization control of pulverizing system to improve the stability and economy of boiler combustion, thereby achieving the clean and efficient use of coal in coal-fired power plants.

The pulverizing system is a typical three-input, three-output, nonlinear, and time-varying system, and there is a serious coupling between each variable. The traditional control system generally consists of three independent single-loop, that is, the mill outlet temperature is controlled by the cold air valve, the primary air flow is controlled by the hot air valve, and the output of the pulverizing system is controlled by the coal feeder, this control method fails to achieve decoupling control of pulverizing system; the output of pulverizing system is generally controlled by the coal feeder indirectly, and its control accuracy is very poor. In addition, the mill outlet temperature is the main factor affecting the degree of dryness and ignition heat of pulverized coal, which is affected by both the raw coal moisture content, the coal feed flow, the primary air flow and the primary air temperature. Among them, the raw coal moisture is an uncontrollable variable, the coal feed flow is controlled with the change of unit load, the primary air flow is controlled with the change of coal feed flow, none of the three can be used as control method for mill outlet temperature, thereby, the mill outlet temperature is essentially controlled by primary air temperature at the inlet of coal mill. The higher the primary air temperature at the inlet of the coal mill, the lower the pulverized coal moisture at the outlet of the coal mill, the

This paper is supported by National Natural Science Foundation of China (51776065); Control Technology on Operating Flexibility of the Thermal Power Unit Based on its Energy Management (2017)

lower the latent heat of vaporization and the ignition heat required for the combustion, which is more conducive to the safe, stable and economical operation of the boiler; however, the excessive primary air temperature at the inlet of coal mill may cause spontaneous combustion of pulverized coal or even an explosion accident, which seriously affect the safety of milling equipment. Therefore, it is of great importance to study the optimal control technology of pulverizing system to realize the safe, stable and economical operation of milling system, and improve the stability and economy of boiler combustion.

Recently, some advanced intelligent control algorithms has been applied to the design of pulverizing control system. Combined the PID algorithm and the predictive control algorithm, Sun[3] et al. proposes a PID-GPC predictive control algorithm, Based on this algorithm, a control scheme for the pulverizing system is designed. The simulation show that the algorithm has better robustness than general feedforward decoupling PID control and GPC control, however, this algorithm fails to consider some practical engineering problems and is not conducive to engineering applications. On the basis of a T-S fuzzy model of a pulverizing system, Zhang[4] et al. present a tracking control scheme for a pulverizing system, and some important performance indicators was considered to ensure the real-time performance of the control system, the simulation verified the effectiveness and real-time performance of the control system, However, this cannot achieve decoupling control of the pulverizing system. Considering the effect of coal moisture on the energy balance of the coal mill, Zeng[5] et al. established a dynamic model of a coal mill and designed an optimized control scheme for the coal mill, the simulation results also show the accuracy of the model and the effectiveness of the control scheme, However, the control scheme is only for the coal mill, the control variable is the inlet primary air temperature and primary air flow, which are not direct control variables of pulverizing system. Through modeling and analysis, Gao[6] et al. proposed an estimation signal for pulverized coal flow at the outlet of coal mill, and this signal was integrated into the design of an intelligent control scheme for the pulverizing system. Finally, a control scheme for the pulverizing system based on state space prediction control was designed, the simulation indicated that the output control precision of the pulverizing system was improved and the ability to resist disturbances was enhanced, however, the control scheme does not consider matrix inversion and tracking switching issues from an engineering perspective, Therefore, it is not conducive to engineering applications.

In summary, the above research content are hard to apply to engineering practice, and only remain in the simulation stage. This article will directly address the engineering applications: 1) the multivariable generalized predictive control algorithm is adopted to realize the decoupling control of pulverizing system, thereby avoiding the coupling fluctuations of the controlled variables; 2) the stair-like solution idea is adopted to solve the control law of the predictive controller, thereby avoiding the inversion problem in the process of solving diophantine equation; and 3) The feedforward experience in traditional control schemes is integrated into the design of this control scheme.

This paper is organized as follows. Section 1 provides a brief introduction for pulverizing systems and simulation models. Section 2 deduces the stair-like multivariable generalized predictive control algorithm. Section 3 designs an optimized control scheme of the pulverizing system on the basis of the algorithm deduced in the former section. Section 4 simulates and verifies the proposed control scheme. Section 5 presents the conclusion of this paper.

II. BRIEF INTRODUCTION FOR PULVERIZING SYSTEMS AND SIMULATION MODELS

A typical positive-pressure, direct-fired, pulverizing system is mainly composed of a coal feeder, a coal mill, a primary fan, a sealed fan, a separator, and a burner (see Fig. 1). The raw coal is fed into the coal mill via a coal feeder, and then ground to pulverized coal; the primary air is boosted by a fan and divided into two parts, one part directly enters the cold air duct, while the other part is heated by an air preheater and then enters the hot air duct. These two parts of wind are mixed and then sent to the coal mill. The mixed primary air temperature and primary air flow are controlled by a cold air valve and a hot valve, these two valves cooperate to complete the drying and conveying tasks of the pulverized coal. In addition, the sealed fan is used to seal the coal mill to prevent the pulverized coal from leaking.

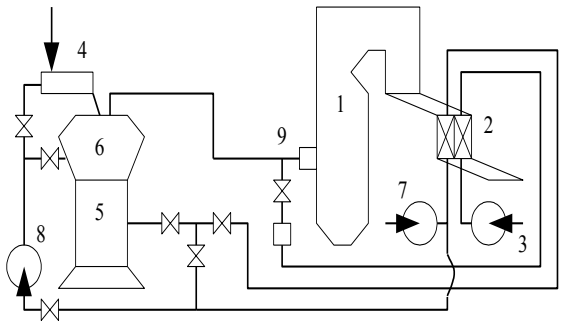

1.boiler furnace, 2.air preheater, 3.air blower, 4. coal feeder, 5. coal mill, 6. Separator, 7. primary fan, 8. sealing fan, 9. burner

Fig.1 Schematic of a medium speed mill, positive-pressure, direct-fired pulverizing system

The research work in this paper is based on a model of a MPS positive-pressure, direct-fired, pulverizing system established in [5]. This model which is established based on the mass balance and energy balance of a coal mill, the specific form of the model is as follows:

Where, W_{air} is primary air flow, kg/s; θ_{in} is primary air temperature, kg/s; M_c is raw coal content in coal mill, kg; M_{pf} is coal powder content in coal mill, kg; θ_{out} is coal mill outlet temperature, °C; u_L is valve opening of cold air, %; u_H is valve opening of hot air, %; W_c is coal feed flow, kg/s; M_{ar} is raw coal moisture, %.

The input of the model are u_L, u_H, and W_c. The output of the model are W_{air}, θ_{out}, and W_{pf}. The states of the model are θ_{in}, W_{air}, M_c, M_{pf}, and θ_{out}. The time-varying parameters is M_{ar}.

$$\begin{cases} \dot{W_{air}} = -0.0971W_{air} + 0.183u_L + 0.551u_H - 22.2 \\ \dot{\theta_{in}} = -0.272\theta_{in} - 198 + \frac{7.98u_L + 192.0u_H}{(0.183u_L + 0.551u_H)(8\theta_{in} \times 10^{-5} + 0.995)} \\ \dot{M_c} = -0.452M_c + W_c \\ \dot{M_{pf}} = 0.452M_c - (0.00285\theta_{in} + 0.778){W_{air}}^2 M_{pf} \times 7.95 \times 10^{-4} \\ \dot{\theta_{out}} = \frac{1}{4171.7}\left(1.1M_c + 0.233M_{pf} + 9.42W_{air} - 2.414W_{air}\theta_{out} + 2.151W_{air}\theta_{in} + tempA + tempB\right) \end{cases}, \quad (1)$$

$$tempA = \frac{2.17u_3(1.88\theta_{out} + 2499)\left(M_{ar} - \frac{1.1M_{ar}}{{\theta_{out}}^{0.45}}\right)}{\left(\frac{1.1M_{ar}}{{\theta_{out}}^{0.45}} - 100\right)}, \quad (2)$$

$$tempB = -2.17\theta_{out}W_c(0.01M_{ar} - 1.0)\left(\frac{4.62M_{ar}}{{\theta_{out}}^{0.45}\left(\frac{1.1M_{ar}}{{\theta_{out}}^{0.45}} - 100\right)} - 1.09\right), \quad (3)$$

III. Optimal Control of the Pulverizing System

In consideration that predictive control algorithms generally perform well in strong coupling multivariable systems without being decoupled [8-10], such an algorithm is adopted as the core of the control system design in this paper, and a stair-like solution idea was adopted to avoid matrix inversion problems.

A. Stair-like multivariable generalized predictive control algorithm

Assume that the system is based on the following discrete-time CARIMA model [8-10]:

$$\boldsymbol{A}(z^{-1})\boldsymbol{y}(k) = \boldsymbol{B}(z^{-1})\boldsymbol{u}(k-1) + \boldsymbol{\xi}(k)/\Delta \quad (4)$$

Where $\boldsymbol{y}(k)$ is the system's m-dimensional output; $\boldsymbol{u}(k)$ is the system's p-dimensional input; $\boldsymbol{\xi}(k)$ is the system's m-dimensional noise vector; and:

$$\boldsymbol{A}(z^{-1}) = 1 + \boldsymbol{A}_1 z^{-1} + \cdots + \boldsymbol{A}_{n_a} z^{-n_a},$$
$$\boldsymbol{B}(z^{-1}) = \boldsymbol{B}_0 + \boldsymbol{B}_1 z^{-1} + \cdots + \boldsymbol{B}_{n_b} z^{-n_b},$$

Where $\boldsymbol{A}_i$ is a m × m dimension matrix, and $\boldsymbol{B}_i$ is a m × m dimension matrix.

Assume that the objective function of the control system is as fellow:

$$\boldsymbol{J} = \sum_{j=1}^{N} \|\hat{\boldsymbol{y}}(k+j|k) - \boldsymbol{y_d}(k+j)\|_{I_m}^2 + \sum_{j=1}^{N_u} \|\boldsymbol{\Delta u}(k+j-1)\|_{\boldsymbol{\Lambda}}^2 \quad (5)$$

Where $\hat{\boldsymbol{y}}(k+j|k)$ is a j-step prediction for $y(k)$; $\boldsymbol{\Lambda}$ is a positive semi-definite matrix, generally take $\boldsymbol{\Lambda} = diag(\lambda_1, \cdots, \lambda_p)$, and $\lambda_i \geq 0$; $\boldsymbol{y}_d(k+j)$ is the softening sequence vector of the set value, which generated by:

$$\begin{cases} \boldsymbol{y}_d(k) = \boldsymbol{y}(k) \\ \boldsymbol{y}_d(k+j) = \boldsymbol{\alpha}\boldsymbol{y}_d(k+j-1) + (\boldsymbol{I}_m - \boldsymbol{\alpha})\boldsymbol{y}_r(k) \ \ (j = 1, \cdots, N) \end{cases} \quad (6)$$

Where $\boldsymbol{\alpha} = diag(\alpha_1, \cdots, \alpha_m)$, and $0 \leq \alpha_i < 1$; $\boldsymbol{y}_r(k)$ is an m-dimensional set value vector.

Introduce the following Diophantine equations:

$$\boldsymbol{I} = \boldsymbol{E}_j\Delta\boldsymbol{A} + z^{-j}\boldsymbol{F}_j \qquad j = 1, \cdots, N,$$
$$\boldsymbol{E}_j\boldsymbol{B} = \boldsymbol{G}_j + z^{-j}\boldsymbol{H}_j \qquad j = 1, \cdots, N,$$

Where,

$$\boldsymbol{E}_j = \boldsymbol{E}^{(0)} + \boldsymbol{E}^{(1)}z^{-1} + \cdots + \boldsymbol{E}^{(j-1)}z^{-(j-1)},$$
$$\boldsymbol{F}_j = \boldsymbol{F}^{(0)} + \boldsymbol{F}^{(1)}z^{-1} + \cdots + \boldsymbol{F}^{(n_a)}z^{-n_a},$$
$$\boldsymbol{G}_j = \boldsymbol{G}^{(0)} + \boldsymbol{G}^{(1)}z^{-1} + \cdots + \boldsymbol{G}^{(j-1)}z^{-(j-1)},$$
$$\boldsymbol{H}_j = \boldsymbol{H}^{(0)} + \boldsymbol{H}^{(1)}z^{-1} + \cdots + \boldsymbol{H}^{(n_b-1)}z^{-(n_b-1)},$$

And $E^{(i)}$, $F^{(i)}$ are m-order square matrixes, $\boldsymbol{G}^{(i)}$, $\boldsymbol{H}^{(i)}$ are p × m dimension matrixes.

Definition:

$$\hat{\boldsymbol{Y}}(k) = \begin{pmatrix} \hat{\boldsymbol{y}}(k+1|k) \\ \vdots \\ \hat{\boldsymbol{y}}(k+j|k) \end{pmatrix}_{m \times N},$$
$$\Delta\boldsymbol{U}(k) = \begin{pmatrix} \Delta\boldsymbol{u}(k) \\ \vdots \\ \Delta\boldsymbol{u}(k+N_u-1) \end{pmatrix}_{p \times N_u}$$

Resolving the Diophantine equations, and then the predictive equations can be obtained as fellow:

$$\hat{\boldsymbol{Y}}(k) = \boldsymbol{G}\Delta\boldsymbol{U}(k) + \boldsymbol{Y}_0(k), \quad (7)$$
$$\boldsymbol{Y}_0(k) = \boldsymbol{F}_j(z^{-1})\boldsymbol{y}(k) + \boldsymbol{H}_j(z^{-1})\Delta\boldsymbol{U}(k-1), \quad (8)$$

Where $\boldsymbol{G} = \begin{bmatrix} \boldsymbol{G}^{(0)} & & \cdots & \\ \boldsymbol{G}^{(1)} & \boldsymbol{G}^{(0)} & \cdots & \\ \vdots & \vdots & \ddots & \\ \boldsymbol{G}^{(N_u-1)} & \boldsymbol{G}^{(N_u-2)} & \cdots & \boldsymbol{G}^{(0)} \\ \vdots & \vdots & \ddots & \vdots \\ \boldsymbol{G}^{(N-1)} & \boldsymbol{G}^{(N-2)} & \cdots & \boldsymbol{G}^{(N-N_u)} \end{bmatrix}$

Let the increment of future control variables be : $\Delta\boldsymbol{u}(k) = \boldsymbol{\delta}$, $\Delta\boldsymbol{u}(k+i) = \beta\Delta\boldsymbol{u}(k+i-1) = \beta^i\boldsymbol{\delta}$, $1 \leq i \leq N_u$

$$\Delta\boldsymbol{U}(k) = (\Delta\boldsymbol{u}(k)\ \Delta\boldsymbol{u}(k+1)\ \cdots\ \Delta\boldsymbol{u}(k+N_u-1))^T = (\boldsymbol{\delta}\ \beta\boldsymbol{\delta}\ \cdots\ \beta^{N_u-1}\boldsymbol{\delta})^T = (1\ \beta\ \cdots\ \beta^{N_u-1})^T\boldsymbol{\delta}$$

$$\boldsymbol{G}\Delta\boldsymbol{U}(k)=\begin{bmatrix}\boldsymbol{G}^{(0)} & & \cdots & \\ \boldsymbol{G}^{(1)} & \boldsymbol{G}^{(0)} & \cdots & \\ \vdots & \vdots & \ddots & \\ \boldsymbol{G}^{(N_u-1)} & \boldsymbol{G}^{(N_u-2)} & \cdots & \boldsymbol{G}^{(0)} \\ \vdots & \vdots & \ddots & \vdots \\ \boldsymbol{G}^{(N-1)} & \boldsymbol{G}^{(N-2)} & \cdots & \boldsymbol{G}^{(N-N_u)}\end{bmatrix}\begin{bmatrix}1\\ \beta\\ \vdots\\ \beta^{N_u-1}\end{bmatrix}\boldsymbol{\delta}$$

$$=\begin{bmatrix}\boldsymbol{G}^{(0)}\\ \boldsymbol{G}^{(1)}+\beta\boldsymbol{G}^{(0)}\\ \vdots\\ \boldsymbol{G}^{(N_u-1)}+\beta\boldsymbol{G}^{(N_u-2)}+\cdots+\beta^{N_u-1}\boldsymbol{G}^{(0)}\\ \vdots\\ \boldsymbol{G}^{(N-1)}+\beta\boldsymbol{G}^{(N-2)}+\cdots+\beta^{N-N_u}\boldsymbol{G}^{(0)}\end{bmatrix}\boldsymbol{\delta}=\widetilde{\boldsymbol{G}}\boldsymbol{\delta}$$

Therefore, the predictive equations can be written as fellow:

$$\widehat{\boldsymbol{Y}}(k)=\widetilde{\boldsymbol{G}}\boldsymbol{\delta}+\boldsymbol{Y}_0(k), \tag{9}$$

$$\min_{\boldsymbol{\delta}}\boldsymbol{J}=\left(\widetilde{\boldsymbol{G}}\boldsymbol{\delta}+\boldsymbol{Y}_0(k)-\boldsymbol{Y}_{\boldsymbol{d}}\right)^T\left(\widetilde{\boldsymbol{G}}\boldsymbol{\delta}+\boldsymbol{Y}_0(k)-\boldsymbol{Y}_{\boldsymbol{d}}\right)+\boldsymbol{\Lambda}(1+\beta^2+\cdots+\beta^{2(N_u-1)})\boldsymbol{\delta}^2, \tag{10}$$

Minimize the objective function $\frac{\partial \boldsymbol{J}}{\partial \boldsymbol{\delta}}=0$, and then obtain the control law as:

$$\boldsymbol{\delta}=\frac{\widetilde{\boldsymbol{G}}^{\boldsymbol{T}}(\boldsymbol{Y}_{\boldsymbol{d}}-\boldsymbol{Y}_0)}{\widetilde{\boldsymbol{G}}^{\boldsymbol{T}}\widetilde{\boldsymbol{G}}+\boldsymbol{\Lambda}(1+\beta^2+\cdots+\beta^{2(N_u-1)})\boldsymbol{\delta}^2}$$

In the control process, only the current control amount $\Delta\boldsymbol{u}(k)=\Delta\boldsymbol{u}(k-1)+\boldsymbol{\delta}$ is implemented.

B. Overall control scheme

Considering that the pulverizing system is a multi-input, multi-output, and non-linear system, the inputs and outputs are strongly coupled, in order to fundamentally realize the decoupling control of the coupled system, a multivariable decoupling control scheme for milling system is designed based on multivariate predictive control algorithm; since the change of coal feed flow affects both the primary air temperature and primary air flow, the coal feed flow is used as feedforward to improve the accuracy of the prediction model. The details are as shown in Fig.2.

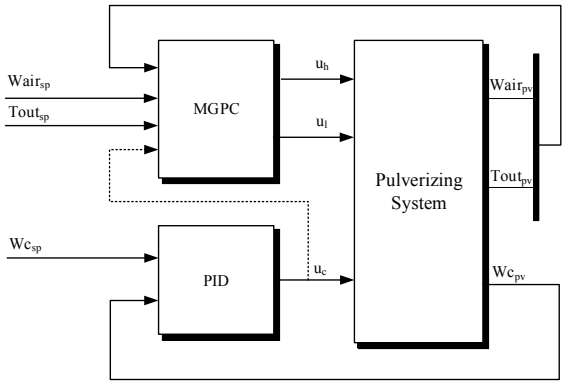

Fig.2 Overall control scheme for the pulverizing system

IV. SIMULATION AND VALIDATION

In order to verify the effectiveness and accuracy of the control scheme, a simulation experiment was conducted on the mill outlet temperature, primary air flow, and coal powder flow at the outlet of the mill respectively, and a 1% white noise was added to the coal supply to reproduce the internal coal disturbance. The specific verification process is as follows:

(1) At 500 seconds, the set value of the pulverized coal flow rate at the mill outlet was increased from 9.67 kg/s to 11.36 kg/s, while keeping the other set values constant. As can be seen from Figure 6, the opening of the cold air valve is reduced, and the opening of the hot air valve is increased, this is due to the increase in the amount of coal feed flow requires more energy to dry the raw coal (Figs.3); the increased coal feed flow causes the action of cold and hot air valve, thereby resulting in a temporary deviation of primary air flow and mill outlet temperatures (Figs.4); and it can be seen from Fig. 5 that since the set value of mill outlet temperature is constant, the pulverized coal moisture quickly recovers after a temporary deviation.

(2) At 1500 seconds, the set value of mill outlet temperature was increased from 71.98°C to 75.98°C, while keeping the other set values constant. as can be seen from Figure 3-4, the opening of the cold air valve is reduced, and the opening of the hot air valve is increased, the mill outlet temperature rises and stabilizes to its set value; as the temperature of the mill outlet rises, the pulverized coal is sufficiently dried, resulting in a decrease in pulverized coal moisture and stabilizing to a new steady state value (Fig. 5).

(3) At 2500 seconds, the set value of primary air flow was increased from 24.6 kg/s to 28.91 kg/s, while keeping the other set values constant. As can be seen from Figure 3-4, the hot and cold air flaps are opened at the same time, and the primary air flow rate increases and stabilizes to its new set value.

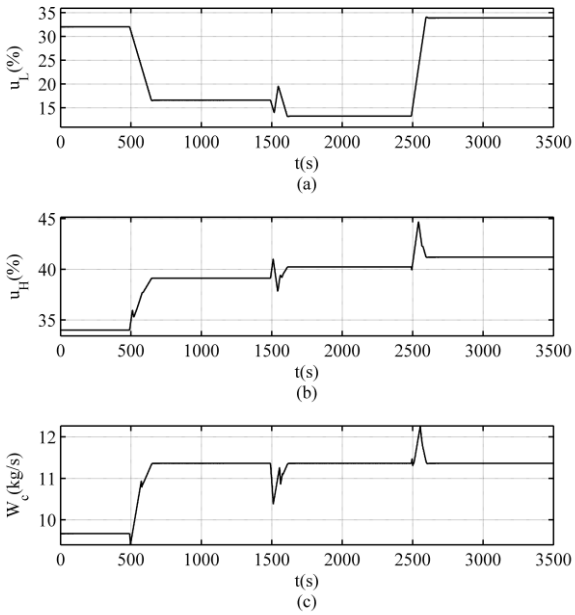

Fig.3 Curve for control variables

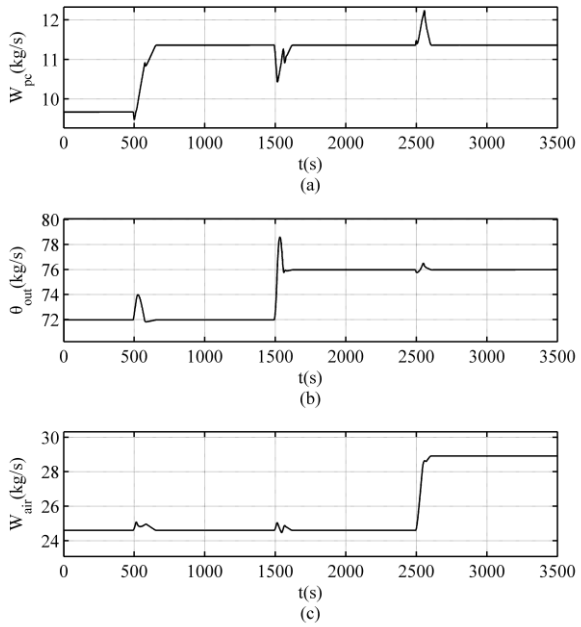

Fig.4 Curve for controlled variables

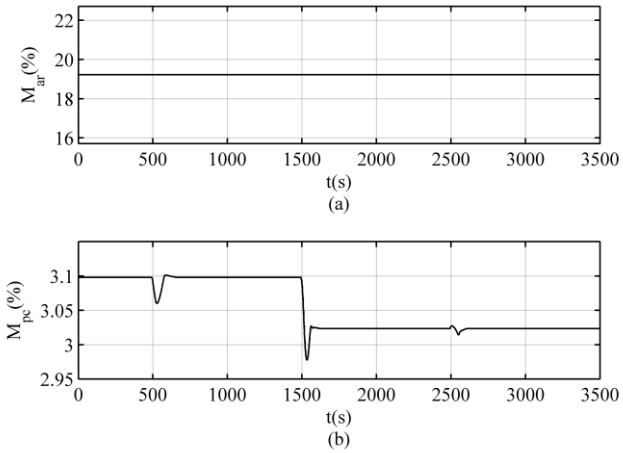

Fig.5 Moisture of Raw coal and coal powder

V. CONCLUSION

In this paper, a control scheme for the pulverizing system based on stair-like multivariable generalized predictive control algorithm is designed. This scheme focuses on the problem of predictive control algorithm in practical application, the pulverized coal at the outlet of coal mill is proposed as a new control target of the pulverizing system's output. Simulation results showed that the scheme can realize decoupling control of the pulverizing system, avoid the problem of matrix inversion, reduce the amount of calculation, and has certain engineering application value, which is of great significance for realizing the clean and efficient utilization of coal in thermal power plants.

REFERENCES

[1] Bugge J, Kjær S, Blum R. High-efficiency coal-fired power plants development and perspectives[J]. Energy, 2006, 31(10): 1437-1445.

[2] Xu C, Yuan Y. Analysis of present operating situation of large size coal-fired utility boilers[J]. Electric Power, 2003, 1: 000.

[3] Sun L, Sun J, Miao Y, et al. Application Research of PID-GPC Algorithm in the Ball Mill System[J]. Open Automation & Control Systems Journal, 2015, 7(1):157-166.

[4] Fei M, Zhang J. Robust Fuzzy Tracking Control Simulation of Medium-speed Pulverizer[M]. Systems Modeling and Simulation. Springer Japan, 2007: 78-82.

[5] Zeng D, Hu Y, Gao S, et al. Modelling and control of pulverizing system considering coal moisture[J]. Energy, 2015, 80: 55-63.

[6] Gao Y, Zeng D, Liu J, et al. Optimization control of a pulverizing system on the basis of the estimation of the outlet coal powder flow of a coal mill[J]. Control Engineering Practice, 2017, 63:69-80.

[7] Gao Y, Zeng D, Liu J. Modeling of a medium speed coal mill[J]. Powder Technology, 2017.

[8] Xiaotian L I, Xin W, Wang Z, et al. A stair-like generalized predictive control algorithm based on multiple models switching[J]. Ciesc Journal, 2012, 63(1):193-197.

[9] Wu G, Peng L X, Sun D M. Application of stair-like generalized predictive control to industrial boiler[C]// IEEE International Symposium on Industrial Electronics. IEEE, 1992:218-221 vol.1.

[10] Qiu X, Xue M, Sun D, et al. The stair-like generalized predictive control for main-steam pressure of boiler in steam-power plant[C]// Intelligent Control and Automation, 2000. Proceedings of the, World Congress on. IEEE Xplore, 2000:3165-3167 vol.5.

Comparison of Solvers Performance for Load Flow Analysis

Vishnu Suresh

***Abstract*—Load flow studies are carried out in order to find a steady state solution of a power system network. It is done to continuously monitor the system and decide upon future expansion of the system. The parameters of the system monitored are voltage magnitude, voltage angle, active and reactive power. This paper presents techniques used in order to obtain such parameters for a standard IEEE – 30 bus and IEEE-57 bus network and makes a comparison into the differences with regard to computational time and performance of each solver. The objective being to first understand the working of each solver and then come to conclusions regarding the best one keeping in mind the network size and complexity so that it can extended to bigger networks for analysis. The methods are evaluated in this study using Matpower which is a tool meant for academical purposes and not intended for on-line use.**

***Index Terms*—Load flow, IEEE 30 bus, IEEE 57 bus Numerical methods.**

I. Introduction

THE load flow problem is an important tool for the operation and control of power systems. It gives the system operator information regarding active power, reactive power demand and consumption, voltage magnitude and voltage angle at every bus within the system which enables the operator to execute an appropriate schedule for dispatch of power. This information is also useful while planning expansion of power systems and helps maintain power system stability [1].

There are many techniques in-order to address the load flow problem [2-4], the techniques are numerical methods that are used to solve non-linear equations in order to obtain the steady state parameters of the system. In [5] network design and load flow analysis were carried out using ETAP and the resulting conclusions were taken as considerations for future expansion of power systems. In [6] load flow studies are performed using Newton-Raphson and decoupled load flow methods and a comparison is made amongst systems with and without unified power system controllers. [7] used '*Distflow*' for comparison of different numerical methods based solvers for the load flow problem. [8] uses a power system analysis toolbox called '*Mipower*' to study the performance of Gauss-Seidel method on an IEEE-3 Bus system. [9] presents a unique power flow iterative algorithm and it is applied to a modified IEEE – 30 consisting of two wind farms in order to validate the model. [10] provides a novel method called Nonsy load flow in which the study has conducted load flow analysis using data that is unsynchronized and is obtained from diesel generators and the main substation in their network. Once this data is obtained other parameters of the network are solved using backward/forward sweep methods. This study makes a comparison of the performance of the methods using Matpower applied to two standard IEEE test bus cases.

Matpower is a useful toolbox in Matlab to solve the load flow problem, it is developed by the power system engineering research center at Cornell University [4]. It is intended for academical use and understanding the different methods for solving load flow problems.

In this paper we compare solving of the load flow problem for a standard IEEE-30 and 57 bus test cases using Gauss-Seidel, Newton-Raphson and Fast decoupled load flow (FDLF) techniques in Matpower and come to conclusions regarding the characteristics of each method. The reason for taking two test cases is to understand how the performance of the solvers varies with increased network size and complexity. Moreover, such a comparison would enable the choosing an appropriate solver for analysis of city sized networks.

The version of Matpower used is 7.0b1, installed in Matlab 2018b in a Windows 10 64-bit system with an i5 core processor. The computational time in this study indicates the overall time take to obtain the solution whereas performance of each solver indicates the time taken per iteration and computational burden refers to the memory that is needed to run each solver. Convergence is defined as a property of a solver to reach the solution vector, It represents the ability of a function to approach a limit as terms in the series increases.

The IEEE-30 bus test case system has a total of 6 generators, 24 loads, transmission lines at 1kV, 11kV, 33kV and 132kV along with capacitor banks at certain buses for reactive power compensation. The IEEE-57 bus test case system has a total of 7 generators, 50 loads, transmission lines along with capacitor banks at certain buses for reactive power compensation. The test systems serve as a representative model to carry out power system studies and load flow analysis. The load flow problem involves solving for 4 parameters at every bus: active power(P_i), reactive power (Q_i), voltage magnitude (V_i) and voltage angle (δ_i) where $i = 1,2,.....,n$ denotes the number of buses and if there are n buses then the total number of variables to be ascertained are $4n$, but power flow studies usually assume bus types which usually

Vishnu Suresh, PhD candidate – Wroclaw University of Science and Technology, Faculty of Electrical Engineering, Wybrzeze Wyspianskiego 27,50-370 Wroclaw, E-mail: vishnu.suresh@pwr.edu.pl.

keeps 2 out of 4 variables as constants, thereby reducing the number of variables to be solved to 2*n*. The bus types are summarized below [2, 3]:

- PQ bus/Load bus: In this type of bus the total active power (P_i) and reactive power (Q_i) at the bus are known, and is calculated as a difference between the active and reactive power injected and consumed in a bus. Hence, the variables to be determined include voltage magnitude (V_i) and voltage angle (δ_i).
- PV bus/Voltage controlled bus/Generator bus: This type of bus is usually preferred for power generating sources. Here, the total active power injected and consumed is known (P_i) and the voltage magnitude is maintained at a particular value by means of reactive power injection. Hence, the unknown variables are total reactive power at the bus (Q_i) and voltage angle (δ_i).
- Swing bus/Slack bus/ Reference bus: In this type of bus the voltage magnitude (V_i) and the voltage angle (δ_i) are known and the active power (P_i) and reactive power (Q_i) are unknown. The slack bus is in-fact a fictitious concept that is created by a power system analyst in order to study the system [2]. In any load flow study, the total active and reactive power (complex power) at every bus is not known since the net complex power flow within the system is unknown including the total loses along transmission lines. Therefore, it is a convention to choose the largest generator in a system to be the slack bus as it is understood that it is capable of producing active and reactive power according to the needs of the system. There is usually only one such bus chosen in a system as a reference.

In the IEEE test bus cases, the largest generator is chosen as the slack bus and the other sources are chosen as PV buses whereas the loads are modeled as load buses. Once the buses are decided the equations to solve are (1).

$$P_i = |V_i| \sum_{k=1}^{n} |V_k||Y_{ik}| \cos(\theta_{ik} + \delta_k - \delta_i) \quad (1)$$

$$Q_i = -|V_i| \sum_{k=1}^{n} |V_k||Y_{ik}| \sin(\theta_{ik} + \delta_k - \delta_i) \quad (2)$$

Where, $i = 1,2,\ldots..,n$. Y_{ik} – represents self and mutual admittances, between buses i and k and forms the bus admittance matrix Y_{bus} that is crucial to obtain the load flow solution.

In order for static load flow equations to match reality as close as possible it is important to incorporate limits pertaining to all components in the network. The constraints are described as follows:

- Voltage magnitude constraints

$$|Vi|_{min} \leq |Vi| \leq |Vi|_{max} \quad (3)$$

- Voltage angle constraints

$$|\delta i - \delta k| \leq |\delta i - \delta k|_{max} \quad (4)$$

This difference with regard to difference of angle during transfer of power between buses i and k is important for system stability.

- Constraints of sources to generate active and reactive power

$$(P_{gi})_{min} \leq P_i \leq (P_{gi})_{max} \quad (5)$$

$$(Q_{gi})_{min} \leq Q_i \leq (Q_{gi})_{max} \quad (6)$$

P_{gi} and Q_{gi} are the active and reactive power generated at bus i

II. Numerical solvers

A. Gauss-Seidel method

This method is used to solve a set of non-linear algebraic equations. It is an iterative method and begins with an assumption of a solution vector. The assumption is made with regard to practical considerations. Revised value of a variable is obtained by substituting in one of the equations in (1) the remaining present variables of the solution vector. Then the solution vector is immediately updated with this new revised variable. This process is done for all variables in the solution vector in one iteration. The iterations continue until a certain degree of accuracy of the solution vector is obtained. The Gauss-Seidel method is very simple in terms of its usage to solve non-linear equations, also it is not necessary to store data from previous iterations to go to the next iteration. On the other hand, this method is very sensitive to the initial assumption of the solution vector, hence the speed of convergence depends on the closeness of the solution vector to the actual solution. In certain cases when the assumption is highly inaccurate the method might fail to converge [2, 3].

The application of this method to the power system is as follows:

1. First, the load demand (P_{di} and Q_{di}) are obtained at all buses, then keeping relevant constraints in mind the active and reactive power generations (P_{gi} and Q_{gi}) are allocated at all generating stations and since the largest generating station is kept as a reference bus the active and reactive power generation at this bus is allowed to change during the iterations.
2. The bus admittance matrix Y_{bus} is assembled with the available line and shunt admittance data
3. To begin the iterative process a flat voltage start is assumed and all buses are set to a voltage magnitude and angle of $1\angle 0^{o}$. Then the voltages at every bus is recalculate by a rearranged version of equation (1) and the iterations continue until an acceptable accuracy is obtained.

$$v_i^{p+1} - v_i^{p} < \varepsilon$$

4. Once the voltage values of all buses are known then active and reactive power at the slack bus is obtained.
5. The last step of the process involves calculating the losses of the system using the line and shunt admittance data along with the known voltage values.

These steps describe the method to obtain all parameters for PQ buses since it begins with an assumption of active and reactive power demand and consumption at every bus. For PV buses the iterative method is different with regard to the assumptions made at the beginning of the iterative process, the detailed procedure is described in [3].

B. Newton-Raphson method

This is a powerful tool for solving a set of non-linear equations, the advantages of this method are that it is not sensitive to the assumption of the solution vector made. The

solution in this case converges in most cases as compared to the Gauss-Seidel method and it is done in a fewer number of iterations. The drawback of this method is increased computational burden and the need of additional storage space since it involves calculation of Jacobian matrices and storage of values of previous iterations.

At any iteration, the function is approximated by a tangent hyperplane and the problem is linearized into a Jacobian-matrix equation [3]. The Jacobian matrix consists of slopes of the tangent hyperplanes.

$$F(X) = — J.\Delta X \quad (7)$$

The problem is solved for the correction ΔX - the correction solved is then added to the previous value of X, so the new updated value is closer to the solution and this iteration process continues until an acceptable accuracy is obtained and the correction values in subsequent iterations are very small.

The application of this method to the power system will be as follows:

1. For a PQ bus for which the values of active and reactive power are known (P_i and Q_i), an initial assumption of the solution for V_i and δ_i is made. Substituting these values in equation (1) the calculated values for P_i and Q_i are obtained then the corrected values are calculated.

$$\Delta P_i = P_{specified} - P_{calculated} \quad (8)$$

$$\Delta Q_i = Q_{specified} - Q_{calculated} \quad (9)$$

   These values ΔP_i and ΔQ_i correspond to F(X) in (6) and the corrected values for V_i and δ_i can be obtained by solving (6).
2. At the slack bus the values of voltage magnitude and angle V_i and δ_i is fixed. Hence, there would be no equations pertaining to the slack bus in the Jacobian.
3. Once the corrected values ΔV_i and $\Delta \delta_i$ are obtained, the next iteration is carried out by adding these corrected values to the previous values of V_i and δ_i and step 1 is repeated. This process continues until the corrected values are very small pertaining to an accuracy that is acceptable.
4. PV buses have constant voltage magnitude and active power at every bus and the iterative process is carried out to obtain values for reactive power and voltage angle.

C. *Fast decoupled load flow methods.*

In transmission systems there is always an interdependence between the voltage angle and active power (*δ-P)* and between voltage magnitude and reactive power (*V-Q).* Hence, the coupling amongst *δ-P* and *V-Q* is weak and this can be exploited in order to make the load flow problem simpler and reduce the computational burden on processing software. This can be done by solving the *δ-P* and *V-Q* problems separately, that is to have two small submatrices for the variables and it is the basis for the decoupled load flow methods. The Jacobian that is formulated in the Newton-Raphson method as mentioned above is simplified by eliminating the elements with weak coupling and it is usually about half of the elements that are eliminated in this manner. This could affect the true convergence of the solution but there is a trade-off between solution accuracy and reduced computational burden which is acceptable [2, 3].

III. LOAD FLOW ANALYSIS

Load flow analysis will be carried out for all three methods mentioned above on IEEE-30 bus and IEEE-57 bus test cases and the results of each will be discussed in-order to understand the advantages and disadvantages of both.

A. *IEEE-30 bus*

The summary of load flow analysis of the ieee-30 bus test case, including the total amount of active and reactive power generated, consumed and line losses using Gauss-Seidel, Newton-Raphson and FDLF methods are presented in Figures 1-3 respectively. The Gauss-Seidel method was able to arrive at the solution in 492 iterations and 0.45 seconds.

The Newton-Raphson method was able to arrive at the solution in 2 iterations and 0.14 seconds.

The FDLF method was able to arrive at the solution in 7 P-iterations and 6 Q-iterations with a total of 13 iterations and in 0.16 seconds. This method takes advantage of the weak coupling between *δ-P* and *V-Q,* hence the equations for both set of variables are solved separately and the number of iterations for the solution also differ.

```
Gauss-Seidel power flow converged in 492 iterations.

Converged in 0.45 seconds
================================================================================
|     System Summary                                                          |
================================================================================

How many?                How much?              P (MW)            Q (MVAr)
---------------------    --------------------  -------------  -----------------
Buses             30     Total Gen Capacity     900.2         -102.0 to 188.0
Generators         6     On-line Capacity       900.2         -102.0 to 188.0
Committed Gens     6     Generation (actual)    301.0              133.9
Loads             21     Load                   283.4              126.2
  Fixed           21       Fixed                283.4              126.2
  Dispatchable     0       Dispatchable          -0.0 of -0.0       -0.0
Shunts             2     Shunt (inj)            -0.0               25.3
Branches          41     Losses (I^2 * Z)       17.56              67.69
Transformers       4     Branch Charging (inj)    -                34.7
Inter-ties         0     Total Inter-tie Flow    0.0                0.0
Areas              1
```

Figure 1. System summary and load flow analysis using Gauss – Seidel numerical method.

```
Newton's method power flow converged in 2 iterations.

Converged in 0.14 seconds
================================================================================
|     System Summary                                                          |
================================================================================

How many?                How much?              P (MW)            Q (MVAr)
---------------------    --------------------  -------------  -----------------
Buses             30     Total Gen Capacity     900.2         -102.0 to 188.0
Generators         6     On-line Capacity       900.2         -102.0 to 188.0
Committed Gens     6     Generation (actual)    301.0              133.9
Loads             21     Load                   283.4              126.2
  Fixed           21       Fixed                283.4              126.2
  Dispatchable     0       Dispatchable          -0.0 of -0.0       -0.0
Shunts             2     Shunt (inj)            -0.0               25.3
Branches          41     Losses (I^2 * Z)       17.56              67.69
Transformers       4     Branch Charging (inj)    -                34.7
Inter-ties         0     Total Inter-tie Flow    0.0                0.0
Areas              1

                          Minimum                      Maximum
                  ------------------------  -------------------------------
Voltage Magnitude   0.992 p.u. @ bus 30      1.082 p.u. @ bus 11
Voltage Angle     -17.64 deg   @ bus 30      0.00 deg   @ bus 1
P Losses (I^2*R)             -              5.21 MW    @ line 1-2
Q Losses (I^2*X)             -              15.61 MVAr  @ line 1-2
```

Figure 2. System summary and load flow analysis using Newton-Raphson numerical method

```
Fast-decoupled power flow converged in 7 P-iterations and 6 Q-iterations.

Converged in 0.16 seconds
================================================================================
|     System Summary                                                          |
================================================================================

How many?               How much?              P (MW)            Q (MVAr)
---------------------   --------------------  -------------  -----------------
Buses              30   Total Gen Capacity      900.2         -102.0 to 188.0
Generators          6   On-line Capacity        900.2         -102.0 to 188.0
Committed Gens      6   Generation (actual)     301.0              133.9
Loads              21   Load                    283.4              126.2
  Fixed            21     Fixed                 283.4              126.2
  Dispatchable      0     Dispatchable          -0.0 of -0.0       -0.0
Shunts              2   Shunt (inj)             -0.0               25.3
Branches           41   Losses (I^2 * Z)         17.56             67.69
Transformers        4   Branch Charging (inj)     -                34.7
Inter-ties          0   Total Inter-tie Flow      0.0               0.0
Areas               1

                          Minimum                      Maximum
                   -------------------------  -------------------------------
Voltage Magnitude    0.992 p.u. @ bus 30        1.082 p.u. @ bus 11
Voltage Angle      -17.64 deg   @ bus 30        0.00 deg   @ bus 1
P Losses (I^2*R)             -                5.21 MW    @ line 1-2
Q Losses (I^2*X)             -               15.61 MVAr  @ line 1-2
```

Figure 3. System summary and load flow analysis using Fast decoupled load flow method

B. IEEE-57 bus

To study the effects of increasing the network size on the performance of numerical solvers, the IEEE-57 bus test case is used and the results are compared with those obtained from the IEEE-30 bus test case. Figures 4-6 represent load flow summary, including the total amount of active and reactive power generated, consumed and line losses using the all 3 methods respectively. The Gauss-Seidel method was able to arrive at the solution in 518 iterations and 0.59 seconds

```
Gauss-Seidel power flow converged in 518 iterations.

Converged in 0.59 seconds
================================================================================
|     System Summary                                                          |
================================================================================

How many?               How much?              P (MW)            Q (MVAr)
---------------------   --------------------  -------------  -----------------
Buses              57   Total Gen Capacity     1975.9         -468.0 to 699.0
Generators          7   On-line Capacity       1975.9         -468.0 to 699.0
Committed Gens      7   Generation (actual)    1278.7              321.1
Loads              42   Load                   1250.8              336.4
  Fixed            42     Fixed                1250.8              336.4
  Dispatchable      0     Dispatchable           -0.0 of -0.0       -0.0
Shunts              3   Shunt (inj)              -0.0               21.6
Branches           80   Losses (I^2 * Z)         27.86             121.67
Transformers       17   Branch Charging (inj)     -                115.3
Inter-ties          0   Total Inter-tie Flow      0.0               0.0
Areas               1

                          Minimum                      Maximum
                   -------------------------  -------------------------------
Voltage Magnitude    0.936 p.u. @ bus 31        1.060 p.u. @ bus 46
Voltage Angle      -19.38 deg   @ bus 31        0.00 deg   @ bus 1
P Losses (I^2*R)             -                3.90 MW    @ line 1-15
Q Losses (I^2*X)             -               19.96 MVAr  @ line 1-15
```

Figure 4. System summary and load flow analysis using Gauss – Seidel numerical method

```
Newton's method power flow converged in 3 iterations.

Converged in 0.15 seconds
================================================================================
|     System Summary                                                          |
================================================================================

How many?               How much?              P (MW)            Q (MVAr)
---------------------   --------------------  -------------  -----------------
Buses              57   Total Gen Capacity     1975.9         -468.0 to 699.0
Generators          7   On-line Capacity       1975.9         -468.0 to 699.0
Committed Gens      7   Generation (actual)    1278.7              321.1
Loads              42   Load                   1250.8              336.4
  Fixed            42     Fixed                1250.8              336.4
  Dispatchable      0     Dispatchable           -0.0 of -0.0       -0.0
Shunts              3   Shunt (inj)              -0.0               21.6
Branches           80   Losses (I^2 * Z)         27.86             121.67
Transformers       17   Branch Charging (inj)     -                115.3
Inter-ties          0   Total Inter-tie Flow      0.0               0.0
Areas               1

                          Minimum                      Maximum
                   -------------------------  -------------------------------
Voltage Magnitude    0.936 p.u. @ bus 31        1.060 p.u. @ bus 46
Voltage Angle      -19.38 deg   @ bus 31        0.00 deg   @ bus 1
P Losses (I^2*R)             -                3.90 MW    @ line 1-15
Q Losses (I^2*X)             -               19.96 MVAr  @ line 1-15
```

Figure 5. System summary and load flow analysis using Newton-Raphson method

```
Fast-decoupled power flow converged in 7 P-iterations and 7 Q-iterations.

Converged in 0.17 seconds
================================================================================
|     System Summary                                                          |
================================================================================

How many?               How much?              P (MW)            Q (MVAr)
---------------------   --------------------  -------------  -----------------
Buses              57   Total Gen Capacity     1975.9         -468.0 to 699.0
Generators          7   On-line Capacity       1975.9         -468.0 to 699.0
Committed Gens      7   Generation (actual)    1278.7              321.1
Loads              42   Load                   1250.8              336.4
  Fixed            42     Fixed                1250.8              336.4
  Dispatchable      0     Dispatchable           -0.0 of -0.0       -0.0
Shunts              3   Shunt (inj)              -0.0               21.6
Branches           80   Losses (I^2 * Z)         27.86             121.67
Transformers       17   Branch Charging (inj)     -                115.3
Inter-ties          0   Total Inter-tie Flow      0.0               0.0
Areas               1

                          Minimum                      Maximum
                   -------------------------  -------------------------------
Voltage Magnitude    0.936 p.u. @ bus 31        1.060 p.u. @ bus 46
Voltage Angle      -19.38 deg   @ bus 31        0.00 deg   @ bus 1
P Losses (I^2*R)             -                3.90 MW    @ line 1-15
Q Losses (I^2*X)             -               19.96 MVAr  @ line 1-15
```

Figure 6. System summary and load flow analysis using Fast decoupled load flow method.

The Newton-Raphson method was able to arrive at the solution in 3 iterations and 0.15 seconds.

The FDLF method was able to arrive at the solution in 7 P-iterations and 7 Q-iterations with a total of 14 iterations and in 0.17 seconds. This method takes advantage of the weak coupling between δ-P and V-Q, hence the equations for both set of variables are solved separately and the number of iterations for the solution also differ.

C. *Convergence of methods*

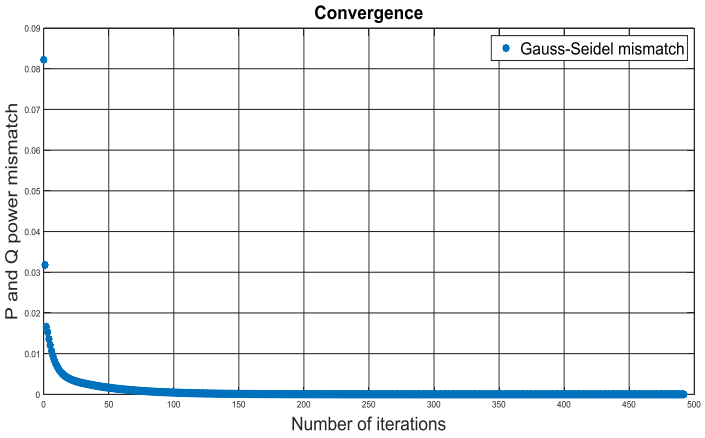

Figure 7. Convergence of Gauss-Seidel method (IEEE-30 bus)

Figure 7 describes the convergence of the Gauss-Seidel method (IEEE-30 bus) and in-comparison with Figure 8 it can be inferred that the slope of convergence is quite gradual in this method and the number of iterations are much higher when compared to the Newton-Raphson and FDLF methods (IEEE – 30 bus) as seen in Figure 8. Figure 8 which describes the convergence of Newton-Raphson and FDLF methods, it can be seen that the Newton-Raphson method takes lesser number of iterations, and from Figure 3 the time taken by the FDLF method is 0.16 seconds compared to 0.14 seconds for the Newton-Raphson method from Figure 2, hence it can be concluded that the per iteration is much higher in the Newton-Raphson method when compared to the FDLF method. This is because the assumptions taken in the FDLF method reduce the computational burden hence accelerating the iterative process. It should also be noted that there is no significant improvement in the overall time taken for the load flow analysis between Newton -Raphson and FDLF methods.

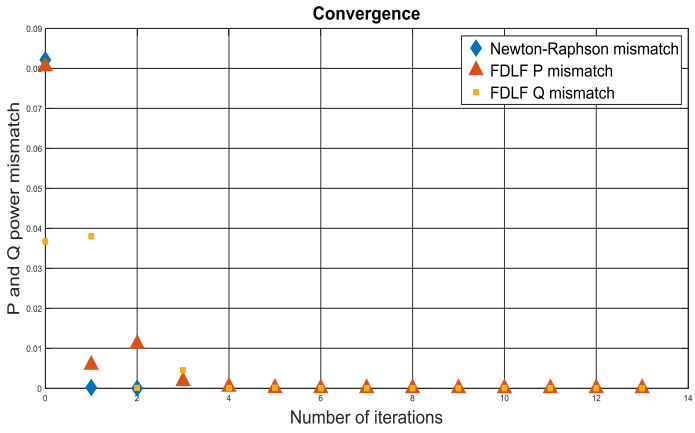

Figure 8. Convergence of Newton-Raphson and FDLF method (IEEE-30 bus)

Figure 9 represents the convergence of the Gauss-Seidel method (IEEE-57 bus) to the solution. It can be noticed that the convergence is gradual and it takes a total of 518 iterations for the method to finish. Figure 10 represents the convergence of the Newton-Raphson and FDLF (IEEE – 57 bus) methods. It can be noticed that the convergence in Figure 10 is much steeper and the solution is obtained in 3 iterations for the Newton-Raphson method and 14 iterations (7 – P iterations and 7 – Q iterations) for the FDLF method.

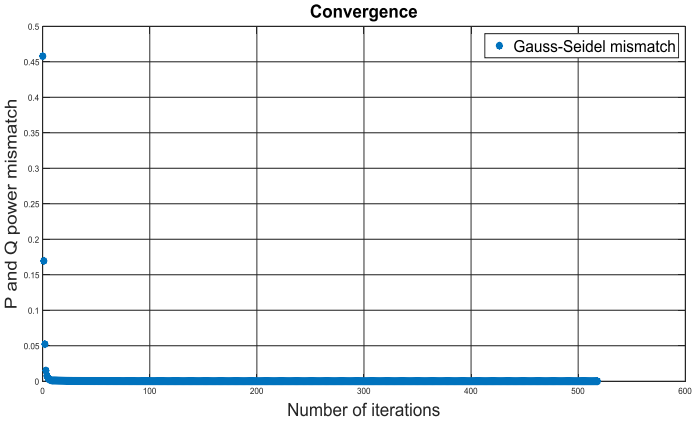

Figure 9. Convergence of Gauss-Seidel method (IEEE-57 bus)

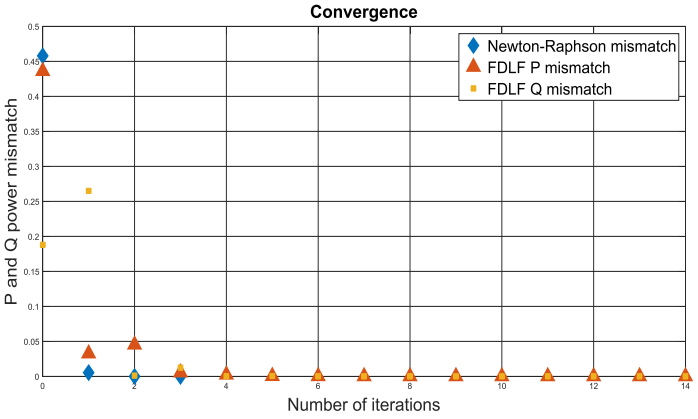

Figure 10. Convergence of Newton-Raphson and FDLF method (IEEE-57 bus)

IV. CONCLUSIONS

A. *Results*

TABLE I
LOAD FLOW RESULTS FOR IEEE – 30 BUS

Characteristics	Gauss-Seidel	Newton-Raphson	FDLF
Iterations	492	2	7 P-iterations 6 Q-iterations Total – 13
Time	0.45	0.14	0.16
Time/iteration	0.0009	0.07	0.0114
Convergence	Gradual	Steep	Steep
Computational burden	Low	High	Higher than Gauss-Seidel, Lower than Newton- Raphson

TABLE II
LOAD FLOW RESULTS FOR IEEE – 57 BUS

Characteristics	Gauss-Seidel	Newton-Raphson	FDLF
Iterations	518	3	7 P-iterations 7 Q-iterations Total – 14
Time	0.59	0.15	0.17
Time/iteration	0.0011	0.05	0.0121
Convergence	Gradual	Steep	Steep
Computational burden	Low	High	Higher than Gauss-Seidel, Lower than Newton-Raphson

B. Discussions

The comparison of different methods to solve the load flow problem yields the following results, the Gauss-Seidel method takes less time to perform one iteration when compared to the Newton-Raphson method, this is because of the fewer number of arithmetic operations involved in completing an iteration, as the calculation of the Jacobian which is an inherent part of the calculations for the Newton-Raphson method. The Newton-Raphson method has a faster rate of convergence because of its quadratic convergence characteristics. The technique is said to 'home-in' to the solution.

For the Gauss-Seidel method the number of iterations increase with the network size i.e. higher the number of buses in the network, the longer it takes for the method to find a solution, this evident from the fact that it takes 518 iterations and 0.59 seconds for the IEEE-57 bus test case to find a solution compared to 492 iterations and 0.45 seconds for the IEEE-30 bus test case. The relationship is not as proportional in the Newton-Raphson method as the time taken for the IEEE-57 test bus case with this method is 0.15 seconds and 3 iterations whereas for the IEEE-30 bus case it is 0.14 seconds and 2 iterations representing only a marginal increase in the computational time. This conclusion holds also for bigger networks with a much higher number of buses [2,3].

The Gauss-Seidel method is relatively easier to implement and does not require a lot of memory, whereas the Newton-Raphson method is complex to implement and does require higher memory and processing capacity.

The Gauss-Seidel method is very sensitive to the selection of the slack bus, In some cases the method is also known to not converge to a solution hence, making the first step of choosing a solution vector very crucial. Inversely, the Newton-Raphson method is not so sensitive to the selection of the slack bus and almost always converges to a solution.

The FDLF method in both cases (IEEE – 30 and 57 bus test cases) takes more iterations and more time to arrive at the solution. It is important to remember that the FDLF method takes into account certain assumptions while searching for the solution making it as fast as the Newton-Raphson method with the advantage of reduced computational needs such as memory and processing capability.

It can be hence concluded that both Newton-Raphson and FDLF methods are efficient and can be extended to bigger and more complex networks but the computational advantage that the FDLF method provides can lead to cost savings. Therefore, the selection of a methods depends on the overall finances involved in solving load flow issues along with speed and accuracy.

Therefore, this paper has described and compared the application of 3 methods in solving the load flow problem for 2 standard IEEE bus test cases and conclusions arrived at commensurate with the objective.

Future study in this regard is to extend the analysis to networks containing renewable energy sources that are unpredictable in their output which makes the load flow problem more complicated and to include time series analysis. The methods can also be executed on other tools and make a comparison as to which tools are most efficient for performing load flow analysis

REFERENCES

[1] Afolabi, O. A., Ali, W. H., Cofie, P., Fuller, J., Obiomon, P., & Kolawole, E. S. (2015). Analysis of the Load Flow Problem in Power System Planning Studies. Energy and Power Engineering, (7), 509–523. https://doi.org/10.4236/epe.2015.710048

[2] Stott, B. (1974). Review of Load-Flow Calculation Methods. Proceedings of the IEEE, 62(7), 916–929. https://doi.org/10.1109/PROC.1974.9544G. O. Young, "Synthetic structure of industrial plastics," in *Plastics,* 2nd ed., vol. 3, J. Peters, Ed. New York: McGraw-Hill, 1964, pp. 15–64.

[3] D. P. Kothari and I. J. Nagrath, "Power System Engineering," 2nd Edition, Tata McGraw Hill, New Delhi, 2007.

[4] R. D. Zimmerman, C. E. Murillo-Sanchez, and R. J. Thomas, \Matpower: Steady- State Operations, Planning and Analysis Tools for Power Systems Research and Education," Power Systems, IEEE Transactions on, vol. 26, no. 1, pp. 12{19, Feb. 2011. DOI: 10.1109/TPWRS.2010.2051168

[5] Prabhu, J. A. X., Sharma, S., Nataraj, M., & Tripathi, D. P. (2016). Design of electrical system based on load flow analysis using ETAP for IEC projects. 2016 IEEE 6th International Conference on Power Systems, ICPS 2016, 1–6. https://doi.org/10.1109/ICPES.2016.7584103.

[6] Model, U. M. (2000). Power Flow Analysis of Power System With Upfc, 00(c), 2–5. Dept. of Electric Power & Automation Engineering Tianjin University, Tianjin (300072)

[7] G.M. Gilbert, D.E. Bouchard, A. Y. C. (2010). Comparison of load. International Journal of Engineering and Advanced Technology, 850–853. Department of Electrical and Computer Engineering Royal Military College of Canada Kingston, Ontario

[8] Kaur, S., Singh, A., & Khela, R. S. (2015). Load Flow Analysis of IEEE-3 bus system by using Mipower Software. International Journal of Engineering Research & Technology (IJERT), 4(03), 9–16.

[9] Phan, T. T., Nguyen, V. L., Hossain, M. J., To, A. N., & Tran, H. T. (2016). An unified iterative algorithm for load flow analysis of power system including wind farms. In L-S. Lê, T. K. Dang, J. Küng, N. Thoai, & R. Wagner (Eds.), 2016 International Conference on Advanced Computing and Applications ACOMP 2016: proceedings (pp. 105-112). Piscataway, NJ: Institute of Electrical and Electronics Engineers (IEEE). https://doi.org/10.1109/ACOMP.2016.024

[10] Bahmanyar, A., Estebsari, A., Bahmanyar, A., & Bompard, E. (2020). Nonsy Load Flow : Smart Grid Load Flow Using Non-Synchronized Measurements. *2017 IEEE International Conference on Environment and Electrical Engineering and 2017 IEEE Industrial and Commercial Power Systems Europe (EEEIC / I&CPS Europe)*, (646568), 1–5. https://doi.org/10.1109/EEEIC.2017.7977509

Literature Survey of Interleaved DC-DC Step-Down Converters for Proton Exchange Membrane Electrolyzer Applications

Vittorio Guida, Damien Guilbert, and Bruno Douine

***Abstract*—Recently, the use of electrolyzers for hydrogen production through water electrolysis is of great interest in the industrial field to replace current hydrogen production pathways based on fossil fuels (e.g. oil, coal). In order to reduce the emission of pollutants into the atmosphere and minimize the cost of electricity, it is preferable to use renewable energy sources (e.g. solar, wind, hydraulic). The electrolyzers must be supplied with a very low DC voltage in order to produce hydrogen from the deionized water. For this reason, DC-DC step-down converters are generally used. However, these topologies present several drawbacks from output current ripple and voltage gain point of view. In order to meet these expectations, interleaved DC-DC step-down converters are considered as promising and interesting candidates to supply proton exchange membrane (PEM) electrolyzers. Indeed, these converters offer some advantages including output current ripple reduction and reliability in case of power switch failures. In addition, over the last decade, many improvements have been brought to these topologies with the aim to enhance their conversion gain. Hence, the main goal of this paper is to carry out a thorough state-of-the-art of different interleaved step-down DC-DC topologies featuring a high voltage gain, needed for PEM electrolyzer applications. Furthermore, a comparison of candidate interleaved step-down converters not only from the voltage ratio point of view but also from the phase and/or output current ripple point of view.**

***Index Terms*— electrolyzer, interleaved converters, renewable sources, conversion ratio, current ripple, energy efficiency, power switch faults, reliability.**

I. Introduction

THE random behavior of the renewable energy sources (RES) makes the hydrogen production and storage an engaging and efficient solution. This is because hydrogen has much higher specific energy than the classical storage devices such as batteries [1]. On planet Earth, there are several resources available for hydrogen production such as fossil fuels (e.g. natural gas and coal), and RES (e.g. biomass and water). However, from an environmental point of view, hydrogen production from fossil fuels (although it does save money) contributes considerably to the release of greenhouse gases and other pollutants into the atmosphere [2]. In this perspective, water is considered an attractive raw material for hydrogen production (having two atoms of hydrogen and one of oxygen, as is well known). Being free of nitrogenous, carbonaceous or sulfured species, water is ideal for hydrogen production, contributing to the reduction of polluting emissions. Among the different hydrogen production processes, starting from water, the most consolidated is electrolysis. Water electrolysis allows obtaining practically pure hydrogen. This process, for which electricity currently has a cost up to three or four times higher than the methane used for steam reforming, becomes economically acceptable as a result of technological innovations and under extremely low-cost conditions of electricity (if electricity is produced from RES) [3]. Water electrolysis is based on an electrochemical reaction using electricity to split water into hydrogen and oxygen; it is carried out by means of an electrolyzer (EL). There are three types of ELs in the literature: proton exchange membrane (PEM) EL, alkaline EL, and solid oxide EL (the latter exists only in the field of research and development) [4].

In order to produce hydrogen from deionized water, the EL must be supplied with a very low DC voltage. Hence, the use of DC-DC converters is decisive to adjust the voltage levels between the EL and the DC bus. Generally, classic DC-DC step-down converters are used for this purpose due to their simplicity and low cost [5,6]. Unfortunately, these converters have several drawbacks from availability in case of electrical failures, output current ripple, conversion ratio, and energy efficiency point of view for EL applications. The same issues have been highlighted regarding classic step-up converters for fuel cell applications [7,8].

Over the last decade, a family of DC-DC step-down converters called interleaved has spread particularly in the research field. Indeed, many interleaved step-down topologies have been proposed in the scientific literature [9-16], bringing improvements (e.g. energy efficiency optimization, output current ripple minimization, and availability in case of electrical failures) compared to the conventional interleaved step-down converter. As it has been mentioned earlier, ELs must be supplied with a very low DC voltage; so interleaved DC-DC step-down converters are suitable for this type of applications.

V. Guida, D. Guilbert, B. Douine are with the Group of Research in Electrical Engineering of Nancy (GREEN), Université de Lorraine, 54500, Vandoeuvre-lès-Nancy, FRANCE (e-mail: vittorio.guida@univ-lorraine.fr , damien.guilbert@univ-lorraine.fr , bruno.douine@univ-lorraine.fr).

Starting from these observations, the main purpose of this work is to carry out a thorough literature survey focused on the family of interleaved DC-DC step-down converters featuring a high voltage gain.

This article is divided into six sections. After this Introduction providing the current state-of-the-art and issues, Section II compares the three existing technologies of ELs with the aim to select the most suitable technology for this study. Then, Section III presents the main requirements of DC-DC converters for EL applications. Afterward, in Section IV, candidate interleaved step-down topologies for EL applications are presented including their advantages and drawbacks. After that, in Section V, a comparison is carried out between candidate interleaved converters, especially from voltage gain and phase and/or output current ripple point of view. Finally, in Section VI, conclusions and perspective of the work are given.

II. Proton Exchange Membrane Technology

Currently, different types of EL can be distinguished by their electrolyte and the charge carrier: (1) alkaline EL; (2) proton exchange membrane (PEM) EL; and (3) solid oxide (SO) EL [2,3]. Table I provides the main features of each technology; while Table II introduces the advantages and drawbacks of each technology. From Tables I and II, alkaline and PEM ELs are currently the two main technologies, which are commercially available. Alkaline ELs are the most mature and widespread compared to PEM ELs (still under development). As highlighted in Tables I and II, alkaline ELs have a higher durability and gas purities, and cheaper catalysts than PEM ELs. However, PEM ELs have several advantages over alkaline ELs, such as compactness, fast system response, wide partial load range and high flexibility in terms of operation. As a result, this technology is an attractive option for integration into the grid including renewable power generating systems [3]. For this reason, PEM ELs are considered within hybrid renewable energy systems and hydrogen production pathways based on renewable energy sources.

III. Main Requirement for DC/DC Converters

Like for fuel cells, DC/DC converters are needed to interface the DC voltage grid and the EL. These converters can be used both for hybrid renewable energy systems (Fig. 1) and hydrogen production pathways based on renewable energy sources (Fig. 2). Generally, a PEM EL needs a very low DC voltage in order to produce hydrogen. Indeed, at rated power, the cell voltage range of a PEM EL is included between 1.75 and 2.2 V [2]. A higher input EL voltage can be obtained by stacking more cells. However, the number of the cells has to be limited in order to guarantee a high reliability of the PEM EL. Currently, this compromise between the EL reliability and its stack voltage (which is the sum of each cell voltage) is a challenging issue for EL applications [4]. Generally, step-down DC/DC converters are used to supply PEM ELs; whereas for fuel cell applications, step-up converters are preferred.

In any systems including a hydrogen buffer storage, DC/DC converter must meet a certain number of requirements,

TABLE I
Main Features of Each Electrolyzer Technology

	Alkaline	PEM	SO
Maturity	Commercial	Commercial medium and small-scale applications	Research and Development
Current density	0.2-0.4 $A{\cdot}cm^{-2}$	0.6-2 $A{\cdot}cm^{-2}$	0.3-0.6 $A{\cdot}cm^{-2}$
Cell area	$<4m^2$	$<0.3\ m^2$	/
Cell voltage	1.8-2.40 V	1.75-2.20 V	/
Hydrogen output pressure	0.05-30 bar	10-30 bar	50 bar
Operating temperature	60-80 °C	50-80 °C	700-800 °C
System efficiency	52-69 %	57-69 %	>90 % (heat and hydrogen) <80% (only for hydrogen)
Indicative system cost	1-1.2 €/W	1.9-2.3 €/W	1.2 €/W
System size range	0.25-760 $Nm^3{\cdot}h^{-1}$ 1.8-5300 kW	0.01-240 $Nm^3{\cdot}h^{-1}$ 0.2-1150 kW	Laboratory scale
Lifetime stack	<90000 h	<60 000 h	≈1000 h

provided below [4]:

1) High energy efficiency.
2) Low electromagnetic disturbances.
3) Reduced cost.
4) High voltage ratio.
5) Low output current ripple (to optimize EL performances).
6) Ability to operate in case of electrical failures.

Among these requirements, the most important feature expected from the DC/DC converter is a high conversion ratio. Indeed, for electrical systems including wind turbines, the DC bus voltage is very high (i.e. between a hundred and a thousand volts) [4]. Besides, current hybrid renewable energy systems with hydrogen storage based on a DC bus configuration are limited to low-power applications due to the use of classic DC/DC converters (buck for PEM EL) [17]. Hence, in order to move towards medium and high-power applications, DC/DC converters must feature high conversion ratio ability [18].

Interleaved step-down DC-DC converter topologies have much to offer for PEM ELs. Some improvements have been reported in the literature to enhance the conversion ratio ability while benefiting low output current ripple, high energy efficiency, and availability in case of electrical failures. Over the last years, many interleaved DC-DC buck converters proposed in the literature [9-16] can be suitable for PEM EL applications. Some candidate topologies with their advantages and drawbacks are presented in the following section.

TABLE II
COMPARISON OF ELECTROLYZER TECHNOLOGIES

	Alkaline	PEM	SO
Advantages	- Mature technology - Long-term stability - High durability and gas purities - Cheaper catalyst - Stacks in the MW range	- High current densities - High voltage efficiency - Fast system response - Compactness - High gas purity - Dynamic operation	- High gas purity - High efficiency - Possible reversibility: operation in fuel cell mode
Drawbacks	- Low current densities - Crossover gases - Low partial load range - Load dynamics - Low operational pressures - Corrosive liquid electrolyte - Low tolerance to impurities in the water	- High cost of components - Technology relatively new - Acidic corrosive environment - Limited durability - Low tolerance to impurities in the water	- Not commercially available (under research and development) - Fragility of materials - Need for a significant heat input - Limited lifetime of ceramics - Long start-up time

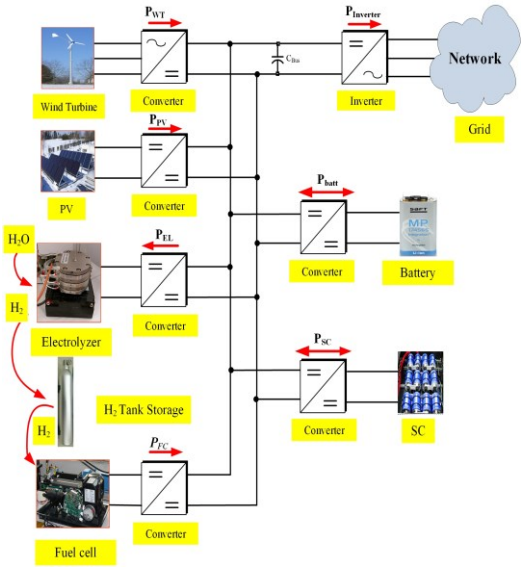

Fig. 1. Hybrid renewable energy system with a hydrogen buffer storage based on a DC bus configuration.

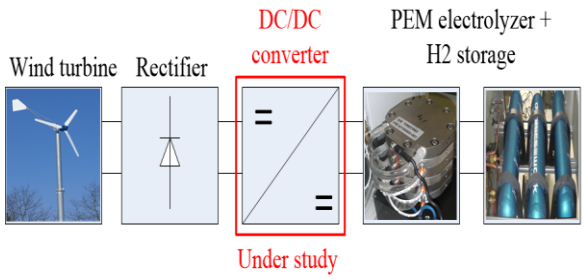

Fig. 2. Hydrogen generation pathways from wind turbines.

IV. CANDIDATE INTERLEAVED DC/DC STEP-DOWN CONVERTERS

A. *Interleaved buck converter*

Based on the classic buck converter, interleaved buck converters can be achieved. These topologies are built by connecting in parallel N buck converters (from N=2 to N=6) with a common DC bus [4]. They present several benefits compared to the classic buck converter, especially from energy efficiency, output current ripple reduction and reliability point of view [4]. Generally, a three-leg interleaved buck converter (IBC) is preferred for optimization reasons (i.e. magnetic component size, output current ripple, energy efficiency) as shown in Fig. 3.

However, IBC topologies present the following drawbacks [4]:

1) Large voltage stresses at the terminals of power switches and diodes (limited energy efficiency).
2) Medium conversion ratio (not suitable for electrolyzers requiring a high voltage ratio).

Over the last decade, many improvements have been brought to the classic IBC, especially from voltage ratio and energy efficiency point of view. These important issues can be solved by modifying the architecture and/or using coupled inductors. In the next subsections, several candidates interleaved buck topologies are presented with the improvements brought to the classic IBC.

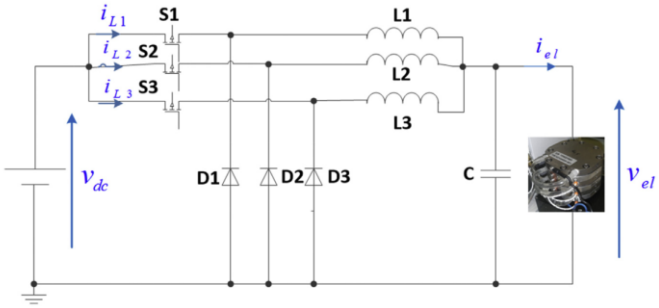

Fig. 3. IBC connected with the electrolyzer.

B. *Interleaved buck converters with a single-capacitor snubber*

The first topology (Fig. 4) differs from the conventional IBC topology for two aspects [9]:

1. a single-capacitor snubber that consists of a resonant capacitor C_1 and either inductor L_1 or L_2;
2. an EI core thanks to which the two coupled inductors (L_1 and L_2) are designed.

The snubber circuit is employed to minimize turn-off losses, switching losses and number of components as well. In addition, it allows limiting the rising rate of the voltage at the terminals of the power switch.

The magnetic core (i.e. EI) is employed to decrease the volume of the converter. Besides, to optimize energy efficiency, the inverse coupling method is used for L_1 and L_2 that leads to better stationary and dynamic performance.

On the one hand, this converter features the same dynamic performance of the classic IBC. On the other hand, IBCs with a single-capacitor snubber can lead up to higher efficiency than conventional IBC for applications requiring a low voltage ratio; whereas for high voltage ratio, the two converters produce approximately the same efficiency.

The voltage ratio of the converter according to the duty cycle D is given by the following equation [9]:

$$\frac{V_o}{V_i} = \frac{(1-D+kD)3D^2}{(7k-3)D^2-(5k-3)D+k} \quad (1)$$

where:

- the coupling coefficient k ($k = M / L$) of the coupled inductors L_1 and L_2 is considered equal to 0.33 [9];
- M is the mutual inductance;

the coupled inductors are made with a symmetric structure ($L_1 = L_2 = L$).

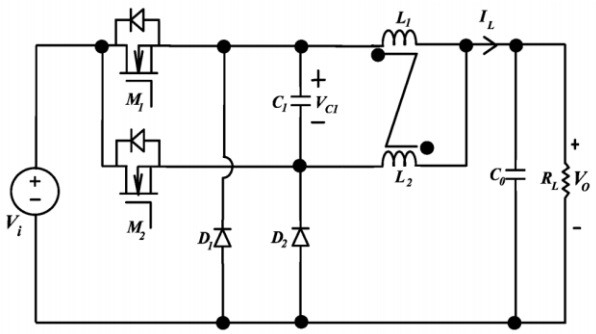

Fig. 4. IBC with a single-capacitor snubber [9].

C. Interleaved buck converter with coupled windings

Compared to the previous topology, the second topology (Fig. 5) is composed of the following elements [10]:

1. two windings coupled with a transformation ratio n, connected to each phase of the converter. Each winding is coupled with the inductance of the corresponding phase;
2. a synchronous IBC composed of two phases.

The addition of the two windings situated before the classic interleaved structure leads to a new topology. It significantly enhances energy efficiency without deteriorating the dynamic response of the converter. Furthermore, it proposes an improved voltage ratio, given by the following expression [10]:

$$\frac{V_o}{V_{in}} = \frac{D}{n+1} \quad (2)$$

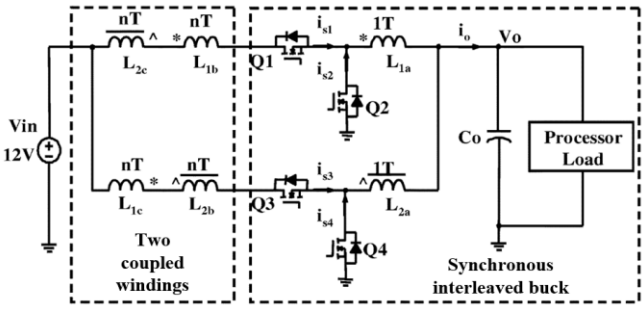

Fig. 5. IBC with coupled windings [10].

D. Interleaved three-level buck converter

The interleaved architecture (Fig. 6) is a three-level DC-DC converter.

In multilevel DC-DC converters, each power switch must withstand only a part of the input voltage and this allows operation with input voltages that are higher than the ratings of the power switches [11].

This topology consists of two interleaved buck converters, each of which includes [11]:

1. the main inductor $L_0/2$;
2. two commutation inductors (L_1, L_2 or L_3, L_4).

The four auxiliary inductors (L_1, L_2, L_3, L_4) allow an important decrease of the power losses related to diode reverse recovery and turn-on transitions at no current.

The interleaved ZCT TL topology is addressed to high-power, high-voltage applications. Furthermore, it can be observed that [11]:

- it can operate at high switching frequencies and this makes easier the design of the output filter;
- all power switches play a part in the power management of the topology and equally divide the electrical power;
- the volume of the converter can be minimized by using coupled inductors.

The converter must operate at duty cycle values smaller than 0.5 permitting the diodes to switch. Otherwise, if the duty cycle is higher than 0.5, the soft switching feature will not be ensured. The conversion gain of the converter is obtained by the following equation [11]:

$$\frac{V_o}{V_{in}} = \frac{2D}{1+\frac{2R_e}{R_o}} \quad (3)$$

where:

- R_e is the lossless resistance ($R_e = 2L_c / T_s$);
- T_s is the switching period;
- L_c is the commutation inductance (if $L_1 = L_2 = L_3 = L_4 = L$: without coupled inductors, $L_c = 2L$, instead of with coupled inductors, $L_c = 4L$);
- R_o is the output load resistance.

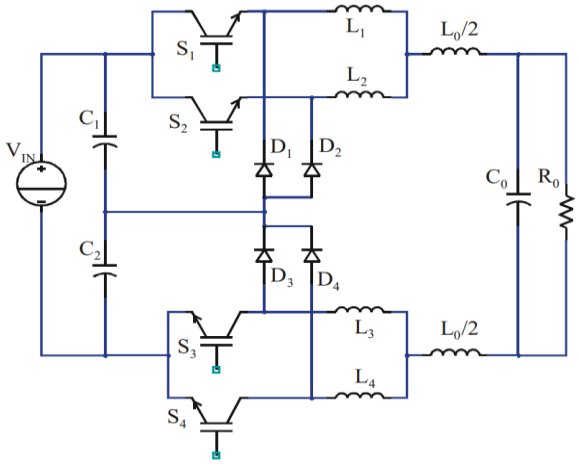

Fig. 6. Interleaved zero current transition (ZCT) three-level (TL) buck converter [11].

E. *Interleaved zero-current-transition buck converter*

The topology (Fig. 7) is an interleaved ZCT buck converter. It differs from the conventional topology since there is an output inductance L_o.

The auxiliary inductors L_1 and L_2 set the current slopes during the switching phases. As the result, these inductors impact the losses related to diode reverse recovery issues. Furthermore, the additional turn-on losses, related to the amount of the leakage diode current, can be guided by the appropriate choice of the auxiliary inductors. The larger the magnetic components (L_1 and L_2), the smaller the reverse recovery and leakage currents. However, the switching times last longer and therefore it is needed to find a compromise [12]. Moreover, these auxiliary magnetic components enable ZCT turn-on.

The output inductor L_o, which is larger than the inductors L_1 and L_2, allows operating at a continuous conduction mode with low output current ripple.

The two power switches contribute towards the power management of the converter. Hence, it makes easier the thermal design and leads to a significant reduction of losses.

Finally, the conversion gain of the converter is provided by the following equation [12]:

$$\frac{V_o}{V_{in}} \approx 2D \tag{4}$$

Equation (4) clearly emphasizes that the complete range of conversion gains ($0 < V_o/V_{in} < 1$) can be achieved by operating each power switch with a duty cycle value included between 0 and 0.5 [12].

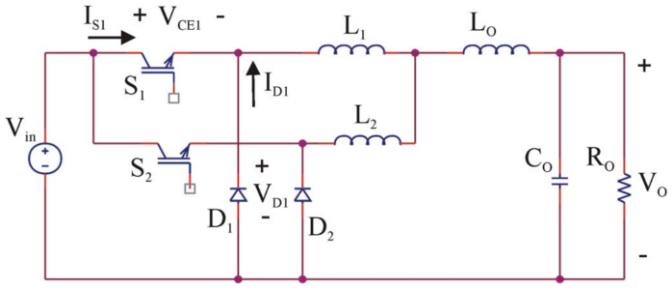

Fig. 7. Interleaved zero-current-transition (ZCT) buck converter [12].

F. *Stacked interleaved converter*

The converter (Fig. 8) is the stacked interleaved topology and it differs from the conventional topology since there is a capacitor (C_S) in the secondary phase.

The capacitor located in the second phase (C_S) stops from flowing the continuous load current from the second phase, making the continuous current for the first phase. This aspect is useful for practical applications where the magnetic components have various parasitic resistances leading up to increasing losses in the secondary phase [13].

The first advantage of the stacked interleaved topology is that it allows a full suppression of the output current ripple whatever the duty cycle values, reducing the needed phases to two (unlike conventional IBC topologies where the number of cancellations strongly depends on the duty cycle and the number of phases).

This current ripple cancellation is achieved through the following components and operation [13]:

- the first phase (S_P, L_P, C_P) connected with the load and operating with a duty cycle D;
- the second phase (S_S, L_S, C_S) no connected with the load and operating with a duty cycle 1-D;

and with the timing chart shown in Fig. 8.

Eliminating the output current ripple, it allows removing the relation between the current ripple of the inductors (L_P and L_S) and the output voltage ripple. As a result, the inductors are smaller than inductors met in IBC. Additionally, the volume reduction of inductors brings more compactness and enhances the dynamic response of the topology.

Connecting the two phases together through a capacitor (C_S), it allows obtaining two different voltages. Indeed, the voltage ratios of the converter are given by the following expressions, respectively for the first and second phase [13]:

$$\frac{V_{OUT}}{V_{IN}} = D \tag{5}$$

and

$$\frac{V_{OUT}}{V_{IN}} = 1 - D \tag{6}$$

The stacked interleaved topology allows coupling the two inductors L_P and L_S. In this case, this coupling permits the reduction of the volume of the inductance, and the attenuation of the current ripple flowing through each inductor.

Therefore, by reducing the current ripple, energy efficiency is improved. In addition, another advantage of using magnetic coupling is the area reduction by stacking the inductors [13].

Finally, as highlighted in [13], all the process effects occurring in a practical implementation, the non-idealities of the converter bring about a delay between the switching transitions. Any overlaps lead up to high current ripples depending on the gain of the magnetic coupling and the duration of the overlaps. The higher the current ripple, the lower the energy efficiency of the converter. In summary, the gain of magnetic coupling has to be chosen judiciously to reduce the effects of time errors [13].

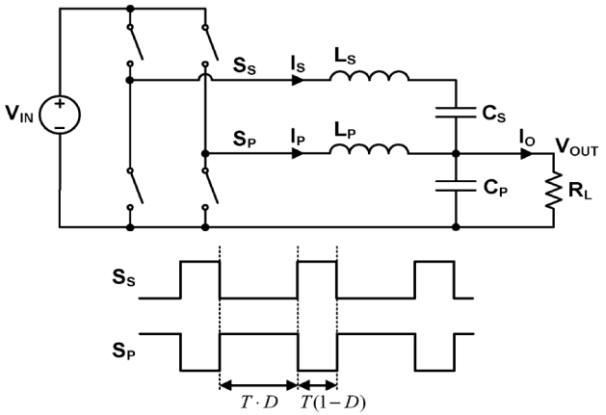

Fig. 8. Stacked interleaved topology and timing chart [13].

G. Interleaved buck converter with winding-cross-coupled inductors and passive-lossless clamp scheme

The topology depicted in Fig. 9 differs from the conventional IBC topology for two aspects:

1. a basic cell with WCCIs and interleaved architecture;
2. a passive-lossless clamp circuit.

The basic cell has two WCCIs (L_1 and L_2). Each WCCI has three windings (L_{1a}, L_{1b}, L_{2c} and L_{2a}, L_{2b}, L_{1c}). The second winding with n_2 turns is linked with the winding in its phase with n_1 turns (L_{1b} versus L_{1a} and L_{2b} versus L_{2a}) and the third winding with n_2 turns is linked with the windings in another phase (L_{1c} versus L_{1a} and L_{1b}, L_{2c} versus L_{2a} and L_{2b}) [14]. The first windings L_{1a} and L_{2a} have similar features as the magnetic components in the basic IBC. The second and the third windings (L_{1b}, L_{1c}, and L_{2b}, L_{2c}) are used as continuous voltage sources and are in series in the circuit to alleviate the power switch voltage stress [14]. Moreover, the use of these windings allows achieving high step-down voltage ratios [14].

The basic cell takes advantage of:

- the basic interleaved structure to decrease the current ripple, which reduces the inductor size, increases the power level and enhances the dynamic response;
- the coupled inductors to obtain a high conversion gain. They aim also at reducing the power switch voltage stress and at avoiding the reduced turnoff pulse operation, which decreases the conduction losses and the current ripple.

On the other side, the fact of using WCCIs leads up to leakage inductances (L_{Lk1} and L_{Lk2}), which result in large switching losses, high voltage spikes, and serious electromagnetic interference (EMI) issues [14].

The drawbacks caused by WCCIs can be solved by means of the passive-lossless clamp circuit. The passive-lossless circuit, consisting of two clamp capacitors (C_{c1} and C_{c2}) and four clamp diodes (D_{c11}, D_{c12}, D_{c21}, D_{c22}), absorbs the voltage spikes on the power switch and reuses the leakage energy [14]. As a result, the energy efficiency of the topology is enhanced, and the electromagnetic disturbances noise is canceled [14].

Compared with the classic IBC, this converter allows decreasing the power switch voltage stress due to the features of the WCCIs. Furthermore, high-performance power semiconductors with low on-state resistances can be used to decrease the conduction losses [14]. The reverse-recovery issue of the output diode (D_{o1}, D_{o2}) is mitigated and the reverse-recovery losses are minimized given that the output diode current falling rate is imposed by the leakage inductance [14].

In summary, this converter is fit for high power applications, high current, high step-down conversion, and to operate at a high switching frequency.

Finally, the conversion gain of the converter is obtained by using this following equation [14]:

$$\frac{V_{out}}{V_{in}} = \frac{D}{N+1} \tag{7}$$

where:

- $D \leq 0.5$;
- N is the turns ratio ($N = n_2/n_1$).

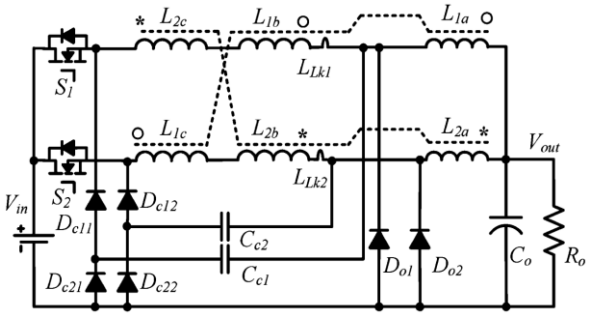

Fig. 9. Interleaved DC–DC high step-down buck converter with winding-cross-coupled inductors (WCCIs) and passive-lossless clamp scheme [14].

H. Interleaved coupled-buck converter with active-clamp circuits

By comparison, this topology (Fig. 10) differs from the conventional topology for these three aspects [15]:

1. two coupled windings on each phase (L_{11} and L_1, L_{22} and L_2 with transformation ratios, respectively indicated n_1 and n_2);
2. a resonance inductance per phase (L_{r1} and L_{r2});
3. an active-clamp circuit per phase (M_{11} and C_{r1}, M_{22} and C_{r2}).

On the one hand, resonant inductors are used to achieve zero voltage switching for the main and auxiliary power switches, and to limit transient reverse currents of freewheeling diodes. Hence, it allows reducing significantly reverse-recovery losses. On the other hand, the active-clamp circuits allow recovering the dispersion energy and limiting the voltage spikes [15].
Like the previous topology, the use of coupled windings allows improving the voltage gain of the converter, provided by the equation (8) [15]:

$$\frac{V_o}{V_i} = \frac{D}{D+n(1-D)} \tag{8}$$

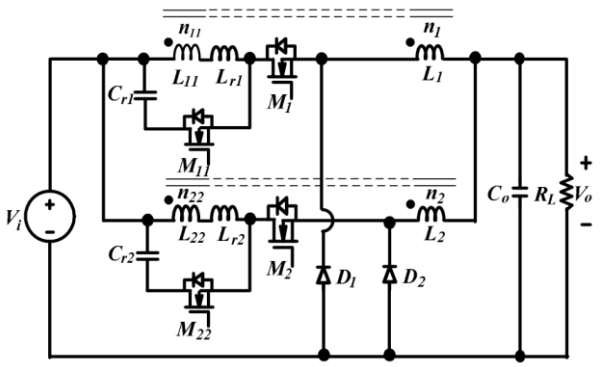

Fig. 10. Interleaved coupled-buck converter with active-clamp circuits [15].

I. Interleaved buck converter with extended duty cycle

The interleaved architecture of Fig. 11 is similar to the conventional IBC, but it differs for two aspects [16]:

1. two active switches, Q_1 and Q_2, are connected in series;
2. a coupling capacitor (C_B) is employed in the power path (it is quite large to be regarded as a voltage source).

The IBC topology with extended duty cycle is particularly suitable for high input voltage applications where the operating duty cycle must be less than or equal to 0.5.
The converter of Fig. 11 presents the following advantages than the conventional IBC [16]:

- a higher step-down conversion ratio;
- a smaller output current ripple (therefore, the inductors with a smaller inductance can be used).

Moreover, the main advantage of this topology is that since the voltage stress across active switches (Q_1 and Q_2) is half of V_S before turn-on or after turn-off when the operating duty cycle is below 50%, the capacitive discharging and switching losses can be reduced substantially; this allows the converter of Fig. 11 to have a higher efficiency than that of the conventional IBC and operate with higher switching frequencies.

The conversion gains of the IBC topology with extended duty cycle are obtained by the following equations [16]:

$$\frac{V_O}{V_S} = \frac{D}{2} \qquad \text{(with } D \leq 0.5\text{)} \qquad (9)$$

and

$$\frac{V_O}{V_S} = D^2 \qquad \text{(with } D > 0.5\text{)} \qquad (10)$$

Finally, we observe that the voltage stress of D_1, during the cold startup, could be higher than V_S. To solve this issue, an auxiliary circuit can be added to the input stage of the converter (Fig. 12).
This auxiliary circuit is composed of:

- two capacitors (C_{add1}, C_{add2});
- a diode (D_{add});
- a resistor (R_{add});

it has the goal of absorbing transient energy generated by parasitic elements during the cold startup.

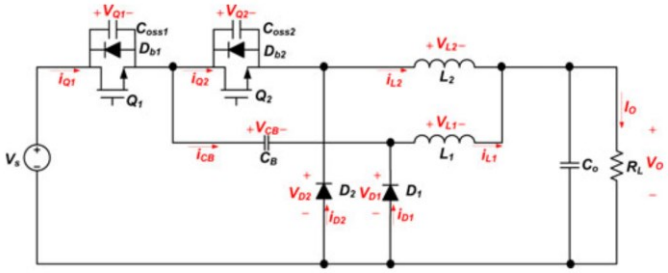

Fig. 11. IBC with extended duty cycle [16].

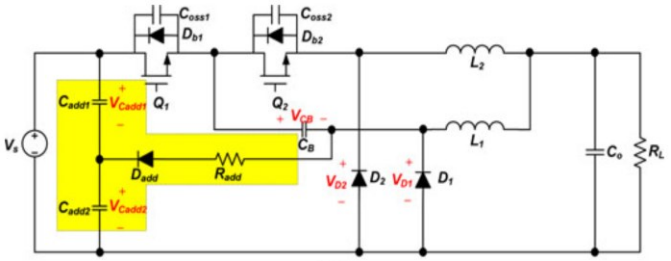

Fig. 12. IBC with extended duty cycle and auxiliary circuit [16].

V. COMPARISON OF CANDIDATE INTERLEAVED STEP-DOWN CONVERTERS

As highlighted in a previous review work [4], three types of DC-DC converters are currently used for PEM EL applications, such as buck, half-bridge, and full-bridge DC-DC converters. However, these classic converters are not optimized from voltage ratio, energy efficiency, output current ripple minimization, and availability point of view. In this article, only interleaved step-down converters have been considered due to their advantages for PEM EL applications. On the one hand, the interleaved step-down converters [9,10], [12-16] are composed of two phases. Despite these topologies are fault-tolerant in case of electrical failures, if one of the phases was faulty, the converter would lose its features [4]. On the other hand, interleaved three-level step-down converter offers an enhanced availability in case of electrical failures [11]. Indeed, this converter is composed of two phases in the non-floating part (upper) and two phases in the floating part (lower). If one of the phases was faulty, the converter could continue to operate without any operation. However, with the aim to improve and optimize the operation of the converter, fault-tolerant strategies must be applied after fault identification and detection.

Availability in the case of electrical failures is not the only requirement for PEM EL. Indeed, one of the most important requirements is a high conversion gain since the PEM EL must be supplied with a very low DC voltage. Furthermore, a low output current ripple (both low and high frequency) is required to optimize PEM EL performance, especially from energy efficiency and hydrogen production point of view. Hence, a thorough analysis of the conversion gain and current ripples is provided in Table III for each interleaved step-down converter. Besides, Fig. 13 shows a comparison between conversion gain according to the duty cycle.

TABLE III

COMPARISON OF INTERLEAVED STEP-DOWN CONVERTERS FROM CONVERSION GAIN AND CURRENT RIPPLE POINT OF VIEW

TOPOLOGY	CONVERSION GAIN		PHASE CURRENT RIPPLE		OUTPUT CURRENT RIPPLE
IBC [4]	$\frac{v_{el}}{v_{dc}} = D$		For the first, second and third phase: $\Delta I_L = \frac{v_{el}(1-D)}{Lf_{sw}}$ with: $L_1 = L_2 = L_3 = L$		$\Delta I = \frac{v_{el}D(1-3D)}{Lf_{sw}}$, $0 < D < \frac{1}{3}$ $\Delta I = \frac{v_{el}(3D-1)(2-3D)}{3Lf_{sw}}$, $\frac{1}{3} < D < \frac{2}{3}$ $\Delta I = \frac{v_{el}(3D-2)D}{Lf_{sw}}$, $\frac{2}{3} < D < 1$
IBC with a single-capacitor snubber [9]	$\frac{V_o}{V_i} = \frac{(1-D+kD)3D^2}{(7k-3)D^2-(5k-3)D+k}$		For the first and second phase: $\Delta I = (V_i - V_o)\frac{[L(1-D)+M\cdot D]^2}{L(L^2-M^2)(1-D)^2}\cdot\frac{D}{f_{sw}}$ where: $0 < D \leq \frac{1}{2}$ M: mutual inductance $L_1 = L_2 = L$		$\Delta I_L = \frac{D(L-M)(V_i-V_o)[L(1-D)+MD]^2-V_oLD(L^2-M^2)(1-D)^2}{L^2(L^2-M^2)(1-D)^2f_{sw}}$ where: $0 < D \leq \frac{1}{2}$ M: mutual inductance $L_1 = L_2 = L$
IBC with coupled windings [10]	$\frac{V_o}{V_{in}} = \frac{D}{n+1}$ n: turns of coupled windings		There is not.		$\Delta I_o = \frac{V_{in}-(n+1)V_o}{L_{eq}}\cdot\frac{D}{f_{sw}} = \frac{(1-D)(n+1)V_o}{L_{eq}}\cdot\frac{1}{f_{sw}}$ where: $L_{eq} = L_{1b} + L_{1a} + 2M$ M: mutual inductance
Interleaved ZCT TL buck converter [11]	$\frac{V_o}{V_{in}} = \frac{2D}{1+\frac{2R_e}{R_o}}$		There is not.		$\Delta I_{L_0} = \frac{V_o(1-4D)}{L_0f_{sw}}$, $0 < D < \frac{1}{4}$ $\Delta I_{L_0} = \frac{V_o(4D-1)(2-4D)}{4DL_0f_{sw}}$, $\frac{1}{4} < D < \frac{1}{2}$ where: $L_0 \gg L_c$ L_c: commutation inductance. L_1 and L_2: two small commutation inductors for the IBC connected to the positive voltage rail. L_3 and L_4: two small commutation inductors for the IBC connected to the negative voltage rail. L_c: sum of the commutation inductors in each of the two IBCs.
Interleaved ZCT buck converter [12]	$\frac{V_o}{V_{in}} \approx 2D$		There is not.		$\Delta I_{L_o} = \frac{V_{in}-V_o}{L+L_o}\cdot\frac{D}{f_{sw}}$ where: $0 < D \leq \frac{1}{2}$
Stacked interleaved converter [13]	For first phase: $\frac{V_{OUT}}{V_{IN}} = D$ where: $0 < D < 1$	For second phase: $\frac{V_{OUT}}{V_{IN}} = 1 - D$ where: $0 < D < 1$	For the first phase (without magnetic coupling between the inductors): $\Delta I_P = (1-D)D\frac{V_{IN}}{Lf_{sw}}$ where: $0 < D < 1$ $L_S = L_P = L$	For the second phase (without magnetic coupling between the inductors): $\Delta I_S = -(1-D)D\frac{V_{IN}}{Lf_{sw}}$ where: $0 < D < 1$ $L_S = L_P = L$	Complete ripple cancellation across all duty cycles ($0 < D < 1$)
			For the first phase (with magnetic coupling between the inductors): $\Delta I_P = = \frac{1}{L(1+k)}D(1-D)V_{IN}\frac{1}{f_{sw}}$ where: $0 < D < 1$ $L_S = L_P = L$ $k = \frac{M}{L}$ k: mutual coupling factor M: mutual inductance	For the second phase (with magnetic coupling between the inductors): $\Delta I_S = = -\frac{1}{L(1+k)}D(1-D)V_{IN}\frac{1}{f_{sw}}$ where: $0 < D < 1$ $L_S = L_P = L$ $k = \frac{M}{L}$ k: mutual coupling factor M: mutual inductance	Complete ripple cancellation across all duty cycles ($0 < D < 1$)
IBC with WCCIs and passive-lossless clamp scheme [14]	$\frac{V_{out}}{V_{in}} = \frac{D}{N+1}$ $N = \frac{n_2}{n_1}$		There is not.		$\Delta I_{out} = \frac{V_{in}-(N+1)V_{out}}{L_{eq}}\cdot\frac{D}{f_{sw}} = \frac{(1-D)(N+1)V_{out}}{L_{eq}}\cdot\frac{1}{f_{sw}}$ where: $0 < D \leq \frac{1}{2}$ $L_{eq} = L_{1b} + L_{1a} + 2M$

TABLE III
(CONTINUATION)

TOPOLOGY	CONVERSION GAIN	PHASE CURRENT RIPPLE	OUTPUT CURRENT RIPPLE
Interleaved coupled-buck converter with active-clamp circuits [15]	$\frac{V_o}{V_i} = \frac{D}{D+n(1-D)}$	For the first and second phase: $\Delta I = \frac{n-1}{n} \cdot \frac{V_i - V_o}{L} \cdot \frac{D_{max}}{f_{sw}}$ where: $0 < D < \frac{1}{2}$ $n = \frac{n_1+n_2}{n_1}$ n: turns ratio of coupled inductors L_1 and L_{11} or L_2 and L_{22}. $L_1 = L_2 = L$	The expression of output current ripple can only be determined experimentally.
IBC with extended duty cycle [16]	$\frac{V_O}{V_S} = \frac{D}{2}$, $0 < D \leq \frac{1}{2}$ $\frac{V_O}{V_S} = D^2$, $\frac{1}{2} \leq D < 1$	$\Delta I_L = \frac{(V_S - 2V_O)D}{2Lf_{sw}}$, $0 < D \leq \frac{1}{2}$ $\Delta I_L = \frac{V_O(1-D)}{Lf_{sw}}$, $\frac{1}{2} \leq D < 1$ with: $L_1 = L_2 = L$	$\Delta I = \frac{(V_S - 4V_O)D}{2Lf_{sw}}$, $0 < D \leq \frac{1}{2}$ $\Delta I = \frac{(V_S - V_O)(2D-1)}{Lf_{sw}}$, $\frac{1}{2} \leq D < 1$ with: $L_1 = L_2 = L$

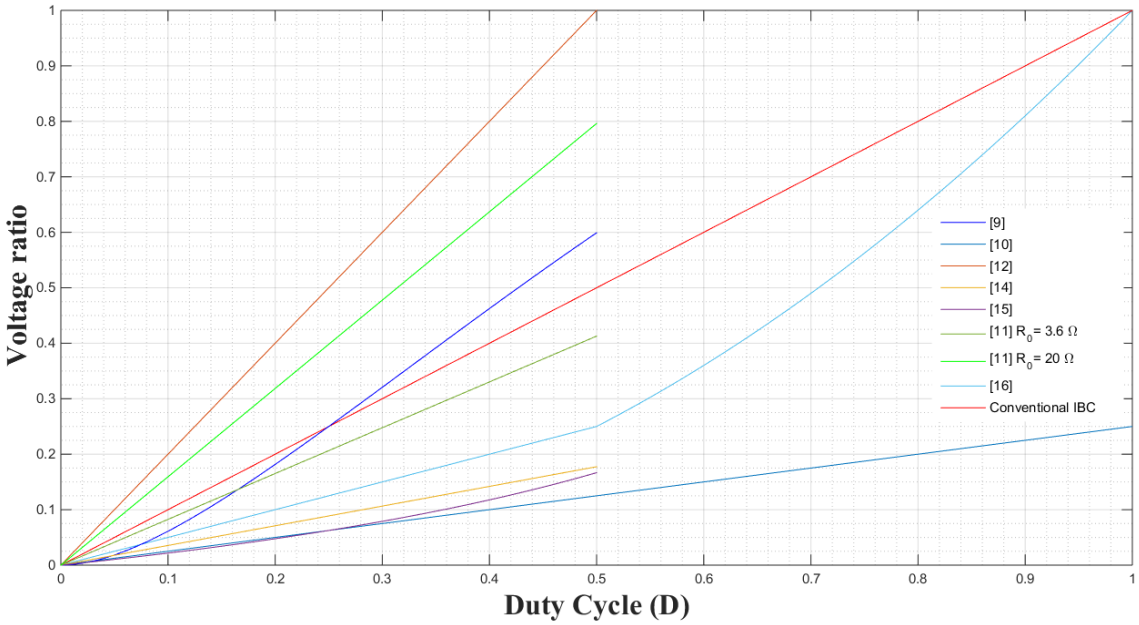

Fig. 13. Comparison of the voltage ratio according to the duty cycle.

Based on Table III and Fig. 13, it can be observed that the classic IBC is not fit for electrolyzers requiring a high voltage gain despite the output current ripples are strongly reduced compared to a classic step-down converter. Indeed, high voltage gain for an IBC leads up to operate at a very low duty cycle [4]. In addition, the most suitable converters for high voltage gain are IBC with coupled windings, IBC high step-down with WCCIs and passive-lossless clamp circuit and interleaved coupled-buck converter with active-clamp circuits. These converters are very interesting for systems based on hydrogen buffer where wind turbines are used. By comparison, the stacked interleaved converter allows canceling the output current ripple whatever the duty cycle value; whereas for IBC topologies, the output current ripple can be canceled for specific duty cycle values [4]. However, this topology suffers from having a low voltage ratio like the classic step-down converter. From output current ripple and availability point of view, the three-level interleaved step-down converter is the most interesting topology for hybrid renewable energy systems with hydrogen storage based on a DC bus configuration.

VI. CONCLUSION

The main objective of this paper is to carry out a thorough literature survey focused on candidate interleaved step-down converters for proton exchange membrane electrolyzer applications. Based on the current literature, it was demonstrated that the classical topologies (e.g. buck, half-bridge, full-bridge) currently used for these applications present several drawbacks. Hence, interleaved DC-DC step-down converters offer several advantages over classical topologies and are promising for these applications.

Based on the classic interleaved DC-DC step-down topology, several candidates interleaved converters were introduced in this article. Each converter was thoroughly analyzed to

determine current ripples and voltage gain expression. From the obtained expressions (summarized in a table and a figure), the most interesting and promising interleaved step-down converters were emphasized from output current ripple reduction and voltage gain point of view.

REFERENCES

[1] T.S. Uyar, D. Beşikci, Integration of hydrogen energy systems into renewable energy systems for better design of 100% renewable energy communities, International Journal of Hydrogen Energy, Vol. 42, Iss. 4, 2017, pp. 2453-2456.

[2] M. Carmo, D.L. Fritz, J. Mergel, D. Stolten, A comprehensive review on PEM water electrolysis, International Journal of Hydrogen Energy, Volume 38, Issue 12, 2013, Pages 4901-4934.

[3] Alexander Buttler, Hartmut Spliethoff, Current status of water electrolysis for energy storage, grid balancing and sector coupling via power-to-gas and power-to-liquids: A review, Renewable and Sustainable Energy Reviews, Volume 82, Part 3, 2018, Pages 2440-2454.

[4] D. Guilbert, S.M. Collura, A. Scipioni, DC/DC converter topologies for electrolyzers: State-of-the-art and remaining key issues, International Journal of Hydrogen Energy, Volume 42, Issue 38, 2017, Pages 23966-23985.

[5] M.E. Sahin, H.I. Okumus, M.T. Aydemir, "Implementation of an electrolysis system with DC/DC synchronous buck converter", International Journal of Hydrogen Energy, vol. 39, iss. 13, p. 6802-6812, 2014.

[6] T. Zhou, B. François, M. El Hadi Lebbal, S. Lecoeuche, "Real-time emulation of a hydrogen-production process for assessment of an active wind-energy conversion system", IEEE Transactions on Industrial Electronics, vol. 56, iss. 3, p. 737-746, 2009.

[7] P. Thounthong, B. Davat, "Study of a multiphase interleaved step-up converter for fuel cell high power applications", Energy Conversion and Management, vol. 51, iss. 4, p. 826-832, 2010.

[8] A. Kolli, A. Gaillard, A. De Bernardinis, O. Bethoux, D. Hissel, Z. Khatir, "A review on DC/DC converter architectures for power fuel cell applications", Energy Conversion and Management, vol. 105, p. 716-730, 2015.

[9] Yaow-Ming Chen, Sheng-Yu Tseng, Cheng-Tao Tsai and Tsai-Fu Wu, "Interleaved buck converters with a single-capacitor turn-off snubber", IEEE Transactions on Aerospace and Electronic Systems, vol. 40, no. 3, pp. 954-967, July 2004.

[10] K. Yao, Y. Qiu, M. Xu and F. C. Lee, "A novel winding-coupled buck converter for high-frequency, high-step-down DC-DC conversion", IEEE Transactions on Power Electronics, vol. 20, iss. 5, p. 1017-1024, 2005.

[11] M. Ilic, B. Hesterman and D. Maksimovic, "Interleaved zero current transition three-level buck converter", in: proceedings of Twenty-First Annual IEEE Applied Power Electronics Conference and Exposition, p. 72-78, 2006.

[12] M. Ilic and D. Maksimovic, "Interleaved Zero-Current-Transition Buck Converter", IEEE Transactions on Industry Applications, vol. 43, no. 6, pp. 1619-1627, 2007.

[13] J. Wibben and R. Harjani, "A High-Efficiency DC–DC Converter Using 2 nH Integrated Inductors", IEEE Journal of Solid-State Circuits, vol. 43, no. 4, pp. 844-854, 2008.

[14] W. Li and X. He, "A Family of Interleaved DC–DC Converters Deduced From a Basic Cell With Winding-Cross-Coupled Inductors (WCCIs) for High Step-Up or Step-Down Conversions", IEEE Transactions on Power Electronics, vol. 23, no. 4, pp. 1791-1801, 2008.

[15] C. T. Tsai and C. L. Shen, "Interleaved soft-switching coupled-buck converter with active-clamp circuits", in: Proceedings of 2009 International Conference on Power Electronics and Drive Systems (PEDS), p. 1113-1118, 2009.

[16] I. Lee, S. Cho and G. Moon, "Interleaved Buck Converter Having Low Switching Losses and Improved Step-Down Conversion Ratio," in IEEE Transactions on Power Electronics, vol. 27, no. 8, pp. 3664-3675, Aug. 2012.

[17] D. Guilbert, B. Yodwong, W. Kaewmanee, P. Phattanasak, Power converters for hybrid renewable energy systems with hydrogen buffer storage: A short review, in: *Proceedings of 6th International Conference on Smart Grid (IEEE ICSMARTGRID)*, 2018, forthcoming.

[18] T. Arunkumari, V. Indragandhi, An overview of high voltage conversion ratio DC-DC converter configurations used in DC micro-grid architectures, Renewable and Sustainable Energy Reviews, Volume 77, 2017, Pages 670-687.

Vittorio Guida was born in Palermo (Italy) in 1984. After obtaining the high school Diploma as "Industrial Expert Technician Specialization Computer", at the "Istituto Tecnico Industriale Statale" of Palermo, he began his academic studies, at the University of Palermo, in Automation Engineering.
First, he obtained the Bachelor's degree with a thesis on the "Automatic Measurement System for the Testing of Electromagnetic Compatibility in Accordance with CEI EN 55014". Subsequently, he obtained the Master's degree with a thesis on the "Adaptive Control for Robotic Systems with Nonsingular Actuator Matrix".
During the academic path, he carried out internships to obtain the respective qualifications. In particular, in 2011, he worked at the "Molino e Pastificio Tomasello S.p.A.", for the implementation of a program in Matlab for image processing. In 2015, he carried out an internship at the University of California Riverside on the "Application of control-theoretic techniques to evaluate the difficulty of different cognitive control tasks, and design of advanced Brain-Computer Interfaces to facilitate the use of EEG signals and to control different dynamical systems".
In May/June 2017, he attended a Java programming course, organized by the QiBit Division (ICT Division of Gi Group S.p.A.), at their offices in Rome.
In October 2017, after passing an international competition, he was admitted to the Ph.D. program in Electrical Engineering, at the University of Lorraine in Longwy (France) with a Ph.D. thesis focused on "Design and realization of a DC/DC converter at high conversion ratio for electrolyzers".

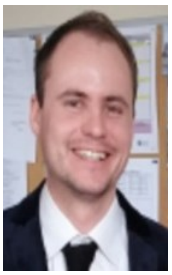

Damien GUILBERT was born in Paris, France, in 1987. He received the M.Sc. degree in electrical engineering and control systems and the Ph.D. degree in electrical engineering from the University of Technology of Belfort-Montbéliard (UTBM), France, in 2011 and 2014 respectively. His current research interests include power electronics, fuel cell, and electrolyzer system, modeling and emulation of PEM electrolyzers, fault-tolerant DC/DC converters for fuel cell/photovoltaic/electrolyzer applications, and fault-tolerant control for fuel cell/electrolyzer systems. He was involved in the creation of the first IEEE/IAS student branch and chapter in France at UTBM, where he was the president in 2015. Since September 2016, he has been Associate Professor at Université de Lorraine and a permanent member of GREEN (Group of Research in Electrical Engineering of Nancy) laboratory.

Bruno Douine was born in Montereau, France, in 1966. He received his Ph. D. in electrical engineering from the University of Nancy, France, in 2001.

He is currently Full Professor at the University of Lorraine and a permanent member of GREEN (Group of Research in Electrical Engineering of Nancy) laboratory. His main topics of research concern characterization of superconducting material and power electronics.

Sustainable Adoption of Connected Vehicles in the Brazilian Landscape: Policies, Technical Specifications and Challenges

Douglas Aguiar do Nascimento, Yuzo Iano, Hermes José Loschi, Navid Razmjooy, Robert Sroufe, Vlademir de Jesus Silva Oliveira, Diego Arturo Pajuelo Castro, Matheus Montagner

***Abstract*—This paper addresses the intervehicular communication in Connected Vehicles (CV) by emphasizing V2V (vehicle-to-vehicle) and V2I (vehicle-to-infrastructure) communications in terms of evolution, current standards, state-of-the-art studies, embedded devices, simulation, trends, challenges, and relevant legislation. To accomplish the objective this review is based on studies conducted from 2003 to 2019, government reports about the sustainable deployment of these technologies and their adoption in the Brazilian automotive market according to experts. Moreover, WAVE (Wireless Access in Vehicular Environment) and DSRC (Dedicated Short-range Communication) standards, the performance analysis of communication parameters and intervehicular available at the market are also described. The current status of ITS (Intelligent Transportation System) development in Brazil is reviewed, as well as the research institutes and governmental actions focused on introducing the concept of connected vehicles into the society. The Brazilian outlook for technological adoption concerning CVs was also discussed. Besides those, challenges related to technical aspects, safety and environmental issues, and the standardization for vehicle communication are also described. Finally, this review highlights the challenges and proposals from available technologies devoted to the roads and vehicular infrastructure communication, their evolution and upcoming trends.**

***Index Terms*—Connected Vehicles, Intelligent Transportation System, Vehicular Communication, Policies, Specification, Sustainability.**

I. Introduction

The number of deaths from traffic accidents has reached about 1.25 million per year around the world, representing the first fatality cause across people aged 15-29 years old [1]. Despite Brazil's legislation on the best traffic practices (prohibiting drunk driving and the awareness of using the helmet, seat belt, and child restraint), the total number of fatalities recorded in 2016 was about 34,850 [2]. It is estimated that Brazil spends US$ 12.3 billion [1] annualy on economic production losses since the victims are absent from work and hospital expenses from traffic accidents on Federal and State highways, municipal and urban agglomerate streets [3]. In 2014, for example, the cost to society was US$ 3.16 billion, due to the 167,247 traffic accidents only on Federal roads, as shown in Table 1. The cost of each accident is the sum of the cost components associated with the control variables of the additive model - costs associated with people, vehicles and other costs.

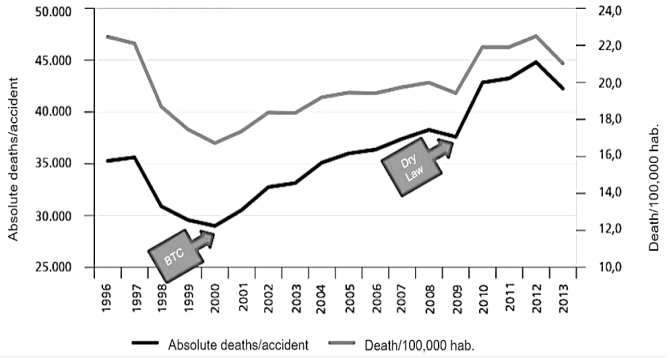

Fig. 1. Evolution of mortality from terrestrial transport [4].

As shown in Figure 1, the economic production losses arising from labor capacity is the most expensive to society due to accidents involving workers.

According to Figure 1, there were some sudden death drops from terrestrial accidents (i.e., 1997-2000 and also 2008-2010), which were caused by the adotion of a more rigid legislation according to the new Brazilian Traffic Code (BTC) and the enforcement of the DWI (Driving While Intoxicated) Law, respectively. The long-term trend is the increase in the number of fatalities. The adoption of public policies introduced by the US Department of Transportation was effective in reducing fatalities and injuries [5]. The adoption of V2V technologies could also help avoid 439,000-615,000 crashes, which represents 13-18% of crashes involving light vechicles, reducing up to 418,000 MAIS (Maximum Abbreviated Injury Scale) within a scale of 1-5 injuries and avoid 746,00 damages

D. A. Nascimento, Y. Iano, H. J. Loschi and D. A. P. Castro were with the Department of Communications, School of Electrical and Computer Engineering, University of Campinas, Campinas, SP, 13083-852 BR, e-mail: eng.douglas.a@ieee.org.

N. Razmjooy is with Tafresh University, Department of Electrical and Control Engineering, Tafresh 39518 79611, Iran.

R. Sroufe is with John F. Donahue School of Business, Duquesne University, Rockwell Hall 820, 600 Forbes Avenue, Pittsburgh, PA 15282, USA.

V. J. S. Oliveira is School of Exact and Technological Sciences, Mato Grosso State University, Av. dos Ingas, 3001, Jardim Imperial, Sinop, MT, 78555-000.

M. Montagner is with Santa Catarina State University, Paulo Malschitzki St., 200, Bairro: Zona Industrial Norte, Joinville, SC, CEP: 89219-710.

Manuscript received on February 10, 2019 and revised on March 17, 2019.

[1] 1 USD: BRL 4.05 (Sept. 22nd, 2018).

TABLE I
ACCIDENT COSTS ON FEDERAL ROADS [3].

Cost	Description	Value ($)	%
People	Hospital expenses; attendance; treatment of injuries; removal of victims; and economic production losses	1,963,186,281.98	62.01
Vehicle	Removal of vehicles; damage to vehicles; and loss of production capacity over its lifetime	1,185,294,508.64	37.44
Institutions and property damage	Attendance; prosecution and damage to public and private properties	17,282,788.40	0.55
Total		3,165,763,579.02	100.00

to PDOVs (Property-damage-only vehicles) [6]. Technologies based on partial automation levels (e.g. ESP - Electronic Stability Control) are responsible for reducing the number of accidents. It is estimated that reducing damages or avoiding crashes in 18% of the total accidents and 34% of those resulting in fatalities is feasible [7]. Regarding secutiry applications, such as CICAS (Cooperative Intersection Collision Avoidance Systems), 80% of crashes could be avoided if 50% of the crossings were equipped with RSU devices (Road-side Unit) from V2I (Vehicle-to-infrastructure). Moreover, 50% of crashes could be avoided if 20% of the crossings were equipped with RSU V2I [5], [8]. Therefore, stakeholders from many countries believe that the systems of connected vehicles (CV – Connected Vehicle), also known as Cooperative Intelligent Transportation System (C-ITS), have the ability to enhance traffic in terms of transport security and efficiency [9]. This scenario of connected cars would be associated to Smart Cities, where several devices are connected in the cloud (data storage network infrastructure) and able to communicate to each other in order to exchange information and data storage. This data, after it was processed and analyzed, would still be useful in providing services and further processing needs. Hence, the term "connected car industry" has been widely used and the revenue forecast for the sales of connected cars is shown in Figure 2 [10].

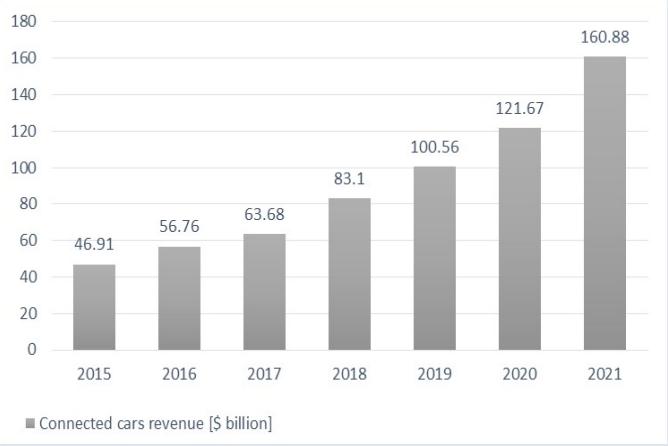

Fig. 2. Global market for connected cars.

Many market surveys provide a number of 380 million connected vehicles [11]–[14]. The development of connected vehicles is taking place in conjuction with underlying technologies devoted to network and communication infrastructure capable of meeting the bandwidth demand required by connected vehicles, such as the 5G mobile communication and WAVE (Wireless

Access in Vehicular Environment) [15]–[18]. Therefore, this work proposes an overview on different types of communication methods for Connected Vehicles and the analysis of prospects and trends for the Brazilian scenario. It is out of the scope of this work covering intelligent cooperative transport systems (CITS) or intervehicular communication for platooning (convoy), since this approach should describe the routing of VANET networks, cognitive applications and case studies in VANET. Readers interested in those technological aspects are encouraged to search elsewhere [19]–[23]. Connected vehicles belong to a new model known as Intelligent Transportation System (ITS), which is focused on improving traffic safety and efficiency by means of wireless electronic communication. Connected vehicles rely on GPS (Global Positioning System) data, connectivity (wireless communication), and data processing to enable vehicles, smart road infrastructure and mobile phones to exchange information for providing warning and security messages to road users [8]. Therefore, this work was structured as follows: Section 2 introduces IoV (Internet of Vehicles) and associated definitions. Section 3 addresses vehicular communication in terms of infrastructure and data exchange, protocols and technologies to connect vehicles. Section 4 describes the Brazilian adoption of vehicular technologies. Section 5 deals with the challenges from technical aspects (e.g., which frequency range to use and allocation issues), safety, and public acceptance within the Brazilian scenario. Section 6 describes the legislation, public policies and legal perspective. Section 7 provides conclusions based on the idea of vehicle communication.

II. INTERNET OF VEHICLES

The Internet of Things (IoT) [25] is a paradigm that establishes a world of embedded physical objects, based on sensors and actuators, connected to wireless networks. They can communicate through the Internet, which gives rise to a network of intelligent objects able to do various types of data processing, get environmental variables, and react to external event. These objects are connected to each other and to other resources (physical or virtual). They can be controlled through the Internet, which allows a plethora of applications that will be able to use new types of data, services and operations available. IoT is an example of an emerging technology that contributes to the achievement of

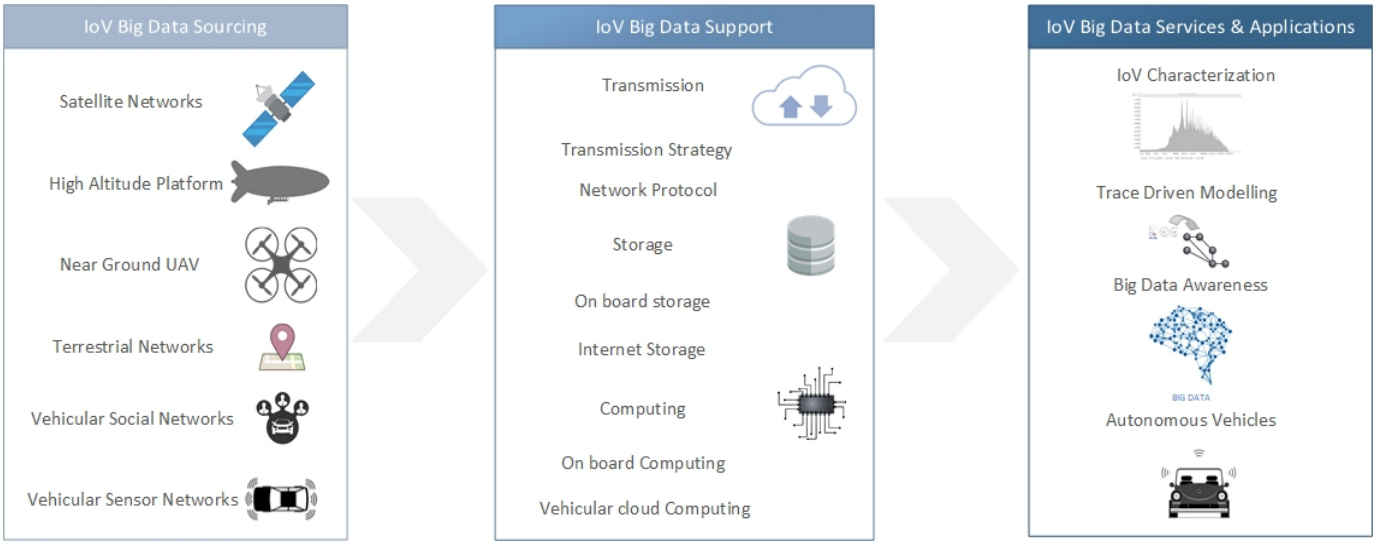

Fig. 3. IoV big data architecture, based on [24].

new fields of application for information and communication technologies (ICTs). One of these domains can be understood as that from smart cities, wherein the use of communication and sensing technologies provides value-added services to the administrative bodies of such cities and their citizens [26], [27]. One of the applications regarding the ICT domain is the intelligent mobility. As described elsewhere [28], mobility is part of the daily life of the modern society, since it requires transportation systems based on different types of vehicles and communication infrastructure. With the recent advances in information and communication technologies, mobility has an important role in providing a better quality of life. The Internet of Things integrates intelligence into existing research and development areas, such as smart-health, smart-home, smart-energy, smart industry and smart transport - or smart mobility as described in [29] (see Figure 3).

The Internet of Vehicles (IoV) is one of the revolutions mobilized by IoT, which involves the concept of VANET - Vehicular Ad hoc Networks, to convey the vision of the smartphone to the smart car [30], [31]. VANET is aimed at improving traffic efficiency and safety by means of real-time communication between advanced wireless access technologies, enabling vehicles with or without RSU (Road Side Unit) [31]. VANETs are a special class of Mobile Ad hoc Networks (MANET) in which the vehicles work as people. These networks are characterized by the high speed of vehicles, low intercontact times among hosts, intermittent connection and real-time data exchange requirements [32]. Moreover, these networks rely on a minimum or temporary infrastructure and are characterized by high mobility, fixed road networks, traffic patterns and predictable speed under traffic congestion conditions, low power requirements, and storage limitations. Even though other communication systems rely on high message throughput, VANETs primarily focus on reliable communication and fast dissemination of safety messages [33]. This way CVs may communicate with each other or with the traffic infrastructure (RSU) by using consolidated Technologies, which are divided as [32]: 1. Vehicle-to-vehicle (V2V) communication; 2. Vehicle-to-infrastructure (V2I) communication; 3. Hybrid communication composed of V2V and V2I, and 4. Vehicle-to-everything (V2X) communication. V2V communication is also known as C2C (Car-to-car), or inter-vehicle communication (IVC). The term “Connected Vehicles” refers to the applications, services, and technologies for connecting vehicles. By adopting a similar definition as New Cars Auto Connected, a connected vehicle is basically formed by the presence of devices that connect this vehicle to other services, devices, networks, applications and services outside the vehicle. Applications include traffic efficiency and safety, infotainment, parking assistance, roadside assistance, remote diagnostics and telematics for self-driving vehicles, and Global Positioning System (GPS). Vehicles with advanced interactive driver-assistance systems (ADAS) and Cooperative Intelligent Transport Systems (C-ITS) can be considered the typical connected vehicles. Safety applications for connected vehicles are designed to increase the awareness and reduce traffic accidents through vehicle to vehicle (V2V) and vehicle to infrastructure (V2I) communications [34], [35]. An increasing number of factories are equiping their vehicles with on-board computers, sensors, and navigating systems able to create mass scale vehicle networks [36]–[38]. By using a myriad of sensors, cameras, computers, and communication services, vehicles are able to harvest, process, analyze, and send information to help drivers [38]. Traffic Information Systems (TISs) allow a better use of road networks by providing real-time traffic conditions and by guiding drivers to make better routing decisions [39], [40]. Vehicle network applications may be classified as [38]: 1. Safety; 2. Entertainment, and 3. Driving assistance. Safety includes applications intended to provide information to the driver about dangerous road conditions,

such as the weather, traffic jams, accidents, etc, with the dissemination of emergency information. The entertainment applications provide the support for Internet access, advertising, content sharing, chats and related services. The driver assistance applications will provide the exchange of information for helping drivers to find gas or power stations, restaurants, and toll roads. Moreover, the systems of CVs also allow: reduction of greenhouse gas emission and fuel consumption, enhanced safety and protection, higher efficiency, mobility and accessibility, besides the adoption of economical opportunities for advancing investments and research on clean technologies [41].

III. Vehicular Communication

It is a global network of WAT (Wireless Access Technology), which includes vehicles, the Internet and other heterogeneous networks, such as the Internet of Vehicles (IoV). The heterogeneous network architecture of IoT includes five types of vehicular communication (Figure 4): V2V (Vehicle-to-Vehicle), by using WAVE (Wireless Acess in Vehicular Environment) through the 802.11p protocol; V2R (Vehicle-to-Roadside unit) with WAVE and 802.11p protocol; V2I (Vehicle-to-Infrastructure) available through Wi-Fi (Wireless Fidellity) 802.11b, Wi-Fi 802.11g and also mobile networks such as 4G, LTE (Long-Term Evolution) and 5G [16], [42], [43]; V2P (Vehicle-to-Personal devices) through technologies such as CarPlay, OAA and NCF, for example; V2S (Vehicle-to-Sensors), in which the ECU (Electronic Control Unit) from vehicles is able to communicate with sensors installed in the vehicle by using protocols such as Ethernet, WiFi and MOST (Media Oriented Systems Transport). Therefore, each vehicle communication from IoV is enabled by using a different WAT, which includes, IEEE WAVE for V2V and V2R, WiFi and 4G/LTE for V2I, CarPlay/NFC for V2P and MOST/WiFi for V2S. The inclusion of a plethora of devices makes the architecture more complex, even though more market oriented, such as VANETs. The structure of a heterogeneous vehicle network of IoV has a significant power for guiding and monitoring vehicles [31], [44], [45].

Even though the vehicle communication technology is mainly used for traffic safety, connected vehicles are also able to support technologies other than safety, such as telematics and traffic management, which includes the control over road congestion, smart tolling and optimization of routes and directions [8]. A suitable description for better understanding this is proposed elsewhere [46], according to the zones of interest, which may be: personal (communication based on PAN), information exchange among vehicles and personal devices; local network (LAN), communication among vehicles and vehicle to vehicle and local infrastructure; and regional (by using mobile networks), applications based on broadcasting, in which the traffic center or manager sends information to vehicles in the region.

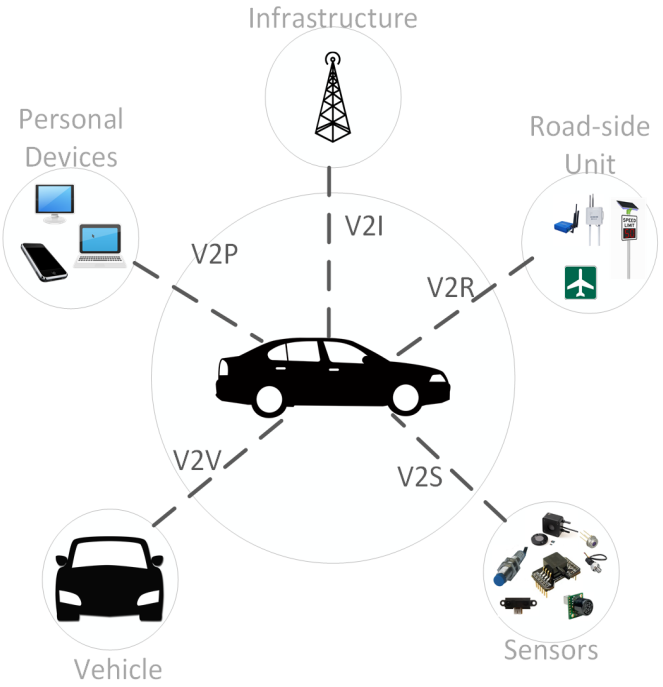

Fig. 4. Types of IoV communication, based on [31].

A. Technologies and Protocols for Vehicular Communication

Within the vehicular communication, each device in the network (vehicle or infrastructure device) is considered a node. The communication among nodes from vehicular networks may be done in three different ways: vehicle to vehicle (V2V), vehicle to infrastructure (V2I), and hybrid (V2X) [47], [48]. The Intervehicular Communication (IVC), which is part of the ITS (Intelligent Transportation System) and its real applications in mobile ad hoc networks, has been researched at the academia and also at industries, most notably in the US, Europe and Japan. The most important achievement from IVC is its ability to expand the horizon of drivers and on-board devices (radar or sensors, for example), besides improving traffic safety and efficiency on the roads [49]. ITS enhances not only transport safety and mobility but also the American economic productivity by integrating advanced communication technologies into transport infrastructure and vehicles. ITS encompasses a myriad of information and electronic technologies based on wired and wireless communication [50]. Table 2 shows an overview from the main countries developing research and the implementing ITS.

There are three different categories for automobile applications based on communication [9], [52]: 1. Safety-driven: examples include the alert for a parked or slow vehicle and electronic emergency brake lights, V2V warning of an accident, an alert for road resources and cooperative collision warning. 2. Comfort-driven: alerts for congested roads, traffic probes, and warning of parking availability, parking lot finder, are some examples. 3. Commercial-driven: such as remote

TABLE II
OVERVIEW OF ITS FOR THE MAIN RESEARCH STUDIES IN DIFFERENT COMMUNITIES [51].

	Japan	USA	Europe
Standard / Committee	ITS-Forum	IEEE802.11p/1609.x	CEN/ETSI EN302 663
Frequency Range	755 – 765 MHz	5850 – 5925 MHz	5855– 5925 MHz
Number of Channels	One 10 MHz channel	Seven 10 MHz channels (Two 20 MHz channels formed by combining 10 MHz channels)	Seven 10 MHz channels
Modulation	OFDM		
Data rate per Channel	3 -18Mbit/s	3 -27Mbit/s	3 - 27Mbit/s
Output power	20 dBm (Antenna input)	23 - 33 dBm (EIRP)	23-33 dBm (EIRP)
Communication	One direction multicasting service (broadcast without ACK)	One direction multicasting service, One to Multi communication, Simplex communication (broadcast without ACK, multicast, unicast with ACK)	
Upper protocol	ARIB STD-T109	WAVE (IEEE 1609) / TCP/IP	ETSI EN 302 665 (incl. e.g.GeoNetworking) TCP/UDP/IP

customization or diagnostics of a vehicle, advertising services, download of contents and real-time video broadcasting.

1) Inter-vehicular Commmunication: WAVE (Wireless Acess in Vehicular Environment) is a wireless technology primarily developed for harsh environments, wherein it enables the fast communication among vehicles with the advantages of high mobility, threshold delays for security messages with severe QoS, optimal energy consumption and respect for privacy and anonymity from roaming users, besides other environmental challenges [53]. According to [47], IEEE has started the standadization of vehicular communcation networks within the IEEE 802.11 working group. This standard has been under development since 2004 and is called IEEE 802.11p – Wireless Acess in Vehicular Environment (WAVE). It is governed by the IEEE 1609 [54] and IEEE 802.11p [55] standards, which establish vehicular communications. A scheme to show the integration among WAVE components is shown in Figure 5.

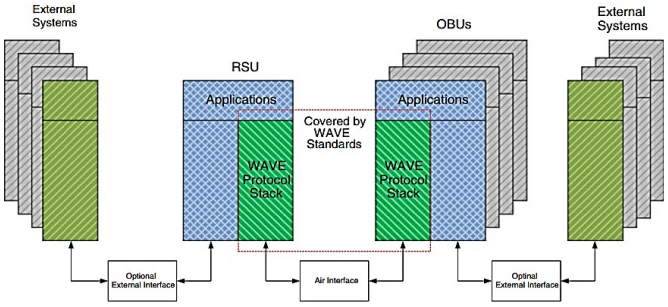

Fig. 5. Example of a WAVE system component, based on [53], [54].

As a global term, WAVE is nowadays employed to define all wireless vehicular communications. It became arbitrarily used as a general term, such as DSRC. Regarding the standardization, WAVE is used for projecting a set of IEEE1609.x standards over the 802.11p standard [53]. Therefore, a DSRC/WAVE offers [8], [54], [56], [57]: 1. Low latency - 802.11p standard states essencial events (functions and services) for data exchange without establishing a Basic Service Set (BSS); 2. Data rate – 802.11 defines a 10 MHz-bandwidth channel and eight data rates' types, i.e. 3, 4, 5, 6, 9, 12, 18, 24, 27 MHz; 3. High reliability – in order to comply within harsh envinronments (sandstorm, rain, etc) IEEE 802.11p stablishes a 10 MHz-bandwidth channel rather 20 MHz; 4. Security and privaty – DSRC protocol provides securing management and messages of application to overcome attacks from malicious and and untrusted events and softwares such as DoD (Denial of Service), eavesdropping and spoofing. The DSRC (Dedicated Short-Range Communication) wireless technology devoted to vehicular communication was designed for ITS applications within vehicular environments. Its primary aim is to offer support to safety applications and the communication among vehicles (V2V), and from vehicle to infrastructure (V2I), this way decreasing the number of accidents. Moreover, DSRC also supports ITS applications, such as managing traffic conditions, information and entertainment (infotainment) [8], [56], [57]. Figure 6 shows the DSRC protocol stack.

The comercial success of the WiFi technology and IEEE 802.11 standards led to the development of a new standard, known as IEEE 802.11p WAVE. IEEE 802.11p is based on the IEEE 802.11a standard, but with improvements on its physical (PHY) and medium access control (MAC), which are aimed at reaching low latency and high communication reliability in short-range radio connections [8], [54], [56]. The IEEE 802.11p standard defines the WAVE physical layers (PHY) and MAC, which are extensions to IEEE 802.11 standard, in order to communicate outside the BSS context. It has also standardized other specifications, such as 5.9 GHz OFDM PHY (within 5,850 – 5,925 GHz in the U.S. and 5,855 – 5,925 GHz in Europe), channel bandwidth, operating

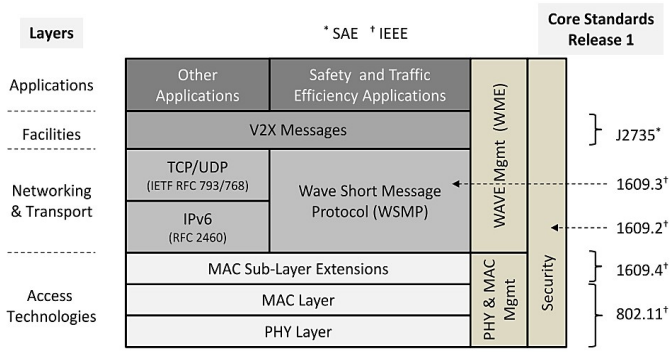

Fig. 6. DSRC protocol stack [58].

ranges, transmission power requirements, transmission masks and alternate channel, and alternate adjacent channel rejection requirements [8]. The IEEE 1609 family of standards defines the architecture and a set of standardized protocols which provide the foundation for a wide range of DSRC/WAVE applications. The most important IEEE 1609.x protocols are [8], [57]: IEEE 1609.3 – defines the using of IPv6 (Internet Protocol version 6) and employs the Wave Short Message Protocol (WSMP) to prevent overhead through the Wave Short Messages (WSM) and the WAVE Service Advertisement (WSA), also setting management functions; IEEE 1609.2 – defines services related to applications and messages of management for authentication using optimal encryption of DSRC messages based upon signals and digital certificates; IEEE 1609.4 – stablishes the multichannel operations by MAC extension and address the channel timing and switching considering IEEE 802.11 standard. Also, it defines the control channel (CCH), created to send messages of advertisement and information through service channels (SCH); SAE j2735 – SAE (Society of Automotive Engineers) standard upper layer containing 15 message, frames and data elements types, and the message specifications; SAE j2945.1 – also defines an upper layer which stablishes the minimum requirements for communication performance. According to [58] the SAE J2735 standard stablishes syntax and semantics of V2X messages and BSM (Basic Safety Message) is the most relevant amongst all other message formats available due BSM address core state information about the broadcasting vehicle and other important informations e.g. location, size, etc. Even though BSM is designed to be compact and efficient, additional frame and data elements may extend it, and add-ons may optionally be added within a subset of messages, such as in every second message. All these DSRC/WAVE functionalities are provided by the communication interface and network technologies as described in the next section.

2) Intra-vehicular Commmunication: Intra vehicular communication allows modules, sensors, and actuators to communicate with each other. It provides the operation for only one vehicle and operates under OBD (On-board diagnostics) services. Local networks also support aftermarket telematic devices, which can access data through OBD's standardized interface. Nowadays, Original Equipment Manufacturers (OEMs) implement sensors and networks shared over the OBD hardware by following OEM standards that carry relevant information for vehicle optimization and support applications concerning future communication. In terms of non-OBD intravehicle communication, communication systems related to drive-by-wire systems are especially built for robustness and security of critical data, whereas other systems host peripheral data, provide fault tolerance, determinism and flexibility, and support network technologies such as CAN, LIN, MOST and FlexRay [59]–[63]. The main traditional intra-vehicular communication networks are [64]:

- LIN (Local Interconnect Network): it is a low-cost and low speed (20 kbps) serial intra-vehicular communication network. LIN is widely used for distributed body control electronic systems in vehicles since it is a user-friendly and a low-cost technology. It is also applied to some comfort functions;
- CAN (Controller Area Network): it is a serial databus communication protocol developed by Robert Bosch GmbH. Nowadays, CAN has become a standard for transmitting data over intra-vehicular networks with a data rate reaching from 125 kbps up to 1 Mbps. It is widely used for automotive communication due to its flexibility and robust nature, which also includes its limited delay, simplicity and low cost;
- Byteflight: it was developed by BMW and supports a data rate of up to 10 Mbps. This network requires broadband services and has been applied to vehicular networks with high level safety requirements (e.g. passive safety);
- TTP/C (Time-Triggered Protocol): it offers a data rate of up to 25 Mbps and is based on TDMA. Despite its complex project, it provides low cost applications. A TTP frame may contain 240 bytes of data and 4 bytes of overhead. The ability to schedule the communication makes the TTP/C protocol less flexible, but its time-triggered communication allows it to be predictable;
- TTCAN (Time-Triggered Controller Area Network): it was also developed by Robert Bosch GmbH and is based on the TDMA mechanism. TTCAN relies on the same standard and message formats from CAN (supports a data rate from 125 kbps up to 1Mbps), but in contrast to CAN, it has a master node responsible for time synchronization among nodes;
- FlexRay: it is used for high speed and flexible intra-vehicular communication and offers a data rate of up to 10 Mbps. It seems to be the best choice for safety and high speed automotive applications. FlexRay is based on TDMA and FTDMA mechanism. It offers star and multiple star topologies. This network exchanges messages with 254 bytes of data and 5 bytes for the header;
- MOST (Media-Oriented Systems Transport): it was developed to make information and entertainment (infotainment) and multimidia systems easier to handle, with a data rate up to 24.8 Mbps for streaming audio, video, data and control information. This allows such a cost-effective technology to offer an efficient data communication infrastructure;

Figure 7 shows the main systems and communication protocols that make up the vehicle, in which the Ethernet protocol was proposed for transmitting and receiving data from the vehicle. The CAN protocol is applied to comfort electronics and powertrain systems. The USB protocol is used for information and entertainment systems, whereas FlexRay is applied to safety systems and chassis control. Considering the main wireless technologies devoted to vehicular communication, it is relevant to mention the review on intra-vehicular communication technologies summarized in Table 3.

According to the work from [68], wireless technologies are preferable over Zigbee and Bluetooth when taking into account

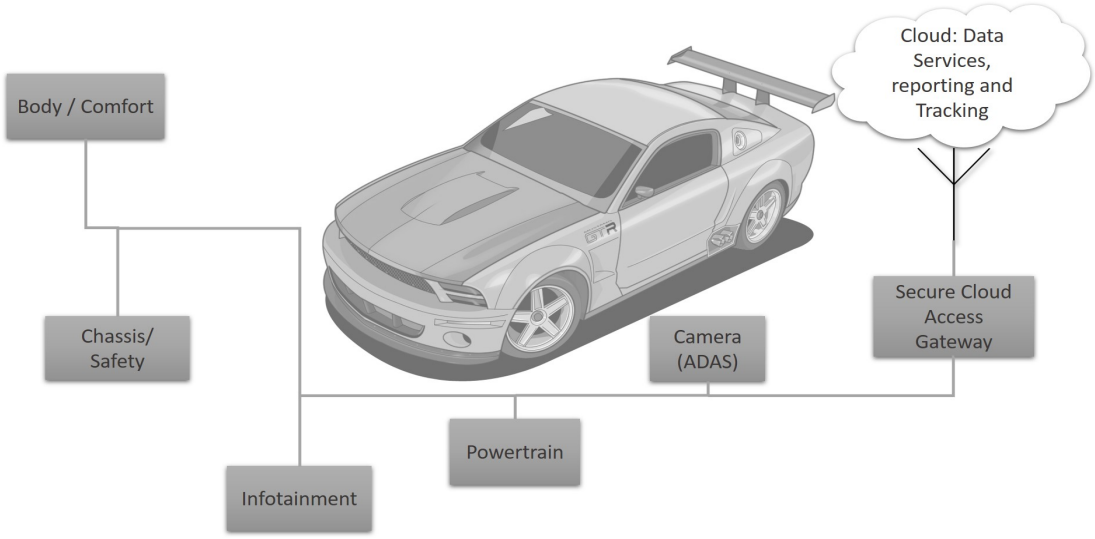

Fig. 7. Example for the application of an in-vehicle communication, based on [65].

TABLE III
THE MOST COMMONLY USED TECHNOLOGIES FOR IN-VEHICLE NEWTWORKS. ADAPTED FROM [66], [67].

Standard	Bluetooth	UWB	ZigBee	Wi-Fi
IEEE specification	802.15.1	802.15.3	802.15.4	802.11a/b/g
In-vehicle applications	In-vehicle communication and device connectivity	High speed intra-vehicular communication environments	In-vehicle communication	In-vehicle communication
Domain	Telematics and body	Telematics and Powertrain	Body	Telematics
Data rate	1 Mbps	100 Mbps	250 Kbps	54 Mbps
Range	10 m	10 m	10-100 m	100 m
Power consumption	Low	Ultra-low	Very low	High
Mode (spreading)	FHSS	DS-UWB	DSSS	DSSS, CCK, OFDM
Modulation type	GFSK	BPSK, QPSK	BPSK, O, QPSK	BPSK, QPSK
Frequency	2.4 GHz	3.1-10.6 GHz	868 MHz, 915 MHz, 2.4 GHz	2.4 GHz, 5 GHz
Data protection	16-bit CRC	32-bit CRC	16-bit CRC	32-bit
Topology	Star	Peer-to-peer	Star/Mesh	Star
Maximum number of cell nodes	8	8	> 6500	Unlimited 2007 (infra-structured)

in-vehicle applications relying on a low bitrate and limited power source, as well as its low power consumption that could provide a longer lifetime. On the other hand, high speed data in-vehicle applications could benefit from the use of UWB and WiFi due to their low normalized energy consumption.

3) Underlying Technologies: The need for inter vehicle communication has grown out of some safety issues, such as maintaining or improving road safety for drivers with the ever increasing traffic density. The initial communication was mainly based on the broadcasting type from one central station spreading traffic information. The need for a feed-back channel beween vehicles was noticed a long time ago and, consequently, the need for inter-vehicle communication regarding safety applications, such as the stopping distance, for example. The main limitations of a vehicular network are the requirements for developing a system with the restrictions of a real-time system, while keeping network latency to safe reaction time limits [69].

The vehicles are connected through multiple radio access technologies, such as DSRC, IEEE 802.11 (Wi-Fi), cellular technologies like LTE and improvements arising from the fifth generation (5G) networks. Although 3rd Generation Partnership Program (3GPP) supports telematics and infotainment services for connected cars, cellular networks have received considerable attention for a broader scope with V2X (3GPP release 14) [15] and with 5G providing ultra-high reliability and ultra-low latency demands of tomorrow V2X applications [70].

Inter-vehicle communication may be carried out by means of existing standards, such as cellular networks (3G, 4G) or satellite communications [69]. LTE is the fourth generation of cellular radio network as defined by 3GPP. Even though LTE has a centralized architecture (similar to earlier generations of cellular radio network systems and lacking a native ad hoc mode), it may be useful as a potential access technology for cellular radio networls due to serveral reasons: high data rates (¿100 Mb/s), which is suitable for information and entertainment services, besides the ability to tolerate high mobility with a low transmission latency. These advantages are relevant for road safety applications. Moreover, LTE can cover

a wider area with a higher penetration rate than 802.11p. Major telecommunication companies have been heavily investing in LTE infrastructure, which has already been deployed in some markets around the world. LTE is a promising technology with the ability to fill in major gaps from IEEE 802.11p, such as intermittent coverage and lower penetration rate. Major stakeholders have been testing the LTE technology for specific road safety applications and traffic efficiency messaging, such as nearby road hazards and traffic alerts over large coverage areas [33].

IV. Adoption of ITS Technologies in Brazil

In Brazil, the implemented ITS covers the dimensions of operation and road services [71]: the traveler; in-transit vehile; support systems; coordination and management systems. The Brazilian ITS communication infrastructure is shown in Figure 8.

Information about general traffic conditions is available to users by means of variable message signs and data centers (Wifi services, web portals and mobile applications). The system can also identify travelers through license plate recognition, transponders (RFID tags), MAC address from mobile devices and from shared tracking data between private and public organizations in association with road management companies. The vehicular control system can identify and monitor vechicles based on their goals (emergency, commercial use, personal use or road operation management vehicles). Besides, the system enables in-vehicle communication through open access networks among vehicles endowed with collision warning systems, which can inform (without human interference) accidents to operational control centers and roadside assistance or emergency vehicles. The structure system to support road operation is composed of field equipments devoted to communication and monitoring, e.g., sensors for counting vehicles, surveillance cameras, general telemetry (such as a weather station), tolls and elements for vehicle classification [71]. Brazil has only one OCC (Operations Control Center) for managing road operations, emergencies and maintenance. Public transport, tolls and commercial fleet management are not under the responsibility of OCC, which requires the implementation of communication subsystems through traffic data telematic infrastructure for communication, monitoring and managing protocols to help decision making [71]. Cameras, speed controllers, and traffic count are currently widely explored on Brazilian highways [72]. The electronic identification of cargo vehicles is under way and the enrolment of drivers is mandatory. Drivers must show the National Register of Road Freight Carriers (RNTR) and in the near future, by means of installed RFID (Radio-Frequency Identification) tags into those vehicles, it will be possible to identify them in order to control overload and minimize cargo theft. The remote operation will be carried out right after the identification and within the OCC of each of the road concession companies wherein Integrated Automation Systems (IAS) will be employed, such as video surveillance, cameras for the automatic recognition and identification of license plates, identification tag readers, roadside variable message signs to display the mandatory entrance to the weigh station and electronic display panels inside the patio from the surveillance checkpoints. Those displays will guide and inform drivers about the overweight and the means to solve the issue [72]. The "SEMPARAR" (Non-Stop) system allows the automatic identification of vehicles, Multi-lane Free Flow, Optical Character Recognition and Mobile resources. It works at the frequency range of 915 Mhz and 5.8Ghz [73].

A standard for communication between field and centralized equipments on Brazilian highways has been defined by the National Agency of Land Transportation (ANTT) through the resolutions 3,323/09, 3,323/09-a and 3,576/10. NTCIP (National Transportation Communications for Intelligent Transportation System Protocol) is a protocol designed from technical standards published by the American Association of State Highway and Transportation Officials (AASHTO). This protocol allows the "center do field" (C2F) or center to center (C2C) communication, which allows the exchange of information between equipments and control centers or among control centers, integrating different agencies. Despite being similar to the IP protocol, the NTCIP provides a dictionary of specific functional data to be used in smart transport systems, simplifying data communication between devices, as well as the installation and configuration of equipments, which allows these systems to be highly interoperable and scalable [71]. Deployment of VANETs in the Brazilian context can follow different directions. This will depend on the public policy that the government will adopt regarding this technology. Possibilities could range from private and public partnerships, which could allow the financial solution for development costs based on strategies to guarantee road safety; or place the radio electromagnetic spectrum for vehicle-to-vehicle communication purposes in a public tender offer. This paper aims at opening academic discussions about these different approaches and bringing to this context current local experiences and success stories from external realities. For example, Michigan University has been studying the transition to a new world of connected and automated vehicles and their work goes beyond technology [74]. Hence, the concept of VANETs is not restricted to the type of medium access technology or routing protocol that may be explored, but the impact that it is going to have on each element of the society. In the Brazilian context, there is a Traffic Engineering Company, Companhia de Engenharia de Tráfego (CET) [75], which is owned by the São Paulo City Hall. It monitors all the intersections with high vehicular load and, this way, can contribute with vehicular data to the civil society for road safety issues, traffic management, etc. Nevertheless, this data does not provide vehicular information to drivers in real time. In other words, it is demonstrated that developing cutting-edge technologies with no interaction with other agents involved in a vehicular environment does not solve the real problem, i.e., preventing accidents. On the other hand, the emergence of applications of GeoReferencing [76], in which drivers interact with each other, by notifying the community that there is an ongoing

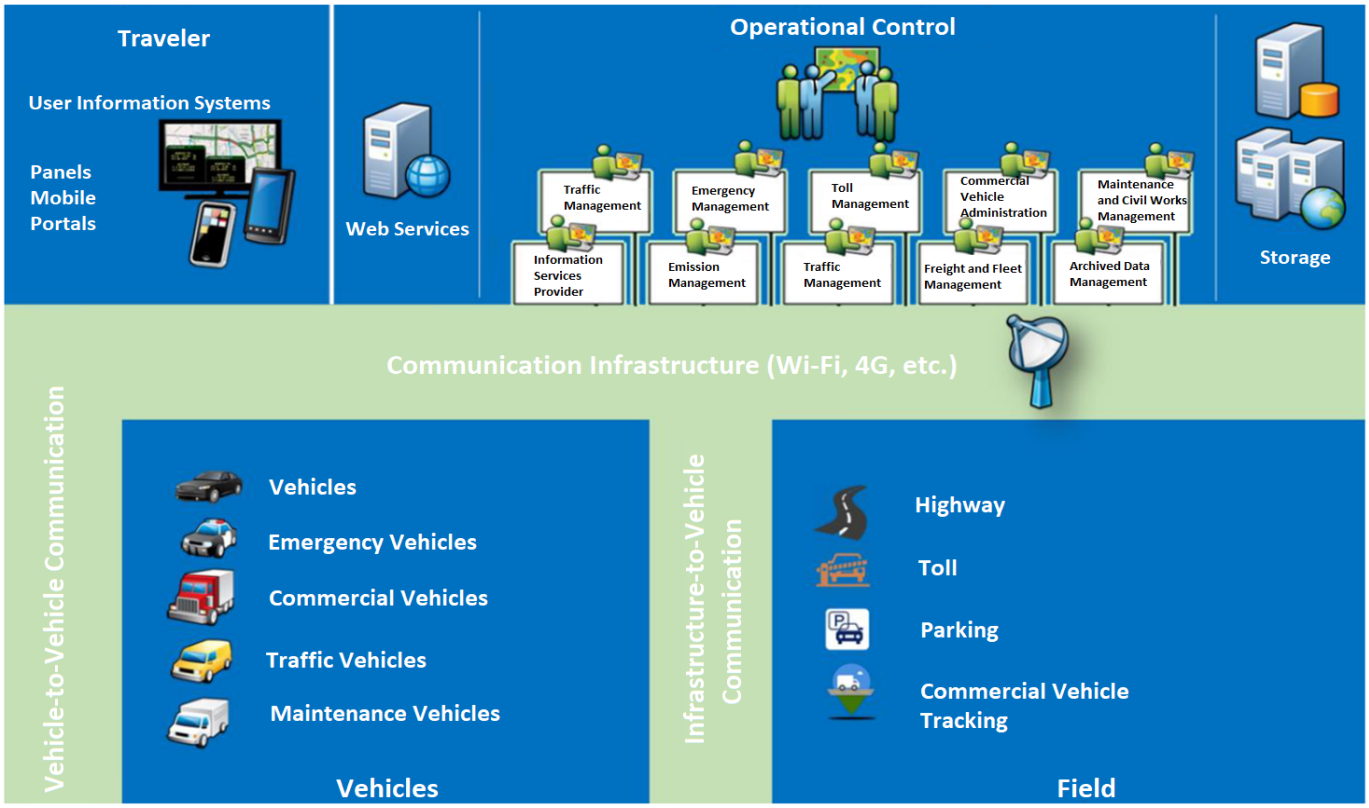

Fig. 8. Brazilian ITS communication infrastructure. Adapted from [71].

operation on a street, the existence of radars or even that an accident happened nearby. Information generated by this type of technology can be fake or cheat because there is no authority who verifies the veracity of posts from users. Again, the lack of communication among users and government agencies is not profitable for the society.

V. Technical Aspects and Challenges of Vehicular Communication

A. Technical Aspects of Vehicular Communication

Smart mobility has a massive interaction with technological advances in the future-driven fields of robotics, artificial intelligence, manufacturing (Industry 4.0), sustainability and global connectivity (Internet of Things) and future vehicles will act autonomously and interact permanently. These systems should undergo a profound change from static and monolithic designs towards much more dynamic and compositional concepts with security, safety, real-time, and maintainability in mind, in order to be prepared for use cases with strict demands on dependability. The concepts must support advanced multi-core and application-specific processor architectures, protection against environmental perturbation and attacks, dynamic update mechanisms, and simplified software portability for long-term operation [29]. The adoption of vehicular communication environments will include big data, security, privacy, reliability, mobility, and standards. These issues should be addressed to make IoV highly reliable and widely adopted. A major challenge is the processing and storage of big data created in IoV due to the large number of connected vehicles. For example, driverless cars are expected to process 1 GB of data per second. Mobile cloud computing and big data analytics will play important role in handling big data. Since IoV involves integrating many different technologies, services and standards, there is the need for data security. As an open, public network, IoV is a target for intrusions and cyber-attacks that may lead to physical damage and privacy leakages. Cars, sensors, and network hardware can malfunction. The system must deal with incorrect data, as well as faulty communications, such as denial of service attacks. As a rule, the safety of the vehicle is more important than entertainment. In a situation where vehicles are moving fast and network topology keeps changing continuously, it is a challenge to keep the nodes connected and provide them with resources to transmit and receive in real time. To accelerate adoption, standardization and interoperability are vital. The lack of standards makes an effective V2V communication more difficult. Adopting open standards will enable smooth sharing of information. Governments should participate and encourage industries to collaborate on the development of technological best practices and open international standards [77]. As discussed elsewhere [33], those authors describe communication and reliability among the technological challenges regarding vehicle communication: 1. Communication: a fully operating vehicular network will require unicast and multicast/broadcast delivery

capabilities for V2P, V2V, V2I and applications. However, this will require communication systems able to support both short-range and long-range communications. In this respect, the speed of vehicle trajectories, network density, changes in network topologies, and constrained bandwidth in vehicular networks are some of the challenges not found in smartphone internet applications. Open problems have not been fully addressed yet by the technology community, such as ensuring communication systems will not interfere with transmission schemes and how to provide low latency and high data rate for vehicular applications; 2. Reliability: it is critical that vehicular communication networks have robust and fault-tolerant softwares able to recover from connection downtime and system errors. Unlike other electronic devices that are prone to frequent hardware turnover, such as in smartphones, the computing hardware for vehicular networks (onboard units, vehicle sensors, etc) must have much longer usage once the lifespan of a vehicle is relatively high (they can last for more than a decade), whereas repair and maintenance may or may not occur according to manufacturers' guidelines. The reliability of both computing software and hardware components remains major technical hurdles which need to be solved so that car manufacturers could adopt and deploy them in large scale. It is possible to assign technological challenges to two communication environments: in-vehicle and inter-vehicle. In vehicle connectivity faces the following drawbacks [68]: harsh environment due to severe scattering in a very limited space and often none-line-of-sight. This is the major reason for extensive effort to characterize the intra-vehicle wireless channels [78]; data transmissions require low latency and high reliability to satisfy the stringent requirement of real-time intra-vehicle control system; Interference from neighboring vehicles in a highly densed urban scenario may not be negligible; security is critical to protect the in-vehicle network and control system from malicious attacks [79]. Moreover, a couple of wireless technologies have been studied to find the most convenient technique for connected vehicles. Inter-vehicle networks include DSRC, WAVE, 4G, LTE, etc, technologies which may allow the V2V, V2I, and V2R communication, regardless of being broadcast or unicast packets. The most cumbersome challenge is to combat the harsh communication environment [68] and the challenges are mainly related to ways for protocol access due to error estimates and high intensity of nodes and the underlying Physics behind vehicle mobility, power consumption, broadcasting support and self-interference, as shown in Table 4.

In urban scenarios, the line-of-sight (LOS) path of V2V communication is often blocked by buildings at intersections. On the other hand, on a highway, the trucks on a communication path may introduce significant signal attenuation and packet loss [81]. Field tests in [82] demonstrated that multipath fading, shadowing, and Doppler effects due to high vehicle mobility and the complex urban environment will lead to severe wireless loss, and with a large scale of vehicles transmitting simultaneously, the mutual interference plays an important role as well. Reference [83] presents an overview of the state-of-the-art vehicular channel measurements. It is noteworthy that there is a lack of unified channel model that can be applied for all scenarios (e.g., urban, rural, and highway), and the existing channel models, only for a specific scenario, have their own merits and deficiencies. The authors also provide suggestions for V2V communication systems based on the channel characterization. The adoption of multiple antennas, for example, would enhance the communication reliability [68]. From a network perspective it is possible to point out the following challenges [68]: 1) The network topology changes frequently and very fast due to high vehicle mobility and different movement trajectory of each vehicle. 2) Due to the high dynamics of network topology and limited range of V2V communication, frequent network partitioning can occur, resulting in data flow disconnections. 3) Surrounding obstacles (e.g., buildings and trucks) can lead to an intermittent link to a mobile vehicle. In addition to the technical challenges, in the [68]: 1) To enable various wireless connectivity, multiple radio interfaces have to be implemented, such as DSRC/WAVE, WiFi, and 3G/4G-LTE interfaces, which may incur a high cost and thereby hinder the development of connected vehicles. A unified solution to provide V2X connectivity with low cost might be required. 2) In-vehicle systems have stringent requirements on latency and reliability for control/monitoring purposes. The full adoption of V2S connectivity may not be feasible in the near future unless V2S connectivity can provide the same performance and reliability as the wired communication [84]. 3) Connected vehicle offers drivers a variety of information. However, research from [85], [86] suggests an up limit on information provided to the driver. Excessive information increases the driver's workload and hence has a negative impact on safety. Therefore, the vehicle information system has to be appropriately designed for offering information to drivers. The Brazilian infrastructure for ITS is still in its infancy and it is not yet integrated to vehicles and RSU. Nonetheless, the ITS communication from center to center through NTCIP C2C is already working [87]. Thus, there are many challenges to adapt Wi-Fi technologies to support the unique requirements of vehicular communications, such as achieving high and reliable performance in highly mobile, often densely populated, and frequently none-line-of-sight environments. The automotive and the communication industries, academia, and governments around the world have been devoting tremendous efforts to address these challenges and significant achievements have been made. Over the last decade, there have been vigorous joint efforts from the industry, academia and government to validate the DSRC technology and also to identify and address key technical and business challenges. In [10] the author provides the lattice AI which gives a solution on how to enable the sync between multiple companies, which provide connected car solutions so that they can connect with each other on a unanimous network running on machine learning and swarm algorithm, and how to share resources. This remark is in good agreement to what happened in Brazil when telecommunication companies deployed cell phone technologies into the national market by the gradual

TABLE IV
CHALLENGES AND SOLUTIONS FOR INTER-VEHICULAR COMMUNICATION. ADAPTED FROM [80].

Medium	Challenge	Proposed solution
PHY Layer	Channel Estimation in Vehicular Environments	a) Turbo receiver: Using tools from modern coding theory to deal with channel estimation errors: e.g. introduce a Turbo receiver [83]; b) Decision feedback receiver: for the case as already-decoded bits as pilots for the remaining packets to improve channel estimation by tracking the channel variations significantly better than standard non-iterative schemes.
	Time selective fading without time interleaving	It can be solved using a better coding scheme (e.g. Turbo or LDPC code). However, this indeed requests a standard change and is better to be addressed in future versions of DSRC
MAC Layer	CSMA behavior at high node density pottentialy resulting in congestion control	A natural approach to reduce congestion is to reduce the number of transmitters within the carrier sense range of each device [59], [84]–[87]. A typical scheme to balance collisions and channel utilization is to use a distributed congestion control mechanism as described in [59], [87]; Another promising method is to use a time-slotted synchronous system with a fixed set of broadcast resources. One can employ a simple MAC protocol, [88], [89] to manage which transmitters should use which resources (e.g., time slots); Slotted TDM systems are typically well suited for periodic transmissions of roughly equal size packets for prolonged durations so the addition of such "hooks" into the DSRC can be beneficial (not specified).
Multi-channel Operations	Single Radio Devices (reduced capacity to support the broadcasting of safety messages)	Many simulation studies have shown that to support vehicle safety broadcasts in typical vehicle densities, most or all of the sync interval would be required; Some studies [80], [81] indicate that even with a fully dedicated 10 MHz channel for safety and control, the channel congestion issues still remain.
	Multiple Radio Devices (The spillage of power into adjacent bands when transmitting and self- interference cancellation)	Certain techniques, which are well studied in the full duplex context, including analog cancelation and digital cancelation can be applied here.

and successful adoption in many cities. This has been shown for the implementation of cellular network technologies such as 2G, 3G, and 4G which reached, respectively, a coverage area of 100% of Brazilian cities (5570 municipalities), 96.46% (5,373 municipalities) and 74.60% (coverage reaches 4,155 municipalities) [88] through investments from companies such as Algar, Claro, Nextel Oi, Sercomtel, Tim and Vivo. They were regulated accordingly by ANATEL (National Telecommunications Agency) based on constitutional principles of economic activity, according to Art. 126 from the General Telecommunications Law, through Personal Mobile Service – SMP [89]. Therefore, it was noticed that the Government has to offer tax breaks for private companies so that they can succeed into the automotive market with less restrictions, but without any reduction in the quality and security of services provided. One of the biggest challenges for ITS is the search for a cooperative and safe environment (C-ITS), which could share data among all the applications developed by the diverse independent players [90]. The success of ITS depends on a significant number of players, such as public administration, transport authorities and companies of various segments such as vehicle manufacturers and OEM (Original Equipment Manufacturer), telecommunication companies, service providers, etc. Within the industrial and technological perspectives, ITS is considered one of the biggest challenges of the TIC community. Therefore, the presence of world standards is a key requirement for exploring its entire potential. Since 1990 standardization efforts have been evolving from various organizations such as IEEE (Institute of Electrical and Electronics Engineers), ISO (International Organization for Standardization), CEN (European Committee for Standardization), ETSI (European Telecommunications Standards Institute), among others [72].

B. Frequency Spectrum Allocation

Even though a global harmonization of DSRC standards and its spectral allocation are not available yet, IEEE committee for standardization (Institute of Electrical and Electronics Engineers) and ETSI (European Telecommunications Standards Institute) have been working on the harmonization of standards for the North American and European regions. There is a second band for DSRC applications (915 MHz for the USA and 700 MHz for Japan), which has been mainly explored for ETC and commercial applications [8]. A complete survey on the history and description of all countries and the allocation spectrum for DSRC is out of the scope of the present study, which is focused on describing only the most important ones. A brief historical study on ITS communication in Japan and in Europe was described herein in Section 2.1. Further information on the architecture and ITS communication concepts in Japan and Europe is available elsewhere [33], [91]. Differently from wireless networks based on frequency ranges from restricted radiation equipments (ISM – Industrial, Scientific and Medical applications), the communication range employed in vehicular networks is exclusive for the DSRC protocol [47]. However, regulations for adotpting dedicated frequency ranges for DSRC in Brazil have not been established yet. Figure 9 depicts the frequency ranges for vehicular communication explored in the main ITS development communities: ITU-R,

Europe, and the United States. It may be noticed that the ITS frequencies chosen in Europe and the United States range from 5.8 and 5.9 GHz.

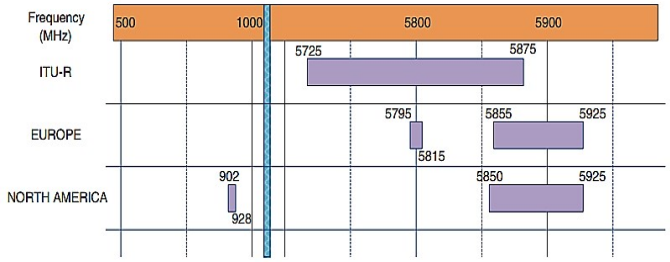

Fig. 9. Spectral range for ITS applications [55].

Regarding spectrum allocation, while FCC (United States Federal Communication Commission) and the Canadian industry allocated a radio band of 75 MHz from 5,850 to 5,925 GHz, in Europe ECC (European Electronic Communications Commitee) assigned 70 MHz from 5,855 to 5,925 GHz, whereas in Japan the allocation was 80 MHz for a band of 5.8 GHz. Nevertheless, in Japan DSRC is not compatible with the American and European standards due to the Japanese development of ETC (Electronic Toll Collection). The frequency range of 75 MHz was allocated by the FCC for vehicular communication in the frequency spectrum of de 5.9 GHz – from 5,850 GHz to 5,925 GHz, which is restricted and licensed to vehicular communications, even though it is free of charge and can be used for free as well. According to the European Telecommunications Standards Institute [92], the following frequency ranges have been reserved for vehicular communications: 5,855 GHz to 5,875 GHz (general applications); 5,875 GHz to 5,905 GHz (emergency applications and traffic security); 5,905 GHz to 5,925 GHz (reserved for future needs) [8], [56]. The standard supports four modulation techniques (BPSK, QPSK, 16-QAM, and 64-QAM). Since a transfer rate of 6 Mbps (QPSK) seems to provide a suitable balance between channel load and noise-to-signal ratio, many tests involving IEEE 802.11p in the United States rely on 6Mbps. In order to reach a higher performance in terms of DSRC communication, the system may adapt its data rate according to the distance between the vehicle and RSU. If a vehicle is away from the RSU (more than 150 km away), for example, it is preferred to send data by using a low data rate. In case the vehicle is rather close to the RSU (less than 150 m), commuting is advisable for reaching higher data rates. The SAE J2945.1 standard defines the requirements for transmitting data, transmit power control and adaptive message rate control [8] in order to allow minimum performance. In Brazil, the organization liable for regulating the automotive sector is ABNT (Brazilian Association of Technical Standards) by means of the Brazilian Automotive Committee ABNT/CB-005 [93], which works on the standardization of different automotive areas (cars, trucks, tractors, buses, mopeds, bicycles, motorcycles, autoparts and components), as well as in vehicle repairs and emissions. Nevertheless, reports or descriptions of connected vehicles or their regulation and legislation have not been found yet on the ABNT database. In terms of the legislation governing telecommunications, ANATEL (Brazilian Telecommunications Agency) is responsible for, among other duties, managing and supervising the use of the frequency spectrum. When searching its database, regulations for the use of the frequency spectrum according to WAVE/DSRC (from 5,850 to 5,925 GHz) standards were not found. By analyzing the Frequency Ranges Assignment, Destination and Distribution Plan in Brazil [94], it was noticed that the frequency ranges for Region 2 (according to ITU – International Telecommunication Union), the geographical location which includes Brazil, have similarities to those currently adopted in Brazil, as shown in Table 5. In Table 5 the labels are space-to-ground (*), ground-to-space(**) and international notes (***).

TABLE V
ASSIGNED SERVICES ACCORDING TO FREQUENCY RANGES [94]

Ranges (MHz)	Region 2 (ITU)	Brazil
5725-5830	Amateur radio Restricted radiation	ANATEL Res. N452/2006 (D.O.U., Official Gov. publication on 12/20/2006) ANATEL Res. N506/2008 (D.O.U., Official Gov. publication on 07/07/2008)
5830-5850	Radiolocation Amateur radio Amateur radio over Satellite* 5.150, 5.453, 5.455***	Radiolocation Amateur radio Amateur radio over Satellite* 5.150***
5850-5925	Fixed Fixed-Satellite** Mobile Amateur radio Radiolocation 5.150***	Fixed-Satellite** Amateur radio 5.150***

The services described for assignment and destination of radiofrequency ranges (see Figure 9) are arranged in two columns: primary service (fixed, limited, etc), were written in upper case letters and secondary service (mobile, plain old telephone service – POTS, etc) were written in lowercase letters. Therefore, it is noticed that the last range (5,650 to 5,925 GHz), which should be assigned to V2X communication, is explored in Brazil for primary services (fixed-satellite) and secondary amateur services, whereas the assignment from ITU is for primary service "Mobile" (cell phones). Such terms (Fixed, Fixed-Satellite, Radiolocation and Mobile) are related to radiocommunication services defined by ITU, under its Radio regulations (RR), which can be reached at: http://www.itu.int/pub/R-REG-RR-2016. Nonetheless, the ANATEL plan contains an international footnote 5,150, which describes the frequency range of 5725-5875 MHz as also devoted to industrial, scientifical and medical (ISM) applications. Radiocommunication services operating within this range should accept harmful interference arising from the use of this range for any application. Therefore, the use of frequency ranges destined by the DSRC protocol may be adopted within the national territory for vehicular applications, as well as VANET. Modeling VANET communication net-

works should consider which infrastructure would be mounted. Re-using existing infrastructure or planning new networks are viable possibilities. LTE infrastructure is well deployed in Brazil and worldwide. VANETs can rely on this network to carry information, despite sharing the same spectrum with other services, such as data, voice or video, which will be a drawback, besides high latency and less reliability [95]. New advances on LTE will allow operators to configure a Broadcast Service, LTE broadcasting or eMBMS (evolved Multimedia Broadcast Multicast Service) [96]; the operators should give up a portion of the spectrum that will be allocated for VANETs communications. The design of how much bandwidth would be allocated for VANETs is a challenge for future networks and additional tests focused on delay measurements in this technology are desirable.

C. Security Aspects in Vehicular Communication

Vehicular applications from IoT have data exchanges involving security and privacy issues [11]. Otherwise, attackers could send corrupt or subverted information aiming at wrong warnings for drivers or even wrong automatic reactions from cars in case of autonomous driving, which could give rise to accidents, injuries or fatalities. An example would be the message of electronic emergency brake light that was fabricated or replayed, which would make the receiving vehicle to immediately brake without any obstable ahead. Thus, safety mechanisms for intelligent transport systems (ITS) are crucial for supporting safety applications based on V2X communication [97]. Many applications for vehicular networks are directly related to reliable information, non-disclosure of sensitive information and the protection between the receptor and the emitter. Many attacks can be done to any kind of electrical vehicle communication, such as those summurized in Table 6.

TABLE VI
VULNERABILITIES RELATED TO CONNECTED VEHICLES [98].

Category	Vulnerability		
V2S	DoS, Jamming, False data injection, GPS deception		
V2V	DoS, Selfish attack, Modification, Sybil attack, False data injection, Eavesdropping, Black Hole, Gray Hole and Wormhole attack.		
V2I	Replay, Router Advertisement Forgey, Privacy, RSU Spoofing, DoS of the DAD		
V2N	Mobile Femtocell	MOBIKE	DoS, MiTM, Spoofing
		Femtocell	Physical Attacks, Configuration Attacks, MiTM, DoS, privacy, among others
	5G	Mmwave and D2D: Eavesdropping, privacy; jamming attack	

According to [98], the communication attacks can be classified according to the communication category, as: Vehicle to Sensor (V2S) attacks – attacks that affects the sensitive data between sensor and vehicle and directly impacts on Urban Platform for Connected Electric Vehicles due to wired communications which are vulnerable to malware, enabling third part to control the communication interface, e.g. CAN bus. It can result in essential services damaged and system failture, i.e. Denial-of-Service attack (DoS) [99]. For Wireless Sensor Network (WSN) attacks, a malicious node can seriously cause malfunctioning of the vehicle operation by executing attacks on the vehicle sensor network such as jamming attack (malicious nodes block legitimate communication by causing intentional interference in networks [100], false data injection attack (sending false data from sensors to ECU), Global Positioning System (GPS) deception (fase information about vehicle location or GPS around) and DoS (uninterrupted message bombarding to ECU); Vehicle-to-Vehicle (V2V) attacks: attacks on communication between two or more vehicles and can be classified as selfish attack (refusing to send or receive message with vehicles or server or message not reaching all vehicles if selfish nodes increase), modification attack (modify or alter content of message sent to server), sybil attack (multiple identities and from different positions to inject false information in the network), false data injection attack (a node sending information to vehicles around to affect the prediction in the server), eavesdropping (detect sensitive information by an unauthorized node about a vehicle and leading to privacy attacks), Black Hole attack (putting a sender node into erroneous condition of shortest path [101], [102]), gray hole attack (extension of black hole attack but dropping messages in a selective way), wormhole attack (by revoking legitimate links between vehicles and hence any data transmitted between legitimate vehicles will pass through the attacker [103]), denial-of-service (when attacker try to cause failure to the system's operation); Vehicle to Infrastructure (V2I) attacks: replay attack (through replaying old messages to neighbors resulting in causing connection failure), router advertisement forgery (forging a router advertisement- RA message with an invalid next hop), privacy attack (assuming that the prefix sent by the RSU in the RA message remains unchanged and prefix is associated to a geographic area, a malicious node on the Internet can create a map based on this association), RSU spoofing (spoof the IP address of the RSU and send an invalid prefix), Duplicate Address Detection (this mechanism is vulnerable to a denial of service attack). The attacker responds to all address duplication detection messages that it has already taken the requested IPv6 address [104]). Vehicle to Network (V2N) attacks: DoS on the road-side WiFi Access Point (WiFi AP), MOBIKE vulnerability - many attacks can be performed on MOBIKE such as Denial of Service (DoS), Man-in-the-Middle (MiTM) and spoofing attacks [105]. Besides that, mobile Femtocell is based on femtocell (Home eNodeB (HeNB) [106]) and it can be subject to several types of attacks as Physical Attacks (the hacker can modify or replace HeNB components), Configuration Attacks (misconfiguration of the Access Control List – ACL - of the targeted HeNB), Protocol Attacks (e.g. man-in-the-middle attacks on HeNB), DoS on Mobile Operator's Core Network, User Data and Identity Privacy Attacks, Radio resource management tampering [107]; 5G technology can be perceived as a revolution for Vehicle to Network communications, even considering vehicles are able to connect to the 5G cellular

network through direct links with the mmWave small cells or by via other devices using D2D communication. The mmWave and the D2D can be subject to the eavesdropping attack [108]. The authors in [109] classify next-generation networks (e.g. 5G) as vulnerable to the jamming attack since they are based on the densification (ultra-dense networks - UDNs). Spoofing attacks have been reported [110], as well as PII (Personally Identifiable Information) and SPI (Serial Peripheral Interface) leaks were some of the threat types for IoT (Internet of Things) in-car WiFi smart appliances. Such attacks could turn cars into mobile hotspots, connecting passenger devices to the Internet and grabbing sensitive information. Some studies have shown some security requirements should be found in vehicular communication environments. These requirements are [97]: 1. confidentiality: overall, V2X communication tries to improve the awarness of car's surroundings, such as the existence of other cars or hazards, for example. Therefore, vehicular communications are typically open, since confidentiality represents a minor requirement. Only some specific issues such as transactional applications (e-tolling, pay-per-view, for example) will require confidentiality. 2. integrity: V2X messages are the basis for decision making, such as in warning drivers or trigerring an automatic response from the vehicle. The latter requires messages in their integrity. Assuring messages were not manipulated may be carried out by using integrity mechanisms, such as digital signature, for example, which has been explored in current Telecommunications Standards [92]; 3. authentication: each message sent over a vehicular network may be authenticated to prevent malicious attackers from inserting messages. The authentication is usually provided by digital signatures and public key infrastructures; 4. Availability: V2X communication must be available for real-time safety applications. Nonetheless, this is a hard task considering that jamming is likely to happen in wireless communication [111]; 5. Protection of privacy: even though there are some requirements for authentication, as described before, vehicles and drivers should not be identifiable, otherwise the location profiling of drivers could be exposed; 6. liability or non-repudiation: this feature requires that any receiving entity could prove to third parties the message was sent by a unique sender. This is somewhat challenging when confronted with privacy protection and the fact that authorized entities, such as those responsible for law enforcement, should identify vehicles or not, is currently under scrutiny. The unique characteristics of moving vehicles have been underlined and some improvement suggestions from literature have been presented elsewhere (improving transport protocols, enhancing MAC protocols for mobility related devices etc.) [68]. As described by [112] main constraints under which VANET must operate, as well as the security requirements: authentication, availability, non-repudiation, privacy, real-time guarantees etc. A novel privacy-preserving randomized authentication protocol is proposed by [113]. The principle of homomorphic encryption is used to allow each individual vehicle to generate its own identities. Therefore, the public acceptance and the addoption of cooperative V2V safety applications will depend on suitable levels of security as an integral part of the system. Differently from other safety technologies, V2V safety applications are cooperative, since both vehicles must send, receive, and analyze data in real time. This cooperative data exchange about potential threats and hazards is crucial for alerting and warning drivers on their decisions and actions towards avoiding imminent accidents. This is a new paradigm which is at odds with stand-alone vehicle systems based on sensors. Nevertheless, a cooperative system can only work when participants in that system trust the alerts and warnings broadcasted by other V2V devices relying on messages from other V2V devices [5]. As described in [114], the already existing and/or proposed mitigation strategies depend on the attack type. But despite this still open emerging security problems such as the trustworthiness evaluation of nodes in VANET, data context trust and verification and so on. The DSRC, for example, received more security and privacy improvements than traditional WiFi and the connected vehicle environment is guarded by physical controls (physical protection around equipment such as tamper-proof casings), technical controls (technologies designed to protect data, such as firewalls, access management, and encryption) and administrative controls (Laws and regulations regarding unauthorized collection, storage, and disclosure of data and fair information practice principles) [5]. Moreover, the polytics for data access and its availabitlity in Brazil provides the confidence to consumers about IoT resources. This may be observed from the Laws: 1. The Brazilian Civil Rights Framework for the Internet (Law 12,965/2014) regulates the use of the internet in terms of principles, warranties, rights, duties and Government actions in order to ensure the organization and order about the Internet; 2. Brazilian General Data Protection Law (Law 13,709/2018) – this law provides on gathering, processing, protecting, and using data by a natural person or legal entity governed by public or private law, in electronic or physical support the processing of personal data. It is expected to go into effect in February 2020. These laws impose criminal and administrative penalties when the norms are violated. However, despite the existence of laws and safety protocols to be followed by information-sharing communication entities, consumers should rely on best practices regarding information security, such as those described elsehwhere [115], as well as general recommendations on information secutiry, e.g.: ensuring all security and operation systems, and technological devices are up-to-date or automatically updated when their hardware or operating system provider issues new fixes; preventig the execution of malicious code on macros (e.g. by disabling automatic runs), analyzing and improving the configuration setup (firewall, sharing, privilege levels and access permission) and generating strong-type passwords and properly store sensitive information.

D. Social Challenges

The organizations liable for managing, regulating, and supervising the National Traffic System in Brazil are public institutions composed by the entities: National Traffic Council

(CONTRAM), National Authority for Terrestrial Transport (ANTT), National transport infrastructure department (DNIT), State Traffic Department (DENATRAM), Federal Highway Police (PRF), State Traffic Council (CETRAN), Department of Roads (DER), Municipal Traffic Department, and Municipal Highway entities [116]. Therefore, the adoption of new technologies on municipal roads or Federal/State highways must undergo the scrutiny of the public jurisdiction before its implementation. This allows for a higher control over traffic infrastructure (e.g. legislation, signaling, road maintenance, and construction of new roads), monitoring traffic conditions, counting vehicles, weighing and tolling. Public institutions must be properly aligned with technological innovations for integrating the Smart Transport System. This way they would enact laws on the adoption of new technologies and vehicle services, such as the frequency spectrum, homologation of electronic equipments (electronic circuits from control circuit, processing, communication and power boards), besides motivating the integration among many technological assets (e.g. vehicles, RSU, infrastructure and personal devices). Therefore, the adoption of a vehicular communication technology will depend on the population, wherein most contributors come from, who should notice the importance of implementing the ITS traffic infrastructure, the gradual incorporation of vehicular technology and the use of information arising from data processing for social welfare, i.e., the best transport option to choose from (subway, bus or private car), traffic and weather conditions, jamming and route optimization (algorithm for predicting arrival times in mobility applications [117], [118]), so that users could reduce their travel time from origin to destination. An example is given by the progressive use of urban mobility services such as 99 (available in 1705 cities) [119], Uber (100 cities) [120] and Cabify (8 cities) [121], thanks to the alliance and mobilization of private companies and the population against polytics favoring taxi services aimed at keeping high transport costs and the restriction of using mobility applications [122]. This was possible because the population noticed the benefits from sustainable mobility arising from mobility applications (affordable prices when compared to conventional transport modes for short distances due to their low operating costs, flexibility in terms of service availability and practicality in terms of service use) and kept aligned to the interests of the companies. This achievement may be understood through methodologies and implemented actions by means of laws or resolutions devoted to make people aware of and show the feasibility of using and adopting new technologies, besides successful case studies such as that from Mcity Driverless Shuttle, developed by the University of Michigan [74] and the awareness of how sustainable urban mobility is in the city of Curitiba [123]. The compelling motivation comes from: 1. Gradual investment in preventing accidents by the use of ITS technologies in order to save 3.1 billion US dollars spent on accidents, as shown in Table 1; 2. Brazil renewed its commitment towards the United Nations, during the Decade of Action for Road Safety 2011/2020, which means reducing by half the number of traffic deaths and injuries through the National Plan for the Reduction of Deaths and Injuries in Road Accidents (Pnatrans), Law 13,614/18, according to [124].

VI. Legislation, Public Policies and Legal Aspects

The adoption of connected vehicles and ITS Technologies in conjuction with the increasing level of vehicular automation has economical, legal, criminal, and administrative consequences. According to [7], the economical consequences impact the allocation of vehicles, the supply chain from automakers, passenger transportation services and the income of those working as drivers, such as taxi services and mobility applications, due to the gradual replacement of the driver; on-demand use of vehicles, instead of a daily rent; and redesign of automakers to adapt themselves to the new consumption requirements without the need of a car per family member. It expected that the productivity of workers increases, once the time for daily trips from home to work and vice-versa (which means 64 minutes on average in Sao Paulo) will be reverted to production capacity by using technological resources (tablets, laptops, etc). Expected legal consequences are the implementation of the social function of property in light of car sharing, which will require usage fees, renting a vehicle and higher traffic efficiency. Finally, there is the civil responsibility and the convenience of compulsory insurance: on the basis of Negligent Entrustment, the Brazilian Superior Court of Justice (STJ) understood that the losses caused to third parties are the responsibility of the owner of the vehicle, even if it is proven that he/she has not driven it, since the owner has the intellectual command and will be responsible for damages caused to third parties independently of being considered guilty. However, in case the damage was caused by a manufacturing defect, it is legal that the owner asks the manufacturer or the company responsible for the maintenance the reimbursement of the amount of money awarded in compensation, on the basis of prohibiting unjust enrichment, according to Article 934 from the Brazilian Civil Code and on the analogical application of Article 13, sole paragraph, from the Brazilian Consumer Defense Code; the same situation happens when a consumer suffers damages arising from an accident. In such a case the legislation must be adapted for enforcing a mandatory insurance from vehicle owners. Therefore, it is noticed that the specific legislation in Brazil for the use of ITS technologies is outdated, even though it was implemented since 2009, it is still restricted to the adoption and implementation of norms, protocols, specifications and prices for highway communication infrastructure, such as ANTT n. 3,323-A on 11/18/2009 [125]. This regulation provides for the adoption of Data Communication Protocols and libraries of data standards from NTCIP (National Transportation Communications) for ITS protocols developed by the National Electronics Manufacturers Association (NEMA), in conjunction with the American Association of State Highway and Transportation Officials (AASHTO), the Institute of Transportation Engineers (ITE) and ANTT n. 3,576 on 09/02/2010 [87]. This resolution

provides for the specifications and prices for ITS systems (Intelligent Transportation Systems) based on Vehicular Traffic Sensing; Variable Message Signs - fixed; of Variable Message Signs - Mobile; Weather sensors; surveillance cameras (CFTV) and height detection to be adopted on Federal concession highways, regulated by ANTT [125]. However, a transport partnership between Brazil and the United States is under way, whose primary aim is to allow a technical exchange in order to boost ITS and reinforce the implementation of National Transportation Communications for Intelligent Transportation System Protocols (NTCIP), besides fostering the discussion on the evolution of the architecture and support for integrating connected vehicles [126].

VII. Conclusion and Prospects

The vehicle communication technology, mainly driven by the development of V2V, V2I, and the IoV concept, is already a reality in the aftermarket and it is possible to acquire equipments to connect vehicles and traffic infrastructure. The connectivity solutions already available in the automotive industry are restricted to V2D communication, via Bluetooth and USB connection applications. Regarding traffic infrastructure solutions, other resources were found, such as e-toll payment and the opening of gates by using RFID. Many researches and practical tests have been carried out since the late 1980s, and today the advance of scientific research is well ahead of the solutions found in the market (such as the use of 5G for V2I communication). In addition, although the current development phase of connected vehicles is not sophisticated, it allows vehicles to communicate with each other and with the traffic infrastructure. It has been found that many countries (from the European Union, the United States, Japan, and China) have their own vehicle communication standards and are implementing tests in real-life traffic situations for later standardization and description of relevant legislation for connected vehicles. This demonstrates the need for harmonization of international standards and further research on standards, vehicle experiments, development and adoption of connected vehicles more efficient and easier. During the research it was noticed that the automobile market is very restrictive in terms of adoptiing new technologies due to the costs of manufacturing and assembly, both to the automakers and to the customers and to the time required for certification and homologation of new equipments. The solution would be the use of technological resources in the aftermarket, where the user could choose the type of equipment to be used and install it in the vehicle, to make it connected. The present work aimed at the research and discussion of main studies in connected vehicles, emphasizing the state-of-the-art V2V and V2I communications. In this case, the goal for state-of-the-art technologies was reached, since many studies were searched over the main databases from the academic environment and reports from entities related to ITS. For this purpose, the article objective was accomplished, pointing out the simulation resources, devices used for vehicular connectivity and practical tests developed for communication evaluation. Research case studies were presented for academic and governmental entities and it was possible to observe a comprehensive, diversified state of the art in the field with well-defined technical specifications through the standards and norms of major regulatory institutions such as ISO, IEEE, ETSI, USDOT, and EC. However, no simulation studies were described, nor was it possible to conduct a case study to obtain all the communication requirements necessary to implement a stand-alone vehicle and to correlate the data achieved with the academic or governmental database. There is still a lot of research and development to be carried out, since the implementation of connected vehicles in real ITS environments is in the initial phase and there is a shortage of transit infrastructure and telecommunications able to support all the applications. As research and future studies, it is proposed searching for each communication requirement to keep the vehicles connected, perform simulation for operation analysis and practical tests involving vehicular applications and traffic infrastructure. Other studies can be developed based on the use of 4G and 5G technologies for broadcasting between the traffic center and the vehicles versus the use of devices connected to the Internet through IoT.

Acknowledgment

The authors are grateful to: Coordenação de Aperfeiçoamento de Pessoal de Nível Superior (CAPES); Conselho Nacional de Desenvolvimento Científico e Tecnológico (CNPq); Fundação de Amparo à Pesquisa do Estado de São Paulo (FAPESP); Departamento de Comunicações (DECOM); Faculdade de Engenharia Elétrica e de Computação (FEEC); Universidade Estadual de Campinas (UNICAMP); for their financial, administrative, and infrastructure support for the development of this research.

References

[1] WHO, "Global Status Safety on Road - Report 2015," World Health Organization, Tech. Rep., 2015. [Online]. Available: http://www.who.int/

[2] V. Maciel, "Óbitos por acidentes de trânsito caem pelo segundo ano consecutivo," 2017.

[3] Institute for Applied Economic Research (Ipea), "Estimativa dos Custos dos Acidentes de Trânsito no Brasil com Base na Atualização Simplificada das Pesquisas Anteriores do Ipea," *Relatório de Pesquisa do Instituto de Pesquisa Econômica Aplicada*, p. 20, 2015. [Online]. Available: http://www.en.ipea.gov.br/

[4] C. H. R. de Carvalho, "Mortes Por Acidentes De Transporte Terrestre No Brasil: Análise Dos Sistemas De Informação Do Ministério Da Saúde," *Instituto de Pesquisa Econômica Aplicada*, p. 50, 2016. [Online]. Available: http://www.ipea.gov.br

[5] J. Harding, G. Powell, R. Yoon, J. Fikentscher, C. Doyle, D. Sade, M. Lukuc, J. Simons, and J. Wang, "Vehicle-to-Vehicle Communications : Readiness of V2V Technology for Application," National Highway Traffic Safety Administration, Washington, DC, Tech. Rep. August, 2014.

[6] NHTSA, "Preliminary Regulatory Impact Analysis FMVSS No. 150 Vehicle-to-Vehicle Communication Technology for Light Vehicles," National Highway Traffic Safety Administration, Tech. Rep., 2016.

[7] C. E. E. de Oliveira and T. A. C. B. Leal, "Considerations on the Autonomous Vehicles - possible economic, urban and legal impacts," Senado Federal, Tech. Rep., 2016. [Online]. Available: https://www12.senado.leg.br/publicacoes/estudos-legislativos/tipos-de-estudos/textos-para-discussao/td214/view

[8] A. Chekkouri, A. Ezzouhairi, and S. Pierre, "Connected vehicles in an intelligent transport system," in *Vehicular Communications and Networks: Architectures, Protocols, Operation and Deployment*, W. Chen, Ed. Elsevier, 2015, vol. 1, ch. 10, pp. 193–.

[9] Q. Hong, E. P. Dennis, R. Wallace, and J. Cregger, "Global harmonization of connected vehicle communication standards," Michigan Department of Transportation and the Center for Automotive Research, Tech. Rep., 2016.

[10] K. Ranjan, "The Lattice: An intelligent grid for connected car Industry," in *2017 IEEE Transportation Electrification Conference (ITEC-India)*, IEEE, Ed., 2017, pp. 1–5.

[11] R. A. Badea and L. Stanciu, "A Survey and Research Model for Vehicular Communication and Security Challenges," *2018 International Conference on Communications (COMM)*, pp. 291–296, 2018.

[12] J. Greenough, "THE CONNECTED CAR REPORT : Forecasts , competing technologies , and leading manufacturers," 2016. [Online]. Available: https://www.businessinsider.com.au/connected-car-forecasts-top-manufacturers-leading-car-makers-2016-4

[13] Statista, "Projected size of the global connected car market in 2016 and 2021, by segment (in billion euros)," 2016. [Online]. Available: https://www.statista.com/statistics/297816/connected-car-market-size-by-segment/

[14] G. V. Research, "Connected Car Market Size To Reach $180.30 Billion By 2022," 2016. [Online]. Available: https://www.grandviewresearch.com/press-release/global-connected-car-market

[15] Z. Ning, F. Xia, N. Ullah, X. Kong, and X. Hu, "Enabling Mobile And Wireless Technologies For Smart Cities: Vehicular Social Networks: Enabling Smart Mobility," *IEEE Communications Magazine*, vol. 55, no. 5, pp. 49–55, 2017.

[16] R. Molina-Masegosa and J. Gozalvez, "LTE-V for Sidelink 5G V2X Vehicular Communications: A New 5G Technology for Short-Range Vehicle-to-Everything Communications," *IEEE vehicular technology magazine*, no. December, 2017.

[17] K. A. Rahman and K. E. Tepe, "Towards a cross-layer based MAC for smooth V2V and V2I communications for safety applications in DSRC/WAVE based systems," *2014 IEEE Intelligent Vehicles Symposium (IV)*, pp. 969–973, 2014.

[18] R. F. Atallah, M. J. Khabbaz, and C. M. Assi, "Vehicular networking: A survey on spectrum access technologies and persisting challenges," *Vehicular Communications*, vol. 2, no. 3, pp. 125–149, 2015. [Online]. Available: http://dx.doi.org/10.1016/j.vehcom.2015.03.005

[19] H. Chenguang, Z. Kaiyu, and W. Shouming, "Analysis of the channel capacity with shadowing fading in VANET," *2018 14th International Wireless Communications & Mobile Computing Conference (IWCMC)*, pp. 577–581, 2018.

[20] P. Salvo, F. Cuomo, A. Baiocchi, and I. Rubin, "Investigating VANET dissemination protocols performance under high throughput conditions," *Vehicular Communications*, vol. 2, no. 4, pp. 185–194, 2015. [Online]. Available: http://dx.doi.org/10.1016/j.vehcom.2015.07.003

[21] D. Das and R. Misra, "Efficient vehicle to vehicle communication protocol for VANETs," *Engineering and Computational Sciences (RAECS), 2014 Recent Advances in*, pp. 1–6, 2014.

[22] M. Amoozadeh, H. Deng, C. N. Chuah, H. M. Zhang, and D. Ghosal, "Platoon management with cooperative adaptive cruise control enabled by VANET," *Vehicular Communications*, vol. 2, no. 2, pp. 110–123, 2015. [Online]. Available: http://dx.doi.org/10.1016/j.vehcom.2015.03.004

[23] C. Campolo, A. Molinaro, A. O. Berthet, and A. Vinel, "Full-Duplex Radios for Vehicular Communications," *IEEE Communications Magazine*, vol. 55, no. 6, pp. 182–189, 2017.

[24] W. Xu, H. Zhou, N. Cheng, F. Lyu, W. Shi, J. Chen, and X. Shen, "Internet of vehicles in big data era," *IEEE/CAA Journal of Automatica Sinica*, vol. 5, no. 1, pp. 19–35, 2018.

[25] L. Atzori, A. Iera, and G. Morabito, "The Internet of Things : A Survey The Internet of Things : A survey," *Computer Networks*, vol. 54, no. 15, pp. 2787–2805, 2010. [Online]. Available: http://dx.doi.org/10.1016/j.comnet.2010.05.010

[26] A. Zanella, N. Bui, A. Castellani, L. Vangelista, and M. Zorzi, "Internet of Things for Smart Cities," *IEEE Internet of Things Journal*, vol. 1, no. 1, pp. 22–32, 2014. [Online]. Available: http://ieeexplore.ieee.org/lpdocs/epic03/wrapper.htm?arnumber=6740844

[27] P. F. Pires, F. C. Delicato, T. Batista, and T. Barros, "Capítulo 3 - Plataformas para a Internet das Coisas," in *XXXIII Simpósio Brasileiro de Redes de Computadores e Sistemas Distribuídos*. Universidade Federal do Espírito Santo, 2015.

[28] F. Cunha, L. Villas, A. Boukerche, G. Maia, A. Viana, R. A. F. Mini, and A. A. F. Loureiro, "Data Communication in VANETs: Survey, Applications and Challenges," *Ad Hoc Networks*, vol. 44, pp. 90–103, 2016. [Online]. Available: http://dx.doi.org/10.1016/j.adhoc.2016.02.017

[29] M. Baunach, R. M. Gomes, M. Malenko, F. Mauroner, L. B. Ribeiro, and T. Scheipel, "Smart mobility of the future – a challenge for embedded automotive systems," *Elektrotechnik & Informationstechnik (2018)*, pp. 304–308, 2018. [Online]. Available: http://dx.doi.org/10.1007/s00502-018-0623-6

[30] S. Q. YANG Fangchun, WANG Shangguang, LI Jinglin, LIU Zhihan, "An Overview of Internet of Vehicles," *China Communications*, no. October, pp. 1–15, 2014.

[31] O. Kaiwartya, A. H. Abdullah, Y. Cao, A. Altameem, M. Prasad, C. T. Lin, and X. Liu, "Internet of Vehicles: Motivation, Layered Architecture, Network Model, Challenges and Future Aspects," *IEEE Access*, vol. PP, no. 99, 2016.

[32] K. Ullah, "On the use of opportunistic vehicular communication for roadside services advertisement and discovery," Ph.D. dissertation, University of São Paulo, 2016.

[33] A. C. Regan and R. Chen, "Chapter 2: Vehicular ad hoc networks," in *Vehicular Communications and Networks: Architectures, Protocols, Operation and Deployment*, W. Chen, Ed. Elsevier, 2015, vol. 1, pp. 29–35.

[34] E. Uhlemann, "Introducing connected vehicles [Connected vehicles]," *IEEE Vehicular Technology Magazine*, vol. 10, no. 1, pp. 23–28, 2015.

[35] IEEE Vehicular Technology Society (VTS), "IEEE Connected Vehicles Initiative," p. 2018, 2018. [Online]. Available: http://sites.ieee.org/connected-vehicles/ieee-connected-vechicles/connected-vehicles/

[36] A. Boukerche, H. A. B. F. Oliveira, E. F. Nakamura, and A. A. F. Loureiro, "Vehicular Ad Hoc Networks : A New Challenge for Localization-Based Systems q," *Computer Communications*, vol. 31, pp. 2838–2849, 2008.

[37] U. Lee and M. G. Bell, "A survey of urban vehicular sensing platforms," *Computer Networks*, vol. 54, no. 4, pp. 527–544, 2010. [Online]. Available: http://dx.doi.org/10.1016/j.comnet.2009.07.011

[38] R. I. Meneguette, G. P. Filho, D. L. Guidoni, G. Pessin, L. A. Villas, and J. Ueyama, "Increasing intelligence in inter-vehicle communications to reduce traffic congestions: Experiments in Urban and highway environments," *PLoS ONE*, vol. 11, no. 8, pp. 1–25, 2016.

[39] D. Levinson, "The value of advanced traveler information systems for route choice," *Transportation Research Part C*, vol. 11, no. 1, pp. 75–87, 2003.

[40] A. Grzybek, G. Danoy, P. Bouvry, and M. Seredynski, "Mitigating flash crowd effect using connected vehicle technology," *Vehicular Communications*, vol. 2, no. 4, pp. 238–250, 2015. [Online]. Available: http://dx.doi.org/10.1016/j.vehcom.2015.10.002

[41] F. R. Yu, "Transportation Systems," *IEEE Transactions on Vehicular Technology*, vol. 65, no. May, pp. 3843–3844, 2016.

[42] S. A. A. Shah, E. Ahmed, M. Imran, and S. Zeadally, "IMMINENT COMMUNICATION TECHNOLOGIES FOR SMART COMMUNITIES: 5G for Vehicular Communications," *IEEE Communications Magazine*, no. January, pp. 111–117, 2018.

[43] A. Mastrosimone and D. Panno, "Moving network based on mmWave technology: a promising solution for 5G vehicular users," *Wireless Networks*, vol. 24, no. 7, pp. 1–18, 2017.

[44] J. Contreras-Castillo, S. Zeadally, and J. Guerrero-Ibañez, "Internet of Vehicles: Architecture, Protocols, and Security," *IEEE Internet of Things Journal*, vol. 4662, no. c, pp. 1–1, 2017. [Online]. Available: http://ieeexplore.ieee.org/document/7892008/

[45] Z. Fantian, L. Chunxiao, Z. Anran, and H. Xuelong, "Review of the key technologies and applications in internet of vehicle," in *2017 IEEE 13th International Conference on Electronic Measurement & Instruments*, 2017, pp. 228–232.

[46] S. Andrews, "Section 9: Vehicular Communications Systems," in *Handbook of Intelligent Vehicles*, A. Eskandarian, Ed. Springer-Verlag London Ltd, 2013, vol. 53, no. 9, pp. 1093–1120.

[47] V. P. Barcelos, "Análise e Experimentaçãoo do Padrão IEEE 802.11P em Redes Veiculares Híbridas," Ph.D. dissertation, Universidade Federal de Lavras, 2014.

[48] M. L. Sichitiu and M. Kihl, "Inter-Vehicle Communication Systems: A Survey," *IEEE Communications Surveys & Tutorials*, vol. 10, no. 2, pp. 88 – 105, 2008.

[49] J. Luo and J.-P. Hubaux, "Nicht zu warm und nicht zu kalt," in *Embedded Security in Cars*. Springer Berlin Heidelberg, 2006, vol. 155, no. 29.

[50] USDOT, "Connected Vehicles: CV Pilot Deployment Program," 2018. [Online]. Available: https://www.its.dot.gov/pilots/cv{_}pilot{_}apps.htm

[51] L. Ward and M. Simon, "Intelligent Transportation Systems Using IEEE 802 . 11p Application Note," Rohde & Schwarz, Tech. Rep., 2015.

[52] F. Bai, H. Krishnan, and V. Sadekar, "Towards Characterizing and Classifying Communication-based Automotive Applications from a Wireless Networking Perspective," *Proceedings of IEEE Workshop on Automotive Networking and Applications (AutoNet)*, pp. 1–25, 2006.

[53] J. M. León-coca, D. G. Reina, S. L. Toral, F. Barrero, and N. Bessis, "Intelligent Transportation Systems and Wireless Access in Vehicular Environment Technology for Developing Smart Cities and Wireless Access in Vehicular Smart Cities," in *Big Data and Internet of Things: A Roadmap for Smart Environments*, N. Bessis and C. Dobre, Eds. Springer, 2014, pp. 285–313.

[54] IEEE, "P1609.0/D13, Oct 2018 - IEEE Draft Guide for Wireless Access in Vehicular Environments (WAVE) - Architecture," IEEE, Tech. Rep., 2018. [Online]. Available: https://ieeexplore.ieee.org/document/8509668

[55] C. S. IEEE, "Specific requirements Part 11 : Wireless LAN Medium Access Control (MAC) and Physical Layer (PHY) Specifications Amendment 5 : Television White Spaces (TVWS) Operation IEEE Computer Society," IEEE Computer Society, Tech. Rep., 2016.

[56] ITERIS, "Dedicated Short Range Communication at 5 . 9 GHz Standards Group," p. 5590, 2016. [Online]. Available: https://local.iteris.com/spc/html/std/stgrdsrc{_}5ghz.htm

[57] J. B. Kenney, G. Bansal, and C. E. Rohrs, "LIMERIC : A Linear Message Rate Control Algorithm for Vehicular DSRC Systems," in *VANET '11 Proceedings of the Eighth ACM international workshop on Vehicular inter-networking*, no. June, 2011.

[58] A. Festag, "Standards for vehicular communication—from IEEE 802.11p to 5G," *Elektrotechnik & Informationstechnik*, vol. 132, no. 7, pp. 409–416, 2015. [Online]. Available: http://dx.doi.org/10.1007/s00502-015-0343-0

[59] T. Noltet, H. Hanssont, and L. L. Bellot, "Automotive Communications - Past, Current and Future," in *2005 IEEE Conference on Emerging Technologies and Factory Automation*, vol. 1. IEEE, 2005, pp. 985–992.

[60] M. Faezipour, M. Nourani, A. Saeed, and S. Addepalli, "Progress and Challenges in Intelligent Vehicle Area Networks," *Communications of the ACM*, vol. 55, no. 2, pp. 90–100, 2012.

[61] D. Paret, *Multiplexed Networks for Embedded Systems: CAN, LIN, FlexRay, Safe-by-Wire...* Wiley, 2007.

[62] S. Tuohy, M. Glavin, C. Hughes, E. Jones, M. Trivedi, and L. Kilmartin, "Intra-Vehicle Networks : A Review," *IEEE TRANSACTIONS ON INTELLIGENT TRANSPORTATION SYSTEMS*, vol. 16, no. 2, pp. 534 – 545, 2014.

[63] J. E. Siegel, D. C. Erb, and S. E. Sarma, "A survey of the connected vehicle Landscape - Architectures, enabling technologies, applications, and development areas," *IEEE Transactions on Intelligent Transportation Systems*, vol. 19, no. 8, pp. 2391–2406, 2018.

[64] Y. Huo, W. Tu, Z. Sheng, and V. C. Leung, "A Survey of In-vehicle Communications : Requirements , Solutions and Opportunities in IoT," *2015 IEEE 2nd World Forum on Internet of Things (WF-IoT)*, 2015.

[65] J. Swanson and M. Serughetti, "Using Ethernet in automotive networks," pp. 1–3, 2014. [Online]. Available: http://www.techdesignforums.com/practice/technique/using-ethernet-automotive-networks/

[66] A. Azman, S. Yogarayan, S. Leong, W. Jian, S. Fatimah, A. Razak, K. J. Raman, M. Fikri, A. Abdullah, S. Z. Ibrahim, A. Hudaya, M. Amin, and K. S. Muthu, "Comprehensive Study of Wireless Communication Technologies for Vehicular Communication," *2018 3rd International Conference on Computer and Communication Systems (ICCCS)*, pp. 314–317, 2018.

[67] M. A. Haque and M. D. Hossain, "Technology survey of wireless communication for in-vehicle applications," *SKIMA 2014 - 8th International Conference on Software, Knowledge, Information Management and Applications*, 2014.

[68] N. Lu, N. Cheng, N. Zhang, X. Shen, and J. W. Mark, "Connected Vehicles : Solutions and Challenges," *IEEE Internet of Things Journal*, vol. 1, no. 4, pp. 289–299, 2014.

[69] M. Ali, "Chapter 8: standards of communications in the intelligent transport systems (ITS)," in *Autonomous Vehicles*, N. Bizon, L. Dascalescu, and N. Tabatabaei, Eds. Nova Science Publishers, 2014, vol. 3, no. 1, pp. 235–246.

[70] RAMON DOS REIS FONTES, CLAUDIA CAMPOLO, CHRISTIAN ESTEVE ROTHENBERG and A. MOLINARO, "From Theory to Experimental Evaluation : Resource Management in Software-Defined Vehicular Networks," *IEEE Access*, vol. 5, 2017.

[71] ENGIMIND, "Relatório final: desenvolvimento de um manual de referência para concepção, dimensionamento e implementação de praças de pedágio em concessões rodoviárias," National Land Transportation Agency (ANTT), Tech. Rep., 2018. [Online]. Available: antt.gov.br/backend/galeria/arquivos/2018/10/16/Relatorio{_}Final.pdf

[72] L. R. Bencke, A. Luiz, F. Perez, and O. Costa, "Smart Roads: an overview of the technologies in Brazil and in the world," *iSys - Revista Brasileira de Sistemas de Informação*, vol. 10, no. 10, pp. 80–102, 2017.

[73] SemParar, "Como funciona," 2018. [Online]. Available: https://www.semparar.com.br/como-funciona

[74] D. ZHAO and H. PENG, "From the Lab to the Street: Solving the Challenge of Accelerating Automated Vehicle Testing," University of Michigan, Tech. Rep. May, 2017.

[75] CET, "Companhia de Engenharia de Trafego," 2019. [Online]. Available: http://www.cetsp.com.br

[76] Waze, "Waze," p. 2019, 2016. [Online]. Available: http://waze.com

[77] M. N. O. Sadiku, M. Tembely, and S. M. Musa, "Internet of Vehicles: An Introduction," *International Journal of Advanced Research in Computer Science and Software Engineering*, vol. 8, no. 1, p. 11, 2018. [Online]. Available: http://ijarcsse.com/index.php/ijarcsse/article/view/512

[78] Z. Wang and M. Hassan, "How Much of DSRC is Available for Non-Safety Use ?" in *VANET '08 Proceedings of the fifth ACM international workshop on VehiculAr Inter-NETworking*, 2008, pp. 23–29.

[79] Q. Chen, D. Jiang, and L. Delgrossi, "IEEE 1609.4 DSRC Multi-Channel Operations and Its Implications on Vehicle Safety Communications," in *2009 IEEE Vehicular Networking Conference (VNC)*. IEEE, 2009, pp. 1–8.

[80] X. Wu, S. Subramanian, R. Guha, R. G. White, J. Li, K. W. Lu, T. Zhang, and A. Bucceri, "Vehicular Communications Using DSRC : Challenges , Enhancements , and Evolution," *IEEE JOURNAL ON SELECTED AREAS IN COMMUNICATIONS/SUPPLEMENT*, vol. 31, no. 9, pp. 399–408, 2013.

[81] M. Boban, T. T. V. Vinhoza, M. Ferreira, J. Barros, and O. K. Tonguz, "Impact of Vehicles as Obstacles in Vehicular Ad Hoc Networks," *IEEE JOURNAL ON SELECTED AREAS IN COMMUNICATIONS*, no. June 2014, 2011.

[82] L. Cheng, B. E. Henty, D. D. Stancil, F. Bai, and P. Mudalige, "Mobile Vehicle-to-Vehicle Narrow-Band Channel Measurement and Characterization of the 5 . 9 GHz Frequency Band," *IEEE JOURNAL ON SELECTED AREAS IN COMMUNICATIONS*, vol. 25, no. 8, pp. 1501–1516, 2007.

[83] C. F. Mecklenbrauker, J. Karedal, A. Paier, T. Zemen, and N. Czink, "Characterization and Its Implications for Wireless System Design and Performance," in *Proceedings of the IEEE*, vol. 99, no. 7. IEEE, 2011.

[84] C. U. Bas and S. C. Ergen, "Ultra-wideband Channel Model for Intra-vehicular Wireless Sensor Networks Beneath the Chassis : From Statistical Model to Simulations," *14 IEEE TRANSACTIONS ON VEHICULAR TECHNOLOGY*, vol. 62, no. 1, pp. 14–25, 2013.

[85] J.-M. Girard, N. Tricot, K. Younsi, and J.-C. Popieul, "When does the driver workload reaches its limits?" in *Proceedings of the 2006 IEEE Intelligent Transportation Systems Conference*. Toronto: IEEE, 2006, pp. 578–583.

[86] C. Wu and Y. Liu, "Queuing Network Modeling of Driver Workload and Performance," *IEEE TRANSACTIONS ON INTELLIGENT TRANSPORTATION SYSTEMS*, vol. 8, no. 3, pp. 528–537, 2007.

[87] N. L. T. A. (ANTT), "Resolução 3576 Resolução nº 3576 , de 02 de setembro de 2010," 2010. [Online]. Available: http://portal.antt.gov.br/

[88] IBGE (Brazilian Institute of Geography and Statistics), "Brazil - Panorama," Brasilia, p. 1, 2018. [Online]. Available: https://cidades.ibge.gov.br/brasil/panorama

[89] N. T. A. (ANATEL), "Mobile Telephony - Municipalities served," 2018. [Online]. Available: http://www.anatel.gov.br/setorregulado/telefonia-movel/115-universalizacao-e-ampliacao-do-acesso/telefonia-movel/423-telefonia-movel-municipios-atendidos

[90] M. Picone, S. Busanelli, M. Amoretti, F. Zanichelli, and G. Ferrari, *Advanced Technologies for Intelligent Transportation Systems*. Springer, 2015.

[91] S. K. Bhoi and P. M. Khilar, "Vehicular communication: a survey," *IET Networks*, vol. 3, no. 3, pp. 204–217, 2014. [Online]. Available: http://digital-library.theiet.org/content/journals/10.1049/iet-net.2013.0065

[92] E. T. S. I. (ETSI), "Intelligent Transport Systems (ITS); Decentralized Congestion Control Mechanisms for Intelligent Transport Systems operating in the 5 GHz range; Access layer part," European Telecommunications Standards Institute, Tech. Rep., 2011.

[93] Brazilian Association of Technical Standards (ABNT), "ABNT / CB-005 - Brazilian Automotive Committee," 2018. [Online]. Available: http://www.abnt.org.br/cb-05

[94] National Telecommunications Agency (ANATEL), "Plan of attribution, destination and distribution of frequency bands in Brazil," Tech. Rep., 2017. [Online]. Available: http://www.anatel.gov.br

[95] L. Zhang, Y. Wu, G. K. Walker, W. Li, K. Salehian, and A. Florea, "Improving LTE eMBMS with extended OFDM parameters and layered-division-multiplexing," *IEEE Transactions on Broadcasting*, vol. 63, no. 1, pp. 32–47, 2017.

[96] D. Lecompte and F. Gabin, "Evolved multimedia broadcast/multicast service (eMBMS) in LTE-advanced: Overview and Rel-11 enhancements," *IEEE Communications Magazine*, vol. 50, no. 11, pp. 68–74, 2012.

[97] F. Kargl and J. Petit, "Chapter 9: Security and privacy in vehicular networks," in *Vehicular Communications and Networks Architectures, Protocols, Operation and Deployment*, W. Chen, Ed. Elsevier, 2015, vol. 1.

[98] Y. Fraiji, L. Ben Azzouz, W. Trojet, and L. Saidane, "Cyber security issues of Internet of electric vehicles," *IEEE Wireless Communications and Networking Conference, WCNC*, vol. 2018-April, pp. 1–6, 2018.

[99] T. Hoppe, S. Kiltz, and J. Dittmann, "Security threats to automotive CAN networksPractical examples and selected short-term countermeasures," *Reliability Engineering and System Safety*, vol. 96, no. 1, pp. 11–25, 2011.

[100] K. Grover, A. Lim, and Q. Yang, "Jamming and anti-jamming techniques in wireless networks: a survey," *International Journal of Ad Hoc and Ubiquitous Computing (IJAHUC)*, vol. 17, no. 4, 2014.

[101] Y. Sun, L. Wu, S. Wu, S. Li, T. Zhang, L. Zhang, J. Xu, Y. Xiong, and X. Cui, "Attacks and countermeasures in the internet of vehicles," *Annales des Telecommunications/Annals of Telecommunications*, vol. 72, no. 5-6, pp. 283–295, 2017.

[102] Y. Sun, L. Wu, S. Wu, S. Li, T. Zhang, L. Zhang, J. Xu, and Y. Xiong, "Security and Privacy in the Internet of Vehicles," *Proceedings - 2015 International Conference on Identification, Information, and Knowledge in the Internet of Things, IIKI 2015*, pp. 116–121, 2016.

[103] B. Lipiński, W. Mazurczyk, K. Szczypiorski, and P. Śmietanka, "Towards Effective Security Framework for Vehicular Ad-Hoc Networks," *Journal of Advances in Computer Networks*, vol. 3, no. 2, 2015.

[104] N. A. Sahloul, L. Benazzouz, and I. Aouini, "Towards an IPsec security GeoNet Architecture," in *Network of the Future NoF'12*, 2012.

[105] S. Namal, M. Liyanage, and A. Gurtov, "Realization of Mobile Femtocells : Operational and Protocol Requirements," *Wireless Personal Communications*, pp. 339–364, 2013.

[106] C.-K. Han, H.-K. Choi, and I.-H. Kim, "Building Femtocell More Secure with Improved Proxy Signature," in *GLOBECOM 2009 - 2009 IEEE Global Telecommunications Conference*, 2009.

[107] G. Mantas, N. Komninos, J. Rodriguez, E. Logota, and H. Marques, "Chapter 9 Security for 5G Communications," in *Fundamentals of 5G Mobile Networks*, 2015. [Online]. Available: http://openaccess.city.ac.uk/13047/Link

[108] M. H. Eiza, Q. Ni, and Q. Shi, "Secure and Privacy-Aware Cloud-Assisted Video Reporting Service in 5G-Enabled Vehicular Networks," *IEEE TRANSACTIONS ON VEHICULAR TECHNOLOGY*, vol. 65, no. 10, pp. 7868–7881, 2016.

[109] P. Gandotra and R. Kumar, "A survey on device-to-device (D2D) communication : Architecture and security issues," *Journal of Network and Computer Applications*, vol. 78, no. October 2016, pp. 9–29, 2017. [Online]. Available: http://dx.doi.org/10.1016/j.jnca.2016.11.002

[110] A. Tarabasz, "The Internet of Things – Digital Revolution in Offline Market. Opportunity or Threat?" *HANDEL WEWNĘTRZNY 2016*, vol. 4, no. 363, pp. 325–337, 2016.

[111] O. Puñal, A. Aguiar, and J. Gross, "In VANETs We Trust ? Characterizing RF Jamming in Vehicular Networks," in *Proceedings of the ninth ACM international workshop on Vehicular inter-networking, systems, and applications,VANET'12*, 2012, pp. 83–92.

[112] N. K. Chaubey, "Security Analysis of Vehicular Ad Hoc Networks (VANETs): A Comprehensive Study," in *International Journal of Security and Its Applications*, vol. 10, no. 5, 2016.

[113] W. Jiang, F. Li, D. Lin, and Elisa Bertino, "No One Can Track You : Randomized Authentication in Vehicular Ad-hoc Networks," *2017 IEEE International Conference on Pervasive Computing and Communications (PerCom) No*, 2017.

[114] H. Hasrouny, A. Ellatif, C. Bassil, and A. Laouiti, "VANet security challenges and solutions : A survey," *Vehicular Communications*, vol. 7, pp. 7–20, 2017. [Online]. Available: http://dx.doi.org/10.1016/j.vehcom.2017.01.002

[115] CERN, "CERN Articles on Computer Security," 2018. [Online]. Available: https://security.web.cern.ch/security/training/en/CERNArticlesOnComputerSecurity(2018).pdf

[116] L. E. d. S. Cardoso, "Sistema Nacional de Trânsito," 2015. [Online]. Available: http://www.conteudojuridico.com.br/?artigos{&}ver=2.52617{&}seo=1{%}3E

[117] Y. Jia, W. Xu, and X. Liu, "An Optimization Framework For Online Ride-sharing Markets."

[118] S. Banerjee, D. Freund, and T. Lykouris, "Pricing and Optimization in Shared Vehicle Systems : An Approximation Framework," in *EC '17 Proceedings of the 2017 ACM Conference on Economics and Computation*, 2017.

[119] 99app, "Cidades: Veja as categorias da 99 em sua cidade," 2018. [Online]. Available: https://99app.com/sobre-a-99/cidades/

[120] Uber, "Descubra quais cidades do Brasil têm Uber," 2018. [Online]. Available: https://www.uber.com/pt-BR/blog/em-quais-cidades-a-uber-esta-no-brasil/

[121] Cabify, "Cidades Cabify. Conheça todas as cidades onde operamos." 2018. [Online]. Available: https://cabify.com/pt-BR

[122] A. Boadle, "Uber, rival apps join forces in Brazil to stem tide of regulation," 2017. [Online]. Available: https://www.reuters.com/article/us-uber-brazil/uber-rival-apps-join-forces-in-brazil-to-stem-tide-of-regulation-idUSKBN1D71KE

[123] H. d. F. Miranda and A. N. R. da Silva, "Benchmarking sustainable urban mobility : The case of Curitiba , Brazil," *Transport Policy*, vol. 21, pp. 141–151, 2012.

[124] J. M. de Araujo, "Plano nacional de redução de mortes e lesões no trânsito," 2018. [Online]. Available: http://www.ctbdigital.com.br/artigo/plano-nacional-de-reducao-de-mortes-e-lesoes-no-transito-por-julyver-modesto-de-a

[125] N. L. T. A. (ANTT), "Resolução ANTT nº 3.323-A de 18/11/2009," Agência Nacional de Transporte Terrestre (ANTT), Tech. Rep., 2009. [Online]. Available: http://www.normasbrasil.com.br/norma/resolucao-3323-2009{_}109723.html

[126] U. D. o. T. (USDOT), "The U . S . Brazil Multimodal Intelligent Transportation Systems (ITS) Workshop," p. 8339, 2017. [Online]. Available: transportation.gov/office-policy/international-policy-and-trade/us-brazil-multimodal-intelligent-transportation-systems